The McGraw-Hill Companies

Optical Fiber Communications

FOURTH EDITION

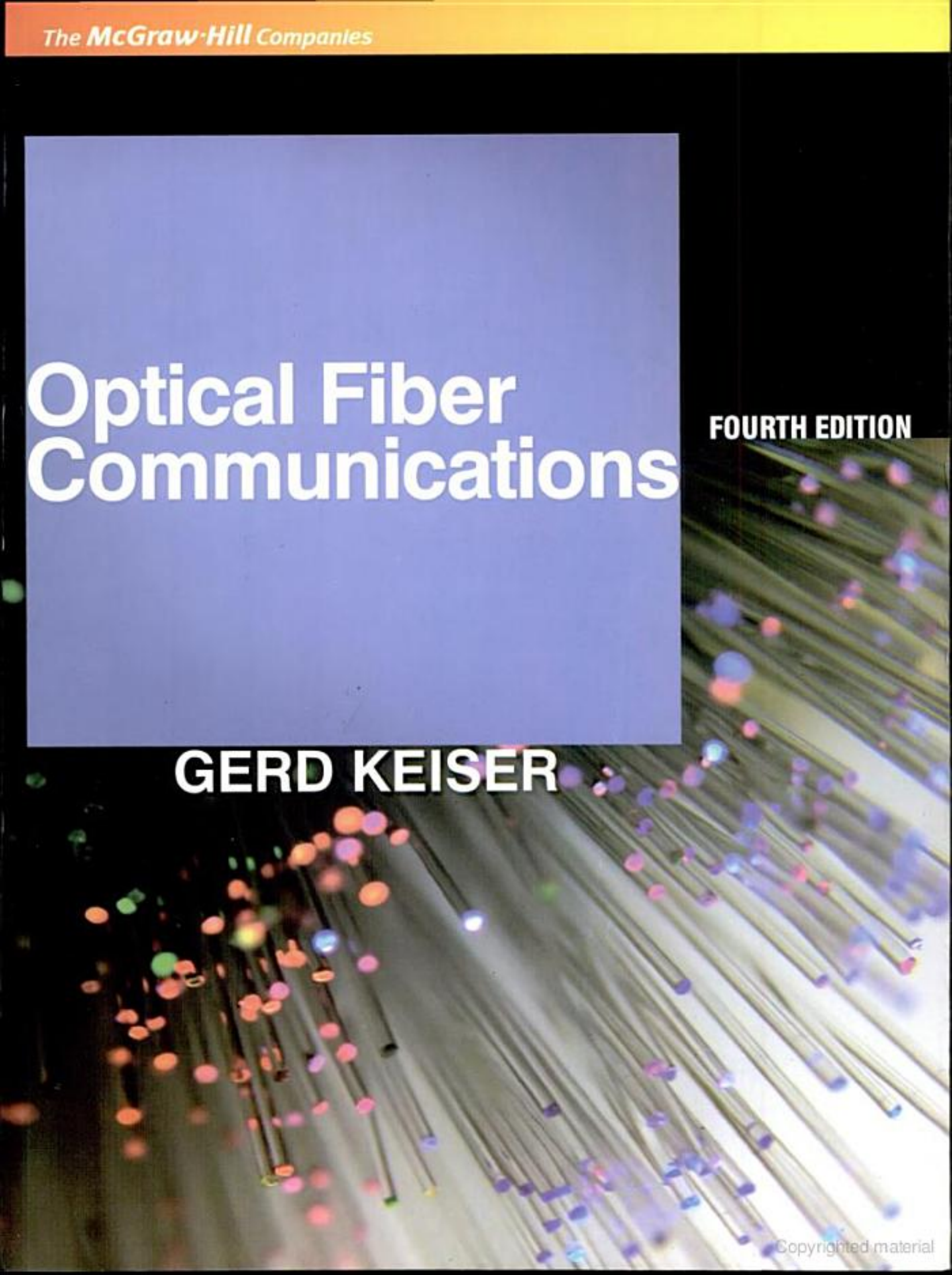

GERD KEISER

Tata McGraw-Hill

Published by the Tata McGraw-Hill Publishing Company Limited,
7 West Patel Nagar, New Delhi 110 008.

Fourth reprint 2008
DZXACRYXRADYD

This edition can be exported from India only by the publishers,
Tata McGraw-Hill Publishing Company Limited.

ISBN 13: 978-0-07-064810-4
ISBN 10: 0-07-064810-7

Managing Director: *Ajay Shukla*

General Manager: Publishing—SEM & Tech Ed: *Vibha Mahajan*
Jr. Editorial Executive: *Sandhya Chandrasekhar*
Asst. Sponsoring Editor: *Shukti Mukherjee*
Executive—Editorial Services: *Sohini Mukherjee*
Senior Production Manager: *P L Pandita*

General Manager: Marketing—Higher Education & School: *Michael J Cruz*
Product Manager: SEM & Tech Ed: *Biju Ganesan*

Controller—Production: *Rajender P Ghansela*
Asst. General Manager—Production: *B L Dogra*

Published by the Tata McGraw-Hill Publishing Company Limited, 7 West Patel Nagar, New Delhi 110 008, typeset at Bukprint India, B-180A, Guru Nanak Pura, Laxmi Nagar-110 092 and printed at Sai Printo-Pack, A-102/4, Okhla Industrial Area, Phase II, New Delhi 110 020

Cover: Rashtriya

This chapter discusses measurements and performance monitoring tests of interest to designers, installers, and operators of fiber optic links and networks. Of particular interest here are measurements for WDM links. Figure 14.1 shows some of the relevant test parameters and at what points in a WDM link they are of importance. The operational impact or impairment for many of these factors can be accounted for and controlled through careful network design. Other parameters may need to be monitored and possibly compensated for dynamically during network operation. In either case, all of these parameters must be measured at some point during the time period ranging from network design concept to service provisioning.

First, Sec. 14.1 addresses internationally recognized measurement standards for component and system evaluations. Next, Sec. 14.2 lists basic test instruments for optical fiber communication link

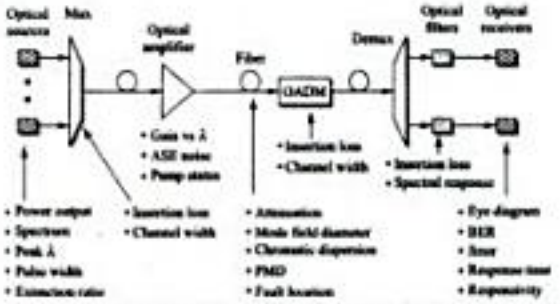

Fig. 14.1 *Components of a typical WDM link and some performance-measurement parameters of user interest*

characterizations. A fundamental unit in lightwave communications is optical power and its measurement with optical power meters, which is the topic of Sec. 14.3. Turning to measurement techniques, Sec. 14.4 gives an overview of methods and specialized equipment for characterizing optical fiber parameters. In addition to determining geometric parameters, this equipment also can measure attenuation and chromatic dispersion. During and after link installation, several basic parameters need to be checked. For example, the error performance can be estimated through eye pattern measurements, which is the topic of Sec. 14.5. The physical integrity of the fielded link typically is checked with an optical time-domain reflectometer, as Sec. 14.6 explains. Finally, Sec. 14.7 discusses optical performance monitoring, which is essential for managing high-capacity lightwave transmission networks. Network functions that need such monitoring include amplifier control, channel identification, and assessment of the integrity of optical signals.

14.1 Measurement Standards

Before examining measurement techniques, let us first look at what standards exist for fiber optics. As summarized in Table 14.1, the three basic classes are primary, component-testing, and system standards.

Link testing setups show what system parameters need to be measured at given points in a link.

Link performance tests illustrate how to assess the performance of a link.

The subscript λ on the $\langle \Delta\tau_{pd} \rangle$ term means that the expected value of the differential group delay is determined over a wavelength span.

14.5 Eye Diagram Tests

The use of an *eye diagram* is a traditional technique for quickly and intuitively assessing the quality of a received signal. Modern bit-error-rate (also called *bit-error-ratio*) measurement instruments construct such eye diagrams by generating a pseudorandom pattern of ones and zeros at a uniform rate but in a random manner. When the pulses in this pattern are superimposed simultaneously, an eye pattern as shown in Fig. 14.14 is formed[29-31]. The word *pseudorandom* means that the generated combination or sequence of ones and zeros will eventually repeat but that it is sufficiently random for test purposes. A *pseudorandom binary sequence* (PRBS) comprises four different 2-bit-long combinations, eight different 3-bit-long combinations, sixteen different 4-bit-long combinations, and so on (that is, sequences of 2^N different N-bit-long combinations) up to a limit set by the instrument. These combinations are randomly selected. The PRBS pattern length is of the form $2^N - 1$, where N is an integer. This choice assures that the pattern-repetition rate is not harmonically related to the data rate. Typical values of N are 7, 10, 15, 20, 23, and 31. After this limit has been reached, the data sequence will repeat.

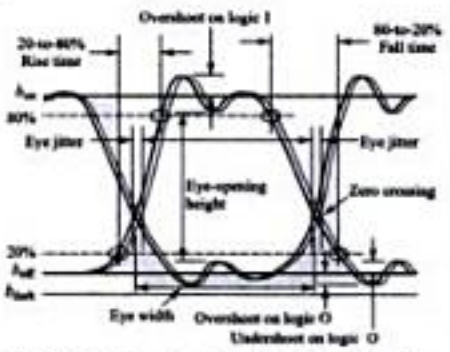

Fig. 14.14 *General configuration of a fairly clean eye diagram showing definitions of fundamental measurement parameters*

Ideally, if the signal impairments are small the received pattern should look like that shown in Fig. 14.14. However, time-varying signal impairments in the transmission path can lead to amplitude variations within the signal and timing skews between the data signal and the associated clock signal. Note that a clock signal, which typically is encoded within a data signal, is used to help the receiver interpret the incoming data correctly. Thus, in an actual link the received pattern will become wider or distorted on the sides and on the top and bottom, as shown in Fig. 14.15.

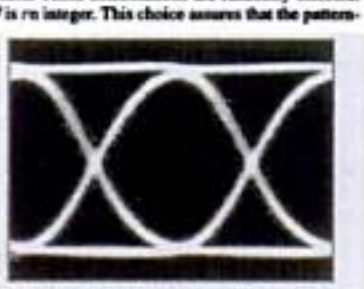

Fig. 14.15 *Signal-distorting effects cause the eye opening to get smaller (Photo provided courtesy of Circadiant Systems; www.circadiant.com)*

temporal characteristics of the waveform of the reflected and back-scattered light. A typical OTDR consists of a light source and receiver, data-acquisition and processing modules, an information-storage unit for retaining data either in the internal memory or on an external disk, and a display. Figure 14.20 shows a portable OTDR for making measurements in the field.

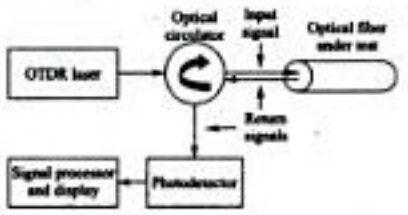

Fig. 14.19 *Operational principle of an OTDR using an optical circulator*

Fig. 14.20 *Example of portable universal test sets that can be used for OTDR traces, optical spectrum analysis, dispersion analysis, and other test functions. (Model FTB-400, photo provided courtesy of EXFO; www.exfo.com.)*

14.6.1 OTDR Trace

Figure 14.21 shows a typical trace as seen on the display screen of an OTDR. The scale of the vertical axis is logarithmic and measures the returning (back-reflected) signal in decibels. The horizontal axis denotes the distance between the instrument and the measurement point in the fiber. In addition to the trace, an OTDR such as the one shown in Fig. 14.20 also can place a number next to an event on the display and give a list of these numbers and their corresponding measurement information in a table below the trace.

The backscattered waveform has four distinct features:

- A large initial pulse resulting from Fresnel reflection at the input end of the fiber.
- A long decaying tail resulting from Rayleigh scattering in the reverse direction as the input pulse travels along the fiber.

Test equipment discussions show the operational principle of major instruments and give examples of commercial gear.

power levels between channels. Other functions of an OPM include determining if a particular channel is active, verifying whether wavelengths match the specified channel plan, and checking whether optical power and OSNR levels are sufficient to meet the QoS requirements.

An OPM may have the following operational characteristics:

- Measures absolute channel power to within ± 0.5 dBm
- Identifies channels without prior knowledge of the wavelength plan
- Makes full S-, C-, or L-band measurements in less than 0.5 seconds
- Measures center wavelength accuracy to better than ± 50 pm
- Determines OSNR with a 35-dB dynamic range to a ± 0.1-dB accuracy

14.7.5 Fault Management

Faults in a network, such as physical cuts in a fiber transmission line or failure of a circuit card or optical amplifier, can cause portions of a network to be inoperable. Since network faults can result in system downtime or unacceptable network degradation, *fault management* is one of the most widely implemented and essential network management functions. As Fig. 14.29 illustrates, fault management involves the following processes:

Network performance management discussions explain the need and procedures for verifying correct and reliable network operations.

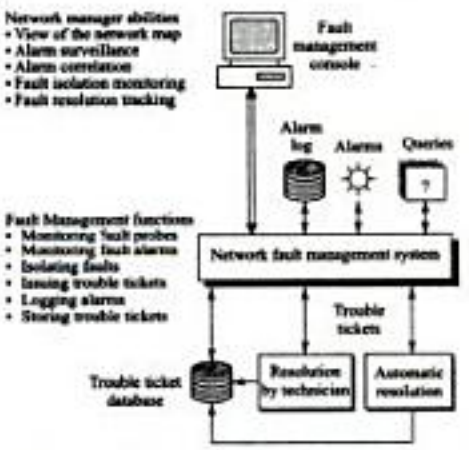

Fig. 14.29 *Functions and interactions of a network fault management system*

- Detecting fault or degradation symptoms. This can be done with *alarm surveillance*, which involves reporting alarms that may have different levels of severity and indicating possible causes of these alarms. Fault management also provides a summary of unresolved alarms and allows the network manager to retrieve and view the alarm information from an alarm log.
- Determining the origin and possible cause of faults either automatically or through the intervention of a network manager. To determine the location or origin of faults, the management system

Contents

Preface

Objective

Optical fiber communications has undergone a fascinating history since the first edition of this book appeared in 1983. Initially the technology focused on simple transmission links but then quickly moved to increasingly sophisticated networks. Along the way many new components and communication techniques were tried. Some of these were highly successful, some faded away perhaps because of their implementation complexity, and others which were ahead of their time are reappearing after being in hibernation for a while. Modern high-capacity telecommunication networks based on optical fiber technology now have become an integral and indispensable part of society. Applications for these sophisticated networks range from simple web browsing and e-mail exchanges to critical health-care diagnosis and complex business transactions. Due to the importance of these networks to everyday life, users have come to expect the communication services to always be available and to function properly. Meeting such a stringent demand requires careful engineering in all technological aspects ranging from component development to system design and installation to network operation and maintenance.

To address the attainment and implementation of these skills, this expanded fourth edition presents the fundamental principles for understanding and applying a wide range of optical fiber technologies to modern communication networks. The sequence of topics takes the reader systematically from the underlying principles of components and their interactions with other devices in an optical fiber link, through descriptions of the architectures and performance characteristics of complex optical links and networks, to essential measurement and test procedures required during network installation and maintenance. By mastering these fundamental topics the reader will be prepared not only to contribute to disciplines such as current device, communication link, or equipment designs, but also to understand quickly any further technology developments for future enhanced networks.

Contents

To accomplish these objectives, Chap. 1 gives a basic overview of how optical communications blend into telecommunication systems. The discussions include the motivations and advantages for using optical fibers, the spectral bands being used, fundamental data communication concepts used in optical communications, how wavelength division multiplexing can boost the transmission capacity of an optical fiber, and what standards are being applied.

Chapters 2 through 11 describe the purpose and performance characteristics of the major elements in an optical link. These elements include optical fibers, light sources, photodetectors, passive optical devices, optical amplifiers, and active optoelectronic devices used in multiple-wavelength networks. Despite its apparent simplicity, an optical fiber is one of the most important elements in a fiber link.

Chapters 2 and 3 give details on the physical structures, constituent materials, attenuation behavior, lightwave propagation mechanisms, and signal distortion characteristics of the wide variety of optical fibers that exist. In addition, Chap. 3 introduces optical fiber fabrication methods and illustrates several generic fiber cable configurations. The new topics in these chapters include a discussion of photonic crystal fibers and a streamlining of the discussions on modal effects and pulse broadening.

Chapter 4 addresses the structures, light-emitting principles, and operating characteristics of light sources used in optical communications. In addition, the discussion includes direct and external modulation techniques, temperature effects, device lifetime considerations, and line coding methods for transporting signals over a fiber. How to couple the light source to a fiber is described in Chap. 5, as well as how to join two fibers in order to ensure a low optical power loss at the joints.

The lightwave receiver has the task of detecting the arriving optical signal and converting it into an electrical signal that can be processed by the receiver electronics. Chapter 6 covers the structures and responses of photodetectors, and Chap. 7 describes the principles and functions of lightwave receivers. The new features in Chap. 7 include a simplified presentation of the operational characteristics of lightwave receivers, the concepts of signal-detection statistics and eye-diagram measurement schemes, basic coherent detection schemes, and a description of burst-mode receivers used for passive optical networks.

Chapters 8 and 9 examine the design methods for digital and analog links, respectively. For Chap. 8 this includes discussions of link power budgets and bandwidth limitations. The new features are an expanded coverage of power penalties and details of error-control methods for digital signals. Additions to Chap. 9 include the concepts of sending radio-frequency (RF) analog signals at microwave frequencies over optical fibers. An expanding application of these RF-over-fiber techniques is for broadband wireless networks.

Chapter 10 addresses the principles of wavelength division multiplexing (WDM), examines the functions of a generic WDM link, and discusses international standards for different WDM schemes. New features in this chapter include expanded descriptions and application examples of passive and active WDM devices, such as fiber Bragg gratings, thin-film filters, arrayed waveguide gratings, diffraction gratings, and variable optical attenuators.

Chapter 11 looks at different concepts for creating optical amplification. Among the topics are semiconductor optical amplifiers, doped-fiber amplifiers, and a new section on Raman amplification schemes. In addition to discussions of the traditional erbium-doped fiber amplifier (EDFA), new structures such as a thulium-doped fiber amplifier (TDFA) for use in the S-band and a gain-shifted EDFA for the L-band are described.

Next, chapters 12 through 14 show how the elements are put together to form links and networks, and explain measurement methodologies used to evaluate the performance of lightwave components and links. A new Chap. 12 is devoted to the origins and effects of nonlinear processes in optical fibers. Some of these nonlinear effects degrade system performance and need to be controlled, whereas others, such as stimulated Raman scattering, can have beneficial uses.

Optical networking concepts for long-haul, metro, local-area, and access networks are presented in an extensively expanded Chap. 13. Among the new topics are high-speed optical links operating up to 160 Gb/s, the concepts of optical add/drop multiplexing and optical cross-connects, wavelength routing, optical packet switching, optical burst switching, passive optical networks, and mitigation techniques for transmission impairments in high-speed networks.

The final chapter discusses performance measurement and monitoring. The topics include a discussion of internationally recognized measurement standards, basic test instruments for optical fiber link

characterization, methods for characterizing optical fibers, and evaluation of link performance through eye-pattern measurements. Particular emphasis is placed on evaluating WDM links. New features in Chap. 14 concerning eye diagrams include the concepts of eye masks, stressed-eye tests, and bit-error-rate eye contours. Another new feature is a discussion of optical performance monitoring. This has become an essential function in optical communication networks, particularly in relation to error monitoring, network maintenance, and fault management.

Use of the Book

This fourth edition provides the basic material for a senior-level or graduate course in the theory and application of optical fiber communication technology. It also will serve well as a working reference for practicing engineers dealing with the design and development of components, transmission equipment, test instruments, and cable plants for optical fiber communication systems. The background required to study the book is that of typical senior-level engineering students. This includes introductory electromagnetic theory, calculus and elementary differential equations, and basic concepts of optics as presented in a freshman physics course. Concise reviews of several background topics, such as optics concepts, electromagnetic theory, and basic semiconductor physics, are included in the main body of the text. Various sections dealing with advanced material (e.g., the applications of Maxwell's equations to cylindrical dielectric waveguides) are designated by a star and can be skipped over without loss of continuity. To assist readers in learning the material and applying it to practical designs, numerous examples are given throughout the book. A collection of 267 homework problems is included to help test the reader's comprehension of the material covered, and to extend and elucidate the text. Instructors can obtain the problem solutions from the publisher.

Numerous references are provided at the end of each chapter as a start for delving deeper into any given topic. Since optical fiber communications brings together research and development efforts from many different scientific and engineering disciplines, there are hundreds of articles in the literature relating to the material covered in each chapter. Even though not all these articles can be cited in the references, the selections represent some of the major contributions to the fiber optics field and can be considered as a good introduction to the literature. Supplementary material and references for up-to-date developments can be found in specialized textbooks and various conference proceedings.

To help the reader understand and use the material in the book, a table in the inside front cover provides a quick reference for various physical constants and units. Appendices A through D give an overview of the international system of units, listings of mathematical formulas needed for homework problems, and discussions on decibels.

Computer-based modeling and simulation tools offer a powerful method to assist in analyzing the design of an optical component, circuit, or network before costly prototypes are built. The book website http://www.mhhe.com/keiser/ofc4e) describes abbreviated interactive demonstration versions of simulation modules. These modules may be downloaded from the websites of several companies that produce simulation tools. The simplified versions contain over 100 predefined component and link configurations that allow interactive concept demonstrations. Although the configurations are fixed, the user can vary certain parameters or turn them on and off to see the effect on system performance.

Book Website

In addition to providing web links for learning about and downloading interactive simuiation

demonstrations, the book website listed earlier has further information on new technology developments, updated reference material related to the book, a link for downloading a selection of the figures in the book for teaching purposes, and a password-protected link for instructors to download the problem solutions. Permission for instructors to access the solutions manual can be obtained from the publisher.

Gerd Keiser

Acknowledgements

In preparing this book and its previous editions, I am extremely grateful to many people with whom I had numerous discussions, who helped me in many different ways, and who supplied me with material for these books. The people from academia include Tri T. Ha, Naval Postgraduate School; John Proakis, Northeastern University and University of California San Diego; Bahaa Saleh, Selim Ünlü, Michael Ruane, Malvin Teich, and Roberto Paiella, Boston University; San-Liang Lee, Jean-Lien Chen, Shih-Hsiang Hsu, Peter Shien-Kuei Liaw, Cheng-Kuang Liu, and Hua-Liang Lo, National Taiwan University of Science and Technology; Hung-Chun Chang, Hen-Wei Tsao, and Chih-Chung Yang, National Taiwan University; Shyh-Lin Tsao, National Taiwan Normal University; Perry Ping Shum, Nanyang Technological University; Arthur Lowery, Monash University; Alan E. Willner, University of Southern California; Daniel Blumenthal, University of California Santa Barbara; Robert Minasian, University of Sydney; Sarah Dods and Elaine Wong, University of Melbourne; Craig Armiento, University of Massachusetts-Lowell; Hui-Chi Chen, Fu-Jen Catholic University; Lian-Kuan Chen and Hon Tsang, Chinese University of Hong Kong; Arthur Chiou and Frank Fu-Jen Kao, National Yang Ming University; Walter Johnstone, University of Strathclyde; and Yung-Sheng Liu, National Tsing Hua University. The people from non-academic institutions include William (Bill) Beck, Troy Bergstrom, Bertand Destieux, Emmanuel Desurvire, Paul Fitzgerald, Doug Forster, Paul Fowler, André Girard, Jim Hayes, Ley Mee Hii, Frank Jaffer, Jan Jakubczyk, Joy Jiang, Kay Iverson, Jack Kretovics, Hui-Ru Lin, Pablo Valente Mena, Rudi Moosburger, J. J. Pan, André Richter, Rosmin Robertson, Dirk Seewald, Douglas Walsh, and Winston Way. I also am indebted to the reviewers of the previous edition who had very helpful suggestions for enhancing and clarifying the material. Particularly encouraging for doing the fourth edition were the many positive comments on the previous editions received from users and adapters at numerous academic institutions worldwide. This edition especially benefitted from the expert guidance of Michael Hackett, Vibha Mahajan, Shalini Jha, Shukti Mukherjee, Stephen M, P L Pandita and Sohini Mukherjee of McGraw-Hill. As a final personal note, I am grateful to my wife Ching-yun and my daughter Nishla for their patience and encouragement during the time I devoted to writing and revising this book.

List of Important Roman Symbols

Symbol	*Definition*
a	Fiber radius
A_{eff}	Effective area
B	Bandwidth
B_e	Receiver electrical bandwidth
c	Speed of light = 2.99793×10^8 m/s
C_j	Detector junction capacitance
D	Dispersion
D_n	Electron diffusion coefficient
D_p	Hole diffusion coefficient
DR	Dynamic range
E	Energy (E = hν)
E	Electric field
E_g	Bandgap energy
E_{LO}	Local oscillator field
f	Frequency of a wave
F	Finesse of a filter
$F(M)$	Noise figure for APD with gain M
$f(s)$	Probability density function
F_{EDFA}	EDFA noise figure
g	Gain coefficient (Fabry-Perot cavity)
G	Amplifier gain
g_B	Brillouin gain coefficient
h	Planck's constant = 6.6256×10^{-34} J-s = 4.14 eV-s
H	Magnetic field
I	Electrical current
I	Optical field intensity
I_B	Bias current
I_D	Photodetector bulk dark current
I_{DD}	Directly detected optical intensity
I_M	Multiplied photocurrent
I_p	Primary photocurrent
$i_p(t)$	Signal photocurrent
I_{th}	Threshold current
$\langle i_s^2 \rangle$	Mean-square signal current

$\langle i_{\text{shot}}^2 \rangle$	Mean-square shot-noise current
$\langle i_{DB}^2 \rangle$	Mean-square detector bulk dark noise current
$\langle i_T^2 \rangle$	Mean-square thermal noise current
J	Current density
J_{th}	Threshold current density
k	Wave propagation constant (k = 2p/l)
K	Stress intensity factor
k_B	Boltzmann's constant = 1.38054×10^{-23} J/K
L	Fiber length
L_c	Connection loss
L_{disp}	Dispersion length
L_{eff}	Effective length
L_F	Fiber coupling loss
L_i	Intrinsic loss
L_n	Electron diffusion length
L_p	Hole diffusion length
L_{period}	Soliton period
L_{split}	Splitting loss
L_{tap}	Tap loss
m	Modulation index or Modulation depth
m	Order of a grating
M	Avalanche photodiode gain
M	Number of modes
m_e	Effective electron mass
MFD	Mode field diameter
m_h	Effective hole mass
n	Index of refraction
$\bar{N}$	Average number of electron-hole pairs
NA	Numerical aperture
n_i	Intrinsic n-type carrier concentration
N_{ph}	Photon density
n_{sp}	Population inversion factor
ORL	Optical return loss
P	Optical power
$P_0(x)$	Probability distribution for a 0 pulse
$P_1(x)$	Probability distribution for a 1 pulse
$P_{\text{amp,sat}}$	Amplifier saturation power
P_{ASE}	ASE noise power
P_e	Probability of error
p_i	Intrinsic p-type carrier concentration
P_{in}	Incident optical power
P_{LO}	Local oscillator optical power

P_{peak}	Soliton peak power
PP_x	Power penalty for impairment x
P_{ref}	Reflected power
$P_{sensitivity}$	Receiver sensitivity
P_{th}	SBS threshold power
q	Electron charge = 1.60218×10^{-19} C
Q	BER parameter
Q	Q factor of a grating
R	Bit rate or Data rate
R	Reflectivity or Fresnel reflection
r	Reflection coefficient
$\mathscr{R}$	Responsivity
$\mathscr{R}_{APD}$	APD responsivity
R_{nr}	Non-radiative recombination rate
R_r	Radiative recombination rate
R_{sp}	Spontaneous emission rate
$S(\lambda)$	Dispersion slope
SNR	Signal-to-noise ratio
T	Period of a wave
T	Absolute temperature
$T_{10\text{-}90}$	10-to-90 percent rise time
T_b	Bit interval, Bit period, or Bit time
t_{GVD}	Rise time from GVD
t_{rx}	Receiver rise time
t_{sys}	System rise time
V	Mode V number

List of Important Greek Symbols

Symbol	*Definition*
α	Refractive index profile shape
α	Optical fiber attenuation
α	Laser linewidth enhancement factor
$\alpha_s(\lambda)$	Photon absorption coefficient at a wavelength λ
β	Mode propagation factor
β_3	Third-order dispersion
Γ	Optical field confinement factor
Δ	Core-cladding index difference
ΔL	Array waveguide path difference
$\Delta\nu_B$	Brillouin linewidth
$\Delta\nu_{opt}$	Optical bandwidth
η	Light coupling efficiency
η	Quantum efficiency
η_{ext}	External quantum efficiency
η_{int}	Internal quantum efficiency
λ	Wavelength
Λ	Period of a grating
λ_B	Bragg wavelength
λ_c	Cutoff wavelength
ν	Frequency
σ_{DB}	Detector dark noise current variance
σ_s	Signal current variance
σ_{shot}	Shot noise current variance
σ_T	Thermal noise current variance
σ_{wg}	Waveguide-induced pulse spreading
τ	Carrier lifetime
τ_{ph}	Photon lifetime
ϕ	Phase of a wave
Φ	Photon flux
χ	Fiber crack depth

List of Acronyms

AGC	Automatic gain control
AM	Amplitude modulation
ANSI	American National Standards Institute
APD	Avalanche photodiode
ARQ	Automatic repeat request
ASE	Amplified spontaneous emission
ASK	Amplitude shift keying
ATM	Asynchronous transfer mode
AWG	Arrayed waveguide grating
BER	Bit error rate
BH	Buried heterostructure
BLSR	Bidirectional line-switched ring
BPON	Broadband PON
BS	Base station
CAD	Computer-aided design
CATV	Cable TV
CNR	Carrier-to-noise ratio
CO	Central office
CRC	Cyclic redundancy check
CRZ	Chirped return-to-zero
CS	Control station
CSO	Composite second order
CTB	Composite triple beat
CW	Continuous wave
CWDM	Course wavelength division multiplexing
DBR	Distributed Bragg reflector
DCE	Dynamic channel equalizer
DCF	Dispersion compensating fiber
DCM	Dispersion compensating module
DFA	Doped-fiber amplifier
DFB	Distributed feedback (laser)
DGD	Differential group delay
DGE	Dynamic gain equalizer
DPSK	Differential phase-shift keying
DQPSK	Differential quadrature phase-shift keying
DR	Dynamic range
DS	Digital system

DSF	Dispersion-shifted fiber
DUT	Device under test
DWDM	Dense wavelength division multiplexing
DXC	Digital cross-connect matrix
EAM	Electro-absorption modulator
EDFA	Erbium-doped fiber amplifier
EDWA	Erbium-doped wave guide amplifier
EH	Hybrid electric-magnetic mode
EHF	Extremely high frequency (30-to-300 GHz)
EIA	Electronics Industries Alliance
EM	Electromagnetic
EMS	Element management system
EO	Electro-optical
EPON	Ethernet PON
ER	Extended reach
FBG	Fiber Bragg grating
FDM	Frequency division multiplexing
FEC	Forward error correction
FM	Frequency modulation
FOTP	Fiber Optic Test Procedure
FP	Fabry-Perot
FSK	Frequency shift keying
FSR	Free spectral range
FTTP	Fiber to the premises
FWHM	Full-width half-maximum
FWM	Four-wave mixing
GE-PON	Gigabit Ethernet PON
GFF	Gain-flattening filter
GPON	Gigabit PON
GR	Generic Requirement
GUI	Graphical user interface
GVD	Group velocity dispersion
HDLC	High-Level Data Link Control
HE	Hybrid magnetic-electric mode
HFC	Hybrid fiber/coax
IEC	International Electrotechnical Commission
IEEE	Institute for Electrical and Electronic Engineers
ILD	Injection laser diode
IM	Intermodulation
IMD	Intermodulation distortion
IM-DD	Intensity-modulated direct-detection
IP	Internet Protocol
ISI	Intersymbol interference
ISO	International Standards Organization
ITU	International Telecommunications Union

ITU-T	Telecommunication Sector of the ITU
LAN	Local area network
LEA	Large effective area
LED	Light-emitting diode
LO	Local oscillator
LP	Linearly polarized
MAN	Metro area network
MCVD	Modified chemical vapor deposition
MEMS	Micro electro-mechanical system
MFD	Mode-field diameter
MIB	Management information base
MQW	Multiple quantum well
MZI	Mach-Zehnder interferometer
NA	Numerical aperture
NF	Noise figure
NIST	National Institute of Standards and Technology
NMS	Network management system
NPL	National Physical Laboratory
NRZ	Non-return-to-zero
NZDSF	Non-zero dispersion-shifted fiber
O/E/O	Optical-to-electrical-to-optical
OADM	Optical add/drop multiplexer
OBS	Optical burst switching
OC	Optical carrier
ODU	Optical channel data unit
OLS	Optical label swapping
OLT	Optical line terminal
OMA	Optical modulation amplitude
OMS	Optical multiplex section
ONT	Optical network terminal
OOK	On-off keying
OPM	Optical performance monitor
OPS	Optical pulse suppressor
OPS	Optical packet switching
OPU	Optical channel payload unit
ORL	Optical return loss
OSA	Optical spectrum analyzer
OSI	Open system interconnect
OSNR	Optical signal-to-noise ratio
OST	Optical standards tester
OTDM	Optical time-division multiplexing
OTDR	Optical time domain reflectometer
OTN	Optical transport network
OTS	Optical transport section
OTU	Optical channel transport unit

OVPO	Outside vapor-phase oxidation
OXC	Optical crossconnect
PBG	Photonic bandgap fiber
PCE	Power conversion efficiency
PCF	Photonic crystal fiber
PCVD	Plasma-activated chemical vapor deposition
PDF	Probability density function
PDH	Plesiochronous digital hierarchy
PDL	Polarization-dependent loss
pin	(*p*-type)-intrinsic-(*n*-type)
PLL	Phase-locked loop
PM	Phase-modulation
PMD	Polarization mode dispersion
POF	Polymer (plastic) optical fiber
POH	Path overhead
PON	Passive optical network
POP	Point of presence
PPP	Point-to-point protocol
PRBS	Pseudorandom binary sequence
PSK	Phase shift keying
PTB	Physikalisch-Technische Bundesanstalt
PVC	Polyvinyl chloride
QCE	Quantum conversion efficiency
QoS	Quality of service
RAPD	Reach-through avalanche photodiode
RC	Resistance-capacitance
RF	Radio-frequency
RFA	Raman fiber amplifier
RIN	Relative intensity noise
RIP	Refractive index profile
rms	Root mean square
ROADM	Reconfigurable OADM
ROF	Radio-over-fiber
RS	Reed-Solomon
RWA	Routing and wavelength assignment
RZ	Return-to-zero
SAM	Separate-absorption-and-multiplication (APD)
SBS	Stimulated Brillouin scattering
SCM	Subcarrier modulation
SDH	Synchronous digital hierarchy
SFDR	Spur-free dynamic range
SFF	Small-form-factor
SFP	Small-form-factor (SFF) pluggable
SHF	Super-high frequency (3-to-30 GHz)
SNMP	Simple network management protocol

SNR	Signal-to-noise ratio
SOA	Semiconductor optical amplifier
SONET	Synchronous optical network
SOP	State of polarization
SPE	Synchronous payload envelope
SPM	Self-phase modulation
SRS	Stimulated Raman scattering
SSMF	Standard single mode fiber
STM	Synchronous transport module
STS	Synchronous transport signal
SWP	Spatial walk-off polarizer
TCP	Transmission control protocol
TDFA	Thulium-doped fiber amplifier
TDM	Time-division multiplexing
TE	Transverse electric
TEC	Thermoelectric cooler
TFF	Thin-film filter
TIA	Telecommunications Industry Association
TM	Transverse magnetic
UHF	Ultra-high frequency (0.3-to-3 GHz)
UPSR	Unidirectional path-switched ring
VAD	Vapor-phase axial deposition
VCSEL	Vertical-cavity surface-emitting laser
VFL	Visual fault locator
VOA	Variable optical attenuator
VSB	Vestigial-sideband
WAN	Wide area network
WDM	Wavelength-division multiplexing
WRN	Wavelength routed network
WSS	Wavelength-selective switch
XPM	Cross-phase modulation
YIG	Yttrium iron garnet

CHAPTER 1

Overview of Optical Fiber Communications

Ever since ancient times, people had a principal need to communicate with one another. This need created interests in devising communication systems for sending messages from one distant place to another. Optical communication methods were of special interest among the many systems that people tried to use. One of the earliest known optical transmission links was a *fire-signal method* used by the Greeks in the eighth century BC for sending alarms, calls for help, or announcements of certain events. Improvements of these optical transmission systems were not pursued very actively because of technology limitations at the time. For example, the speed of sending information over the communication link was limited since the transmission rate depended on how fast the senders could move their hands, the optical signal receiver was the error-prone human eye, line-of-sight transmission paths were required, and atmospheric effects such as fog and rain made the transmission path unreliable. Thus it turned out to be faster, more efficient, and more dependable to send messages by a courier over the road network.

Subsequently, no significant advances for optical communications appeared until the invention of the laser in the early 1960s and a series of technology developments related to optical fibers around 1970. These events finally allowed practical *lightwave communication systems* to start being fielded worldwide in 1978. These systems operate in the near-infrared region of the electromagnetic spectrum and use optical fibers as the transmission medium. The goal of this book is to describe the various technologies, implementation methodologies, and performance measurement techniques that make optical fiber communication systems possible. The reader can find additional information on the theory of light propagation in fibers, the design of links and networks, and the evolution of optical fibers, photonic devices, and optical fiber communication systems in a variety of books and conference proceedings.[1–23]

This chapter gives an overview of fundamental communications concepts and illustrates how optical fiber transmission systems operate. First, Sec. 1.1 gives the motivations behind developing optical fiber transmission systems. Next Sec. 1.2 defines the different spectral bands which describe various operational wavelength regions used in optical communications. Section 1.3 explains fundamental data communication concepts, encoding methods, channel capacity, and the decibel notation for expressing optical power levels. Section 1.4 gives the basic hierarchy for multiplexing digitized information streams used on optical links and Sec. 1.5 describes how wavelength division multiplexing can boost the

transmission capacity of an optical fiber significantly. Next, Sec. 1.6 introduces the functions and implementation considerations of the key elements used in optical fiber systems.

An important aspect of realizing a smoothly interacting worldwide lightwave network is to have well-established international standards for all aspects of components and networks. Section 1.7 discusses the organizations that are involved with this standardization activity and lists the main classes of standards related to optical communication components, system operations, and installation procedures. Finally, Sec. 1.8 gives an introduction to modeling and simulation tools that have been developed to aid in the design of optical fibers, passive and active devices, links, and networks.

Chapters 2 through 10 describe the purpose and performance characteristics of the major elements in an optical link. These elements include optical fibers, light sources, photodetectors, passive optical devices, optical amplifiers, and active optoelectronic devices used in multiple-wavelength networks. Then Chapters 11 through 14 show how the elements are put together to form links and networks, and explain measurement methodologies used to evaluate the performance of lightwave components and links.

1.1 Motivations for Lightwave Communications

1.1.1 The Path to Optical Networks

Prior to about 1980 most communication technologies involved some type of electrical transmission mechanism. The era of electrical communications started in 1837 with the invention of the telegraph by Samuel F. B. Morse. The telegraph system used the Morse code, which represents letters and numbers by a coded series of dots and dashes. The encoded symbols were conveyed by sending short and long pulses of electricity over a copper wire at a rate of tens of pulses per second. More advanced telegraph schemes, such as the Baudot system invented in 1874, enabled the information speeds to increase to about 120 bits per second (b/s), but required the use of skilled operators. Shortly thereafter in 1876 Alexander Graham Bell developed a fundamentally different device that could transmit the entire voice signal in an analog form and which did not require any expertise to use.[24, 25]

Both the telegraph and the analog voice signals were sent using a baseband transmission mode. *Baseband* refers to the technology in which a signal is transmitted directly over a channel. For example, this method is used on standard twisted-pair wire links running from an analog telephone to the nearest switching interface equipment. The same baseband method is used widely in optical communications, that is, the optical output from a light source is turned on and off in response to the variations in voltage levels of an information-bearing electrical signal.

In the ensuing years an increasingly larger portion of the electromagnetic spectrum was utilized to develop and deploy progressively more sophisticated and reliable electrical communication systems with larger capacities for conveying information from one place to another. The basic motivations behind each new system application were to improve the transmission fidelity so that fewer distortions or errors occur in the received message, to increase the data rate or capacity of a communication link so that more information can be sent, or to increase the transmission distance between in-line repeater or amplification stations so that messages can be sent farther without the need to restore the signal amplitude or fidelity periodically along its path. These activities led to the birth of a wide variety of communication systems that are based on using high-capacity long-distance terrestrial and undersea copper-based wire lines and wireless radio-frequency (RF), microwave, and satellite links.

In these developments the basic trend for advancing the link capacity was to use increasingly higher channel frequencies. The reason for this trend is that a time-varying baseband information-bearing signal may be transferred over a communication channel by superimposing it onto a sinusoidal electromagnetic wave, which is known as the *carrier wave* or simply *carrier*. At the destination the baseband information signal is removed from the carrier wave and processed as desired. Since the amount of information that can be transmitted is directly related to the frequency range over which the carrier operates, increasing the carrier frequency theoretically increases the available transmission bandwidth and consequently, provides a larger information capacity.[25–28] For example, Fig. 1.1 shows

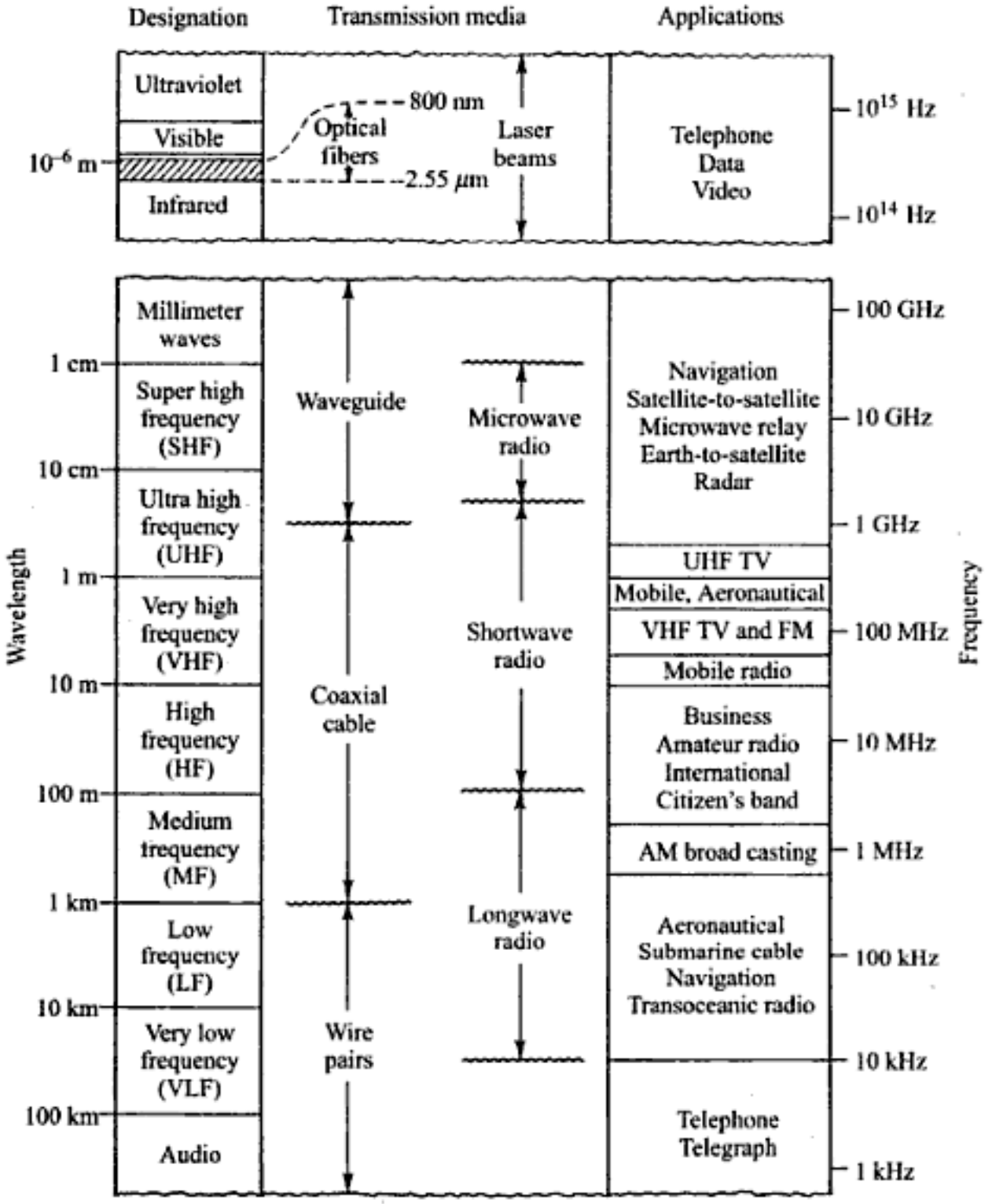

Fig. 1.1 *The regions of the electromagnetic spectrum used for radio and optical fiber communications. (Used with permission from A. B. Carlson, Communication Systems, © 1986, McGraw-Hill Book Company.)*

the electromagnetic spectral bands used for radio transmission. As the diverse radio technologies move from high frequency (HF) to very high frequency (VHF) to ultra high frequency (UHF) bands with nominal carrier frequencies of 10^7, 10^8, and 10^9 Hz, respectively, increasingly higher information transmission speeds can be employed to provide a higher link capacity. Thus the trend in electrical communication system developments was to use progressively higher frequencies, which offer corresponding increases in bandwidth or information capacity.

As Fig. 1.1 also shows, optical frequencies are several orders of magnitude higher than those used by electrical communication systems. Thus the invention of the laser in the early 1960s aroused a curiosity about the possibility of using the optical region of the electromagnetic spectrum for transmitting information. Of particular interest is the near-infrared spectral band ranging from about 770 to 1675 nm, since this is a low-loss region in silica glass fibers.[18-20] The technical breakthrough for optical fiber communications started in 1970 when researchers at Corning demonstrated the feasibility of producing a glass fiber having an optical power loss that was low enough for a practical transmission link.[20, 29]

As research progressed, it became clear that many complex problems made it extremely difficult to extend the carrier concept for achieving a super broadband optical communication link. Nevertheless, the unique properties of optical fibers gave them a number of performance advantages compared to copper wires, so that optical links operating in a simple on-off keyed baseband mode were attractive applications.

The first installed optical fiber links which appeared in the late 1970s were used for transmitting telephony signals at about 6 Mb/s over distances of around 10 km. As research and development progressed, the sophistication and capabilities of these systems increased rapidly during the 1980s to create links carrying aggregated data rates beyond terabits per second over distances of hundreds of kilometers without the need to restore signal fidelity along the path length.

Starting in the 1990s there was a burgeoning demand on communication-network assets for bandwidth-hungry services such as database queries, home shopping, high-definition interactive video, remote education, telemedicine and e-health, high-resolution editing of home videos, blogging, and large-scale high-capacity e-science and Grid computing.[30-33] This demand was fueled by the rapid proliferation of personal computers (PCs) coupled with a phenomenal increase in their storage capacity and processing capabilities, the widespread availability and continuous expansion of the Internet, and an extensive choice of remotely accessible programs and information databases. To handle the ever-increasing demand for high-bandwidth services from ranging from home-based PC users to large businesses and research organizations, telecommunication companies worldwide greatly enhanced the capacity of fiber lines by adding more independent signal-carrying wavelengths on individual fibers and increasing the transmission speed of information being carried by each wavelength.

1.1.2 Advantages of Optical Fibers

The advantages of optical fibers compared to copper wires include the following:

Long Distance Transmission Optical fibers have lower transmission losses compared to copper wires. Consequently data can be sent over longer distances, thereby reducing the number of intermediate repeaters needed to boost and restore signals in long spans. This reduction in equipment and components decreases system cost and complexity.

Large Information Capacity Optical fibers have wider bandwidths than copper wires, so that more information can be sent over a single physical line. This property decreases the number of physical lines needed for sending a given amount of information.

Small Size and Low Weight The low weight and the small dimensions of fibers offer a distinct advantage over heavy, bulky wire cables in crowded underground city ducts or in ceiling-mounted cable trays. This feature also is of importance in aircraft, satellites, and ships where small, lightweight cables are advantageous, and in tactical military applications where large amounts of cable must be unreeled and retrieved rapidly.[34]

Immunity to Electrical Interference An especially important feature of an optical fiber relates to the fact that it is a dielectric material, which means it does not conduct electricity. This makes optical fibers immune to the electromagnetic interference effects seen in copper wires, such as inductive pickup from other adjacent signal-carrying wires or coupling of electrical noise into the line from any type of nearby equipment.

Enhanced Safety Optical fibers offer a high degree of operational safety, since they do not have the problems of ground loops, sparks, and potentially high voltages inherent in copper lines. However, precautions with respect to laser light emissions need to be observed to prevent possible eye damage.

Increased Signal Security An optical fiber offers a high degree of data security, since the optical signal is well-confined within the fiber and an opaque coating around the fiber absorbs any signal emissions. This feature is in contrast to copper wires where electrical signals potentially could be tapped off easily. Thus fibers are attractive in applications where information security is important, such as financial, legal, government, and military systems.

1.2 Optical Spectral Bands

All telecommunication systems use some form of electromagnetic energy to transmit signals. The *spectrum* of electromagnetic (EM) radiation is shown in Fig. 1.2. *Electromagnetic energy* is a combination of

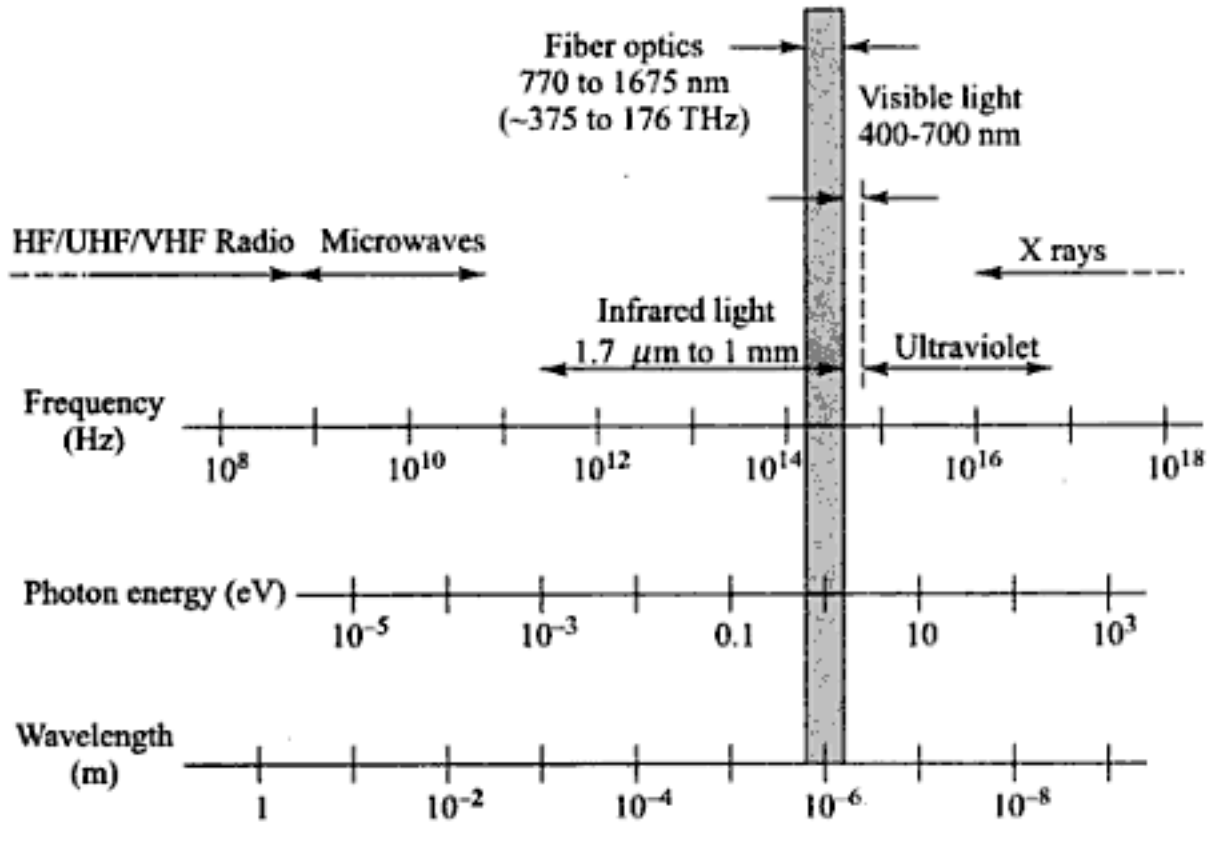

Fig. 1.2 *The spectrum of electromagnetic radiation*

electrical and magnetic fields and includes power, radio waves, microwaves, infrared light, visible light, ultraviolet light, x rays, and gamma rays. Each discipline takes up a portion (or band) of the electromagnetic spectrum. The fundamental nature of all radiation within this spectrum is that it can be viewed as electromagnetic waves that travel at the speed of light, which is about $c = 3 \times 10^8$ m/s in a vacuum. Note that the speed of light s in a material is smaller by the refractive-index factor n than the speed c in a vacuum, as Chapter 2 describes. For example, $n \approx 1.45$ for silica glass, so that the speed of light in this material is about $s = 2 \times 10^8$ m/s.

The physical properties of the waves in different parts of the spectrum can be measured in several interrelated ways. These are the length of one period of the wave, the energy contained in the wave, or the oscillating frequency of the wave. Whereas electrical signal transmission tends to use frequency to designate the signal operating bands, optical communication generally uses *wavelength* to designate the spectral operating region and *photon energy* or *optical power* when discussing topics such as signal strength or electro-optical component performance.

As can be seen from Fig. 1.2, there are three different ways to measure the physical properties of a wave in various regions in the EM spectrum. These measurement units are related by some simple equations. First of all, in a vacuum the speed of light c is equal to the wavelength λ times the frequency ν, so that

$$c = \lambda\nu \tag{1.1}$$

where the frequency ν is measured in cycles per second or *hertz* (Hz).

The relationship between the energy of a photon and its frequency (or wavelength) is determined by the equation known as *Planck's Law*

$$E = h\nu \tag{1.2}$$

where the parameter $h = 6.63 \times 10^{-34}$ J-s = 4.14 eV-s is *Planck's constant*. The unit J means *joules* and the unit eV stands for *electron volts*. In terms of wavelength (measured in units of μm), the energy in electron volts is given by

$$E(eV) = \frac{1.2406}{\lambda(\mu m)} \tag{1.3}$$

Figure 1.2 shows, the optical spectrum ranges from about 5 nm in the ultraviolet region to 1 mm for far-infrared radiation. In between these limits is the 400-to-700-nm *visible band*. Optical fiber communications use the *near-infrared spectral band* ranging from nominally 770 to 1675 nm.

The International Telecommunications Union (ITU) has designated six spectral bands for use in optical fiber communications within the 1260-to-1675-nm region.[35] These long-wavelength band designations arose from the attenuation characteristics of optical fibers and the performance behaviour of an erbium-doped fiber amplifier (EDFA), which Chapters 3 and 10 describe, respectively. Figure 1.3 shows and Table 1.1 defines the regions which are known by the letters O, E, S, C, L, and U.

The 770-to-910 nm band is used for shorter-wavelength multimode fiber systems. Thus this region is designated as the *short-wavelength* or *multimode fiber band*. Later chapters describe the operational performance characteristics and applications of optical fibers, electro-optic components, and other passive optical devices for use in the short- and long-wavelength bands.

Table 1.1 *Spectral band designations used in optical fiber communications*

Name	*Designation*	*Spectrum (nm)*	*Origin of Name*
Original band	O-band	1260 to 1360	Original (first) region used for single-mode fiber links
Extended band	E-band	1360 to 1460	Link use can extend into this region for fibers with low water content
Short band	S-band	1460 to 1530	Wavelengths are shorter than the C-band but higher than the E-band
Conventional band	C-band	1530 to 1565	Wavelength region used by a conventional EDFA
Long band	L-band	1565 to 1625	Gain decreases steadily to 1 at 1625 nm in this longer wavelength band
Ultra-long band	U-band	1625 to 1675	Region beyond the response capability of an EDFA

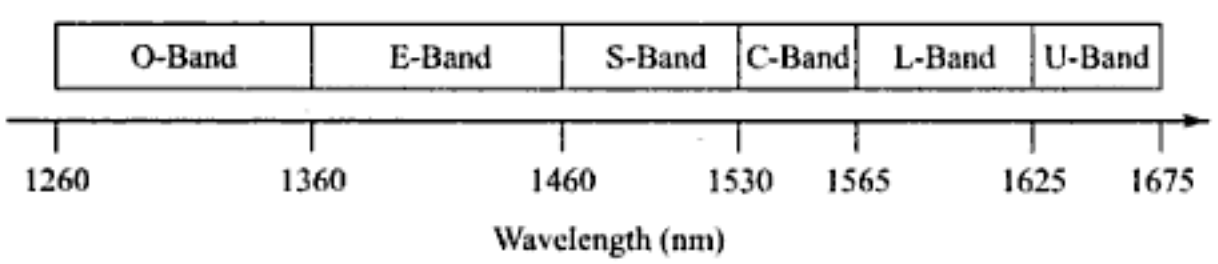

Fig. 1.3 *Designations of spectral bands used for optical fiber communications*

1.3 Fundamental Data Communication Concepts

The exchange of information between any two devices across a communication channel involves using some type of electrical or optical signal which carries this information. The channel could be a wire, radio, microwave, satellite, atmospheric infrared, or optical fiber link. Each type of channel medium has unique transmission performance characteristics associated with it, which ideally should match the properties of the signal. However, regardless of its type the medium degrades the fidelity of the transmitted signal because of an imperfect reproduction of the signal format and because of the unavoidable presence of electrical and optical noise and interference. These impairments can lead to misinterpretations of the signal by the electronics at the receiving end.

1.3.1 Elementary Communication Link

Figure 1.4 shows a block diagram of an elementary communication link. The user or device where the message originates is called a *source* and the final receiving user or device is called the *destination*. The output of the information source serves as the message input to a transmitter. The function of the *transmitter* is to couple the message onto a *transmission channel* in the form of a time-varying signal that matches the transfer properties of the channel. This process is known as *encoding*.

As the signal travels through the channel, various imperfect properties of the channel medium and of various link components induce impairments into the signal. These include electrical or optical noise effects, signal distortions, and signal attenuation. In the presence of these impairments, the function of the *receiver* is to extract the weakened and distorted signal from the channel, amplify it, and restore it as close as possible to its original encoded form before *decoding* it and passing it on to the message destination.

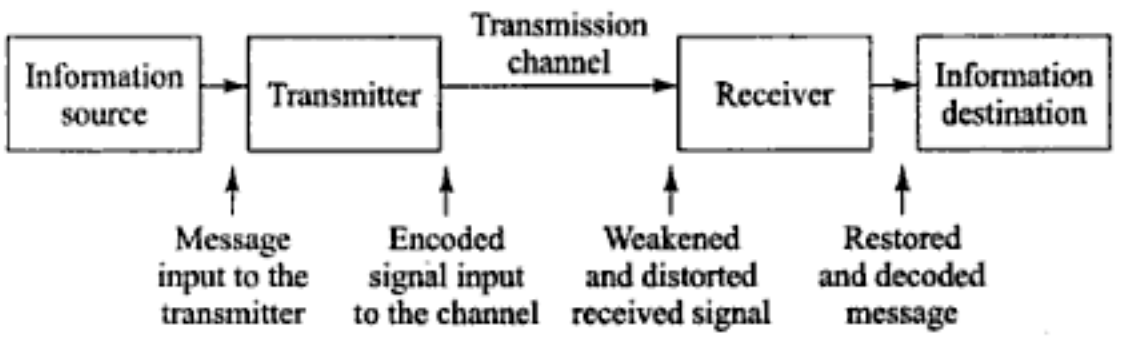

Fig. 1.4 *The main components in an elementary communication link*

1.3.2 Analog Signals

The format of a signal is an important factor in efficiently and reliably sending the signal across a network. The signals emitted by information sources can be classified into analog and digital formats. An *analog signal* conveys information through a *continuous and smooth variation in time* of a physical quantity such as optical, electrical, or acoustical intensities and frequencies. For example, voice, music, electronic hum, and video information streams are well-known analog signals.

A fundamental *analog signal* is the periodic *sine wave*, shown in Fig. 1.5. Its three main characteristics are its amplitude, period or frequency, and phase. The *amplitude* is the size or magnitude of the waveform.

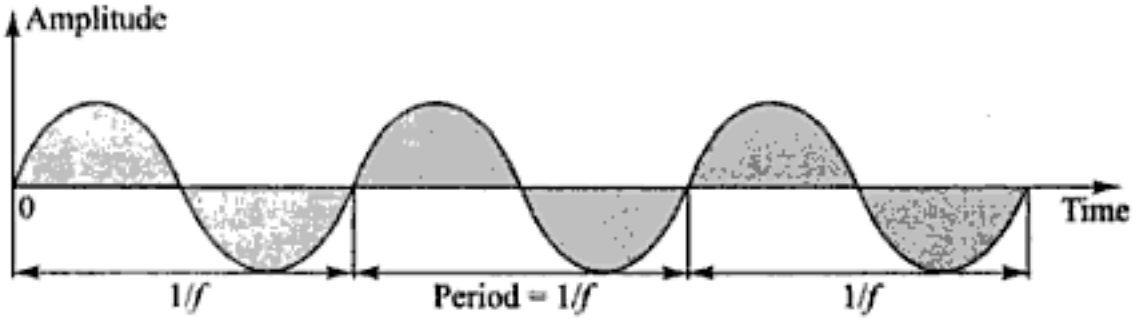

Fig. 1.5 *Frequency, period, and amplitude characteristics of a basic sine wave*

Amplitude is designated by the symbol A and is measured in volts, amperes, or watts, depending on the signal type. The *frequency* (designated by f) is the number of cycles per second that the wave undergoes (i.e., the number of times it oscillates per second), which is expressed in units of hertz (Hz). A hertz refers to a complete cycle of the wave. The *period* of a wave (represented by the symbol T) is the inverse of the frequency, that is period = $T = 1/f$. The term *phase* (designated by the symbol ϕ) describes the position of the waveform relative to time zero. Phase is measured in degrees or radians, where 180 degrees = π radians.

If the crests and troughs (high and low points) of two waves with identical periods are aligned, they are said to be *in phase*. For example, wave 1 and wave 2 shown in Fig. 1.6 are in phase. Let wave 1 have an

---

Example 1.1 A sine wave has a frequency $f = 100$ kHz. Its period is $T = /10^5$ s = 0.01 ms.

A sine wave has period $T = 1$ ns. Its frequency is $f = 1/(10^{-9}\text{s}) = 1$ GHz.

A sine wave is offset by 1/4 of a cycle with respect to time zero. since one cycle if 360 degrees, the phase shit is $\phi = 0.25 \times 360$ degrees = 90 degrees = $\pi/2$ radian

---

amplitude A_1 and let wave 2 have an amplitude A_2. If these two waves are added together, the amplitude A of the resulting wave will be the sum $A = A_1 + A_2$. This effect is known as *constructive interference.*

Figure 1.7 illustrates four *phase shifts* of a wave relative to time zero. When two waves differ slightly in their relative positions, they are said to be *out of phase*. As an illustration, the wave shown in Fig. 1.7(c) is 180° (π radians) out of phase with the wave shown in Fig. 1.7(a). If the two waves in Fig. 1.7(a) and 1.7(c) have identical periods, the resulting wave amplitude will be the sum $A = A_1 + A_2$. If the two waves also have the same amplitudes, then they undergo *destructive interference* so that $A = 0$, that is they will cancel each other out. These interference concepts are important when considering the operation of devices such as laser diodes, thin-film filters, and optical couplers.

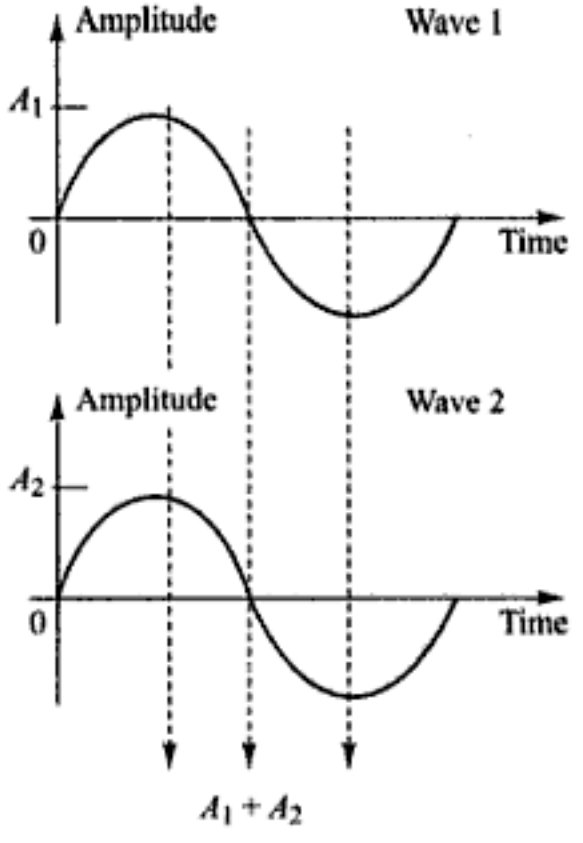

Fig. 1.6 *Two in-phase waves with the same period will add constructively*

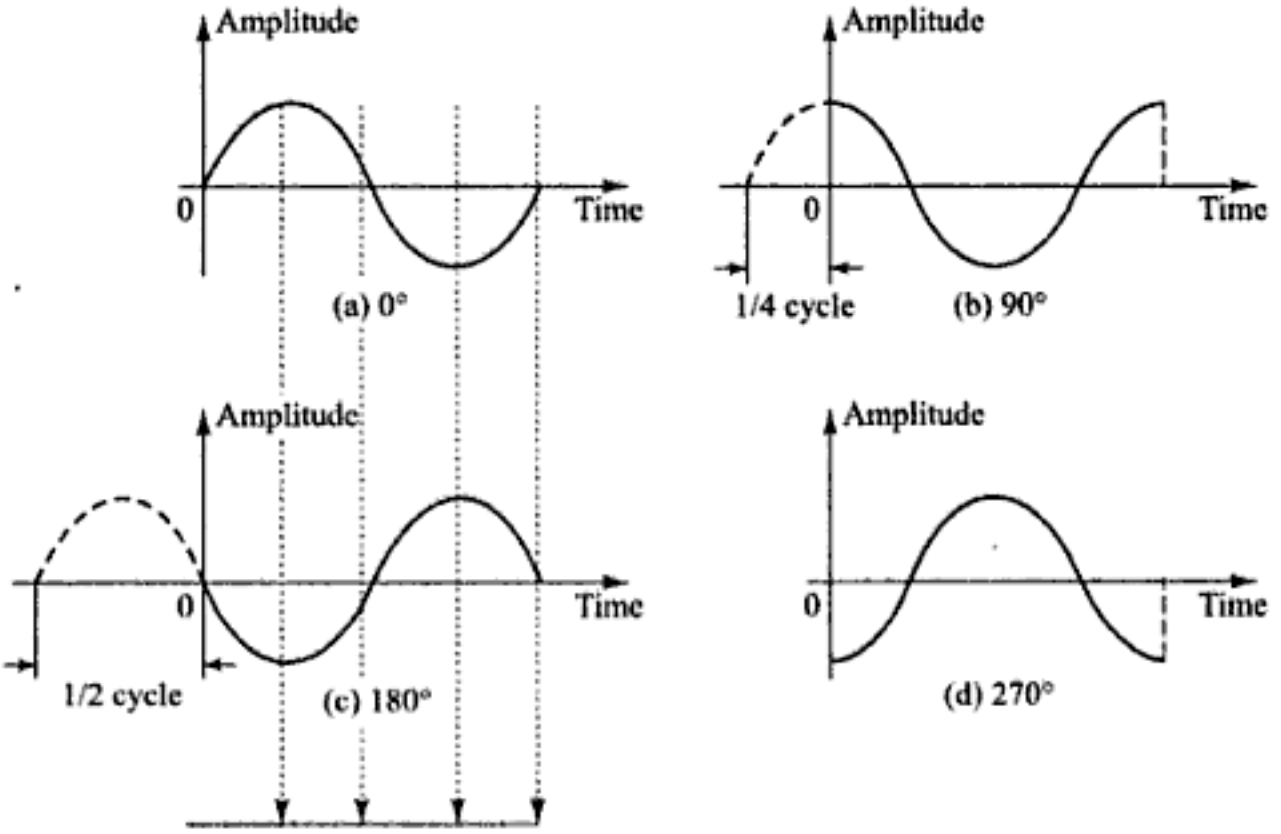

Fig. 1.7 *Illustration of four phase shifts of a wave relative to time zero. Two identical waves that are 180° out of phase will interfere destructively.*

Example 1.2 If the spectrum of a signal ranges from its lowest frequency f_{low} = 10 kHz to its highest frequency f_{high} = 100 kHz, then the bandwidth $B = f_{high} - f_{low}$ = 90 kHz.

Two further common characteristics in communications are the frequency spectrum (or simply spectrum) and the bandwidth of a signal. The *spectrum* of a signal is the range of frequencies that it contains. That is, the spectrum of a signal is the combination of all the individual sine waves of different frequencies which make up that signal. The *bandwidth* (designated by B) refers to the width of this spectrum. The bandwidth commonly is specified in units such as kilohertz (kHz), megahertz (MHz), or gigahertz (GHz).

1.3.3 Digital Signals

A *digital signal* is an ordered sequence of *discrete symbols* selected from a finite set of elements, for example, the letters of an alphabet, numbers, and other symbols such as @, #, or %. A common digital signal configuration is the *binary waveform*, which consists of two pulse types of known shape as shown in Fig. 1.8. The information contained in a digital signal is given by the particular sequence of the presence (a *binary one*, or simply either *one* or 1) and absence (a *binary zero*, or simply either *zero* or 0) of these pulses or *bits*. These bits often are referred to as a *logic one* (or *logic* 1) and a *logic zero* (or *logic* 0), respectively.

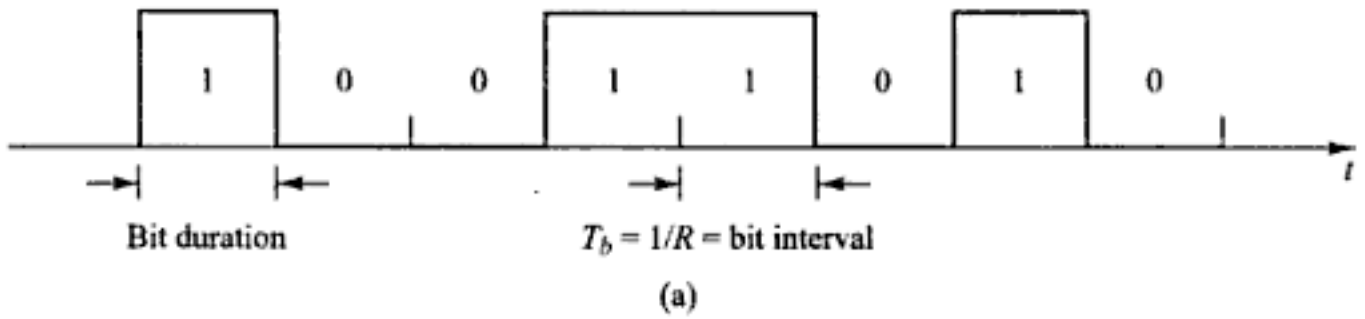

Fig. 1.8 *Examples of two binary waveforms showing their amplitude, period, and bit duration. (a) The bit fills the entire bit period for the 1 bit only; (b) a 1 bit fills the first half and a 0 bit fills the second half of a bit time slot*

The time slot T_b in which a bit occurs is called either the *bit interval*, *bit period*, or *bit time*. The bit intervals are spaced regularly and occur every $1/R$ seconds, or at a rate of R *bits per second* (b/s), where R is the *bit rate* or the *data rate*. The data rate commonly is specified in units such as kilobits per second

(kb/s), megabits per second (Mb/s), or gigabits per second (Gb/s). As an example, a data rate of 2×10^9 b/s = 2 Gb/s. A bit can fill the entire bit interval or part of it, as shown in Fig. 1.8(a) and Fig. 1.8(b), respectively. A block of eight bits often is used to represent an encoded symbol or word and is called an *octet* or a *byte*.

1.3.4 Digitization of Analog Signals

To send a signal in an analog format, the transmission channel typically cannot achieve perfect reproduction of the signal at the destination, so there always will be some degree of distortion. Furthermore, different types of analog signals may require different channel responses. This puts a strain on the design of a multipurpose analog link. In addition, noises that get added to the analog signal as it passes through multiple repeaters cannot be eliminated, which further degrades the signal.

In contrast, digital signals can undergo a great amount of distortion and still allow the information to be extracted with a high degree of fidelity. To avoid the shortcomings of analog signals and to create networks that can multiplex and switch any type of information, most information is sent in a digital format. To achieve this network flexibility, most analog signals need to be converted to a digital format. However, as Chapter 9 describes, there are a number of situations in which it is advantageous to send high-speed analog signals in their native form over relatively short distances. One example is the transmission of microwave signals from a satellite dish to a processing station located less than a kilometer away.

An analog signal can be transformed into a digital signal through a process of periodic sampling and the assignment of quantized values to represent the intensity of the signal at regular intervals of time. To convert an analog signal to a digital form, one starts by taking instantaneous measures of the height of the signal wave at regular intervals, which is called *sampling* the signal. The simplest, but not necessarily the best, way to convert these analog samples to a digital format is to divide the amplitude excursion of the analog signal into N equally spaced levels and assign a discrete binary word to each level. Each analog sample is then assigned one of these level values. This process is known as *quantization*. Since the signal varies continuously in time, this process generates a sequence of real numbers.

Example 1.3 Figure 1.9 shows an example of digitization. Here the allowed voltage-amplitude excursion is divided into eight equally spaced levels ranging from zero to V volts. In this figure, samples are taken every microsecond and the nearest discrete quantization level is chosen as the one to be transmitted, according to the 3-bit binary code listed next to the quantized levels shown in Fig. 1.9. At the receiver this digital signal is then demodulated. That is, the quantized levels are reassembled into a continuously varying analog waveform.

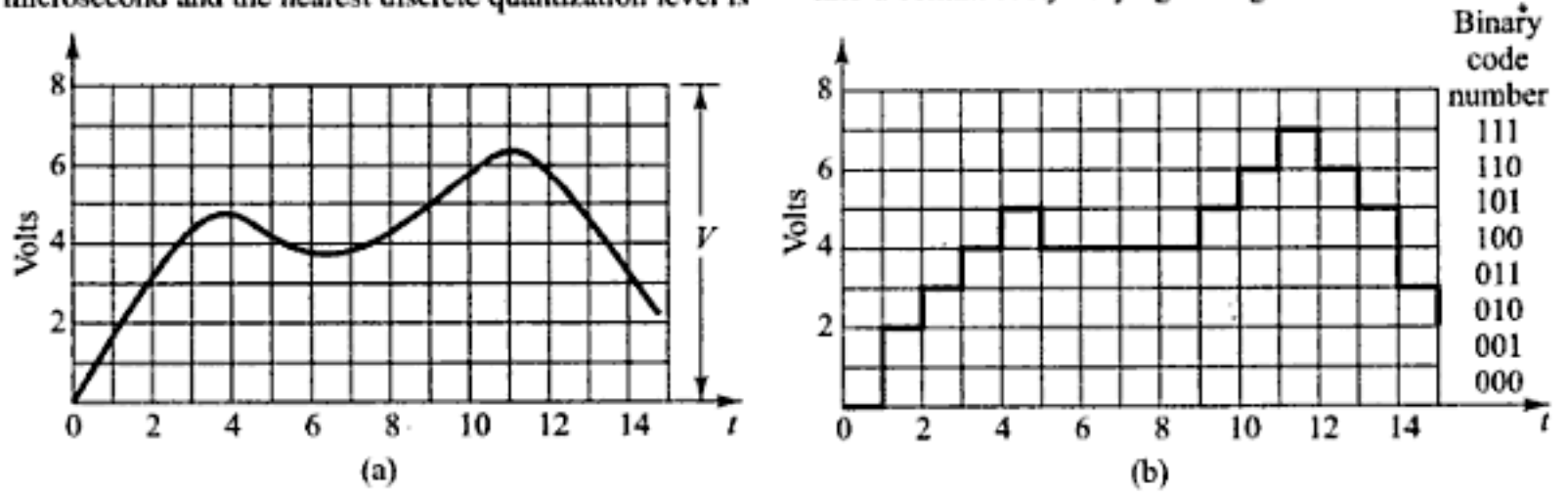

Fig. 1.9 *Concept for digitization of analog signals. (a) Original signal varying between 0 and V volts; (b) Sampled and quantized digital version*

Intuitively, one can see from Fig. 1.9 that if the digitization samples are taken frequently enough relative to the rate at which the signal varies, then to a good approximation the signal can be recovered from the samples by drawing a straight line between the sample points. The resemblance of the reproduced signal to the original signal depends on the fineness of the quantizing process and on the effect of noise and distortion added into the transmission system. According to the *Nyquist theorem*, if the sampling rate is at least two times the highest frequency, then the receiving device can faithfully reconstruct the analog signal.[25-28] Thus, if a signal is limited to a bandwidth of B hertz, then the signal can be reproduced without distortion if it is sampled at a rate of $2B$ times per second. These data samples are represented by a binary code. As noted in Fig. 1.9, eight quantized levels having upper bounds V_1, V_2, ..., V can be described by 3 binary digits ($2^3 = 8$). More digits can be used to give finer sampling levels. That is, if n binary digits represent each sample, then one can have 2^n quantization levels.

1.3.5 Channel Capacity

In the analysis of any communication network, an important factor is *channel capacity*. This is the maximum rate at which data can be sent across a channel from the message source to the user destination. A fundamental and important theorem for this is the *Shannon capacity formula*. This theorem states that if a channel has a bandwidth B (measured in hertz) then the maximum information-transmission *capacity* C of that channel is given in *bits per second* by the relationship[25-28, 36]

$$C = B \log_2 (1 + S/N) \tag{1.4}$$

Here $\log_2$ represents the base-2 logarithm, and S and N are the average signal power and noise power, respectively. Typically these powers are measured at the receiver, since it is at this point that a signal is extracted from the channel and processed. Note: For simplicity of calculation, the following relationship may be useful to find $\log_2 x$:

$$\log_2 x = (\log_{10} x)/(\log_{10} 2) = (\log_{10} x)/0.3 \tag{1.5}$$

The parameter S/N is the *signal-to-noise ratio* (*SNR*), which is the ratio of the power in a signal to the power contained in the noise at a particular measurement point. This ratio is often expressed in decibels:

$$SNR_{\text{dB}} = 10 \log \frac{\text{signal power}}{\text{noise power}} = 10 \log \frac{S}{N} \tag{1.6}$$

The Shannon formula indicates the theoretical maximum capacity that can be achieved. In practice this capacity cannot be reached, since the formula only takes into account thermal noise and does not consider factors such as impulse noise, attenuation distortion, or delay distortion. Furthermore, intuitively it might seem that the capacity can be increased merely by raising the signal strength. However, raising the signal level also increases nonlinear effects in the system, which leads to higher noise powers. Also note that increasing the bandwidth B decreases the ratio S/N, since the wider the bandwidth the more noise is introduced into the system.

Example 1.4 Suppose we have a noisy channel with a 1-MHz bandwidth in which the signal-to-noise ratio is 1. From Eq. (1.4), the maximum capacity for this channel is

$$C = B \log_2 (1 + S/N) = 10^6 \log_2 (1 + 1) = 10^6 \log_2 (2)$$
$$= 10^6 (1.0) = 1 \text{ Mb/s}$$

Example 1.5 Let us find the capacity of a channel that operates between 3 MHz and 4 MHz and in which the signal-to-noise ratio is 20 dB. Then the bandwidth is

$$B = (4 \text{ MHz}) - (3 \text{ MHz}) = 1 \text{ MHz}.$$

and, from Eq. (1.6),

$$S/N = 10^{20/10} = 100$$

Then

$$C = 10^6 \log_2 (1 + 100) = [10^6 \log_{10} (101)]/0.3$$
$$= 10^6 (2.0)/0.3 = 6.7 \text{ Mb/s}$$

1.3.6 Decibel Units

Reduction or attenuation of signal strength arises from various loss mechanisms in a transmission medium. For example, electric power is lost through heat generation as an electric signal flows along a wire, and optical power is attenuated through scattering and absorption processes in a glass fiber or in an atmospheric channel. To compensate for these energy losses, amplifiers are used periodically along a channel path to boost the signal level, as shown in Fig. 1.10.

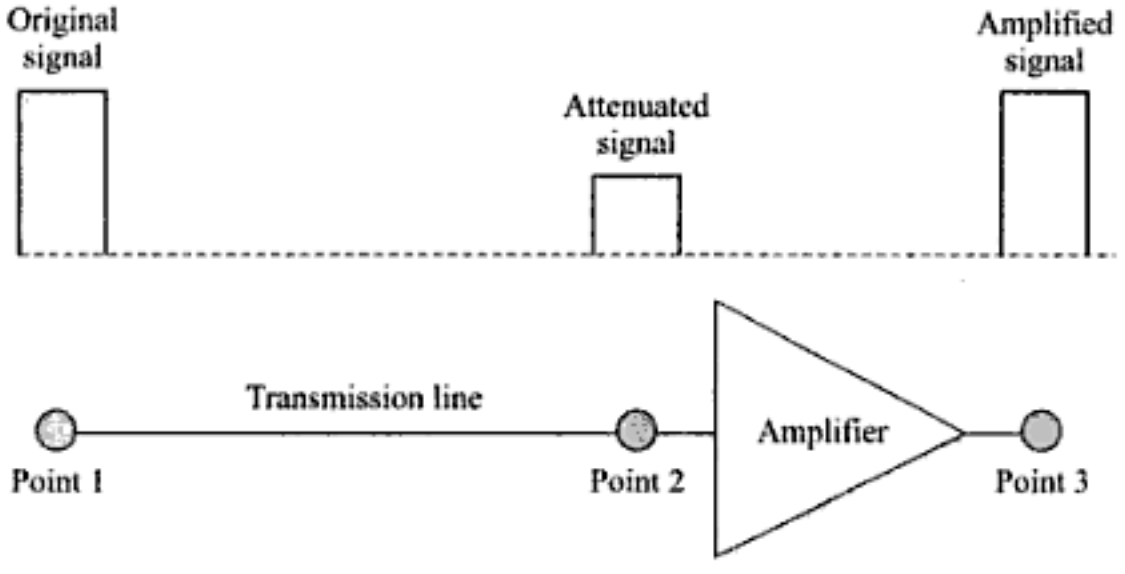

Fig. 1.10 *Periodically placed amplifiers compensate for energy losses along a link*

A standard and convenient method for measuring attenuation through a link or a device is to reference the output signal level to the input level. For guided media such as an optical fiber, the signal strength normally decays exponentially. Thus, for convenience one can designate it in terms of a logarithmic power ratio measured in *decibels* (dB). The dB unit is defined by

$$\text{Power ratio in dB} = 10 \log \frac{P_2}{P_1} \tag{1.7}$$

where P_1 and P_2 are the electrical or optical power levels of a signal at points 1 and 2 in Fig. 1.11, and *log* is the base-10 logarithm. The logarithmic nature of the decibel allows a large ratio to be expressed in a fairly simple manner. Power levels differing by many orders of magnitude can be compared easily when they are in decibel form. Another attractive feature of the decibel is that to measure the changes in the strength of a signal, one merely adds or subtracts the decibel numbers between two different points.

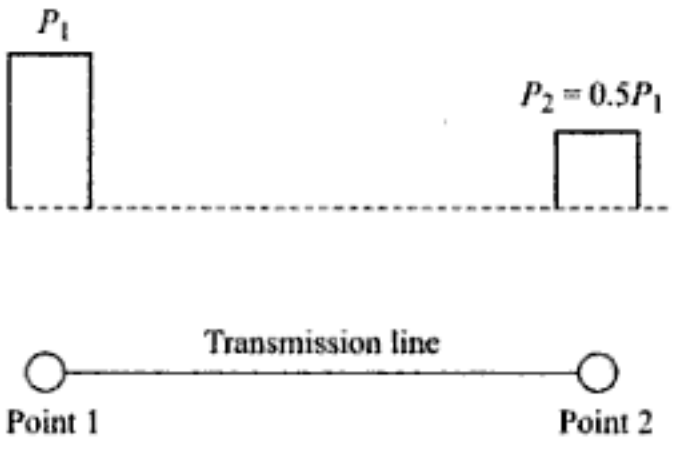

Fig. 1.11 *Example of pulse attenuation in a link. P_1 and P_2 are the power levels of a signal at points 1 and 2*

Example 1.6 Assume that after traveling a certain distance in some transmission medium, the power of a signal is reduced to half, that is, $P_2 = 0.5\,P_1$ in Fig. 1.11. At this point, using Eq. (1.7) the attenuation or loss of power is

$$10 \log \frac{P_2}{P_1} = 10 \log \frac{0.5\,P_1}{P_1} = 10 \log 0.5 = 10(-0.3) = -3 \text{ dB}$$

Thus, −3 dB (or a 3-dB attenuation or loss) means that the signal has lost half its power. If an amplifier is inserted into the link at this point to boost the signal back to its original level, then that amplifier has a 3-dB gain. If the amplifier has a 6-dB gain then it boosts the signal power level to twice the original value.

Table 1.2 shows some sample values of power loss given in decibels and the percent of power remaining after this loss. These types of numbers are important when considering factors such as the effects of tapping off a small part of an optical signal for monitoring purposes, for examining the power loss through some optical element, or when calculating the signal attenuation in a specific length of optical fiber.

Table 1.2 *Representative values of decibel power loss and the remaining percentages*

Power loss (in dB)	*Percent of power left*
0.1	98
0.5	89
1	79
2	63
3	50
6	25
10	10
20	1

Example 1.7 Consider the transmission path from point 1 to point 4 shown in Fig. 1.12. Here the signal is attenuated by 9 dB between points 1 and 2. After getting a 14-dB boost from an amplifier at point 3, it is again attenuated by 3 dB between points 3 and 4. Relative to point 1, the signal level in dB at point 4 is

$$\begin{aligned}\text{dB level at point 4} &= (\text{loss in line 1}) + (\text{amplifier gain}) \\ &\quad + (\text{loss in line 2}) \\ &= (-9\text{ dB}) + (14\text{ dB}) + (-3\text{ dB}) = +2\text{ dB}\end{aligned}$$

Thus the signal has a 2-dB (a factor of $10^{0.2} = 1.58$) gain in power in going from point 1 to point 4.

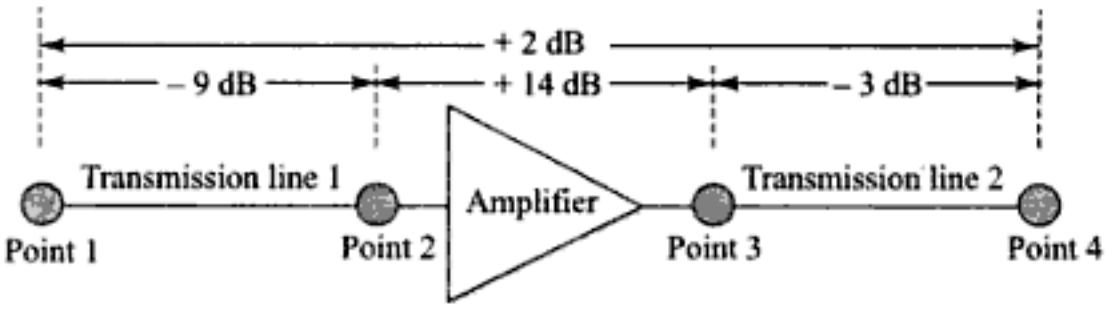

Fig. 1.12 *Example of signal attenuation and amplification in a transmission path*

Since the decibel is used to refer to ratios or relative units, it gives no indication of the absolute power level. However, a derived unit can be used for this. Such a unit that is particularly common in optical fiber communications is the dBm (simply pronounced *dee bee em*). This unit expresses the power level P as a logarithmic ratio of P referred to 1 mW. In this case, the power in dBm is an absolute value defined by

$$\text{Power level (in dBm)} = 10 \log \frac{P\,(\text{in mW})}{1\ \text{mW}} \qquad (1.8)$$

An important rule-of-thumb relationship to remember for optical fiber communications is 0 dBm = 1 mW. Therefore, positive values of dBm are greater than 1 mW and negative values are less than 1 mW.

Table 1.3 lists some examples of optical power levels and their dBm equivalents.

Table 1.3 *Examples of optical power levels and their dBm equivalents*

Power	*dBm equivalent*
200 mW	23
100 mW	20
10 mW	10
1 mW	0
100 μW	–10
10 μW	–20
1 μW	–30
100 nW	–40
10 nW	–50
1 nW	–60
100 pW	–70
10 pW	–80
1 pW	–90

1.4 Network Information Rates

To handle the continuously rising demand for high-bandwidth services from users ranging from individuals to large businesses and research organizations, telecommunication companies worldwide are implementing increasingly sophisticated digital multiplexing techniques that allow a larger number of independent information streams to share the same physical transmission channel. This section describes some common digital signal multiplexing techniques.

1.4.1 Telecom Signal Multiplexing

Table 1.4 gives examples of information rates for some typical telecom services. To send these services from one user to another, network providers combine the signals from many different users and send the aggregate signal over a single transmission line. This scheme is known as *time-division-multiplexing* (TDM) wherein N independent information streams, each running at a data rate of R b/s, are interleaved electrically into a single information stream operating at a higher rate of $N \times R$ b/s. To get a detailed perspective of this methodology, let us look at the multiplexing schemes used in telecommunications.

Early applications of fiber optic transmission links were mainly for large capacity telephone lines. These digital links consisted of time-division-multiplexed 64-kb/s voice channels. The multiplexing was developed in the 1960s and is based on what is known as the *plesiochronous digital hierarchy* (PDH). Figure 1.13 shows the digital transmission hierarchy used in the North American telephone network.

The fundamental building block is a 1.544-Mb/s transmission rate known as a *DS*1 rate, where *DS* stands for *digital system*. It is formed by time-division-multiplexing twenty-four voice channels, each digitized at a 64-kb/s rate (which is referred to as *DS*0). *Framing bits*, which indicate where an information unit starts and ends, are added along with these voice channels to yield the 1.544-Mb/s bit stream. Framing and other control bits that may get added to an information unit in a digital stream are called *overhead* bits. At any multiplexing level a signal at the designated input rate is combined with other input signals at the same rate.

Table 1.4 *Examples of information rates for some typical services*

Type of service	*Data rate*
Video on demand/interactive TV	1.5 to 6 Mb/s
Video games	1 to 2 Mb/s
Remote education	1.5 to 3 Mb/s
Electronic shopping	1.5 to 6 Mb/s
Data transfer or telecommuting	1 to 3 Mb/s
Video conferencing	0.384 to 2 Mb/s
Voice (single telephone channel)	33.6 to 56 kb/s

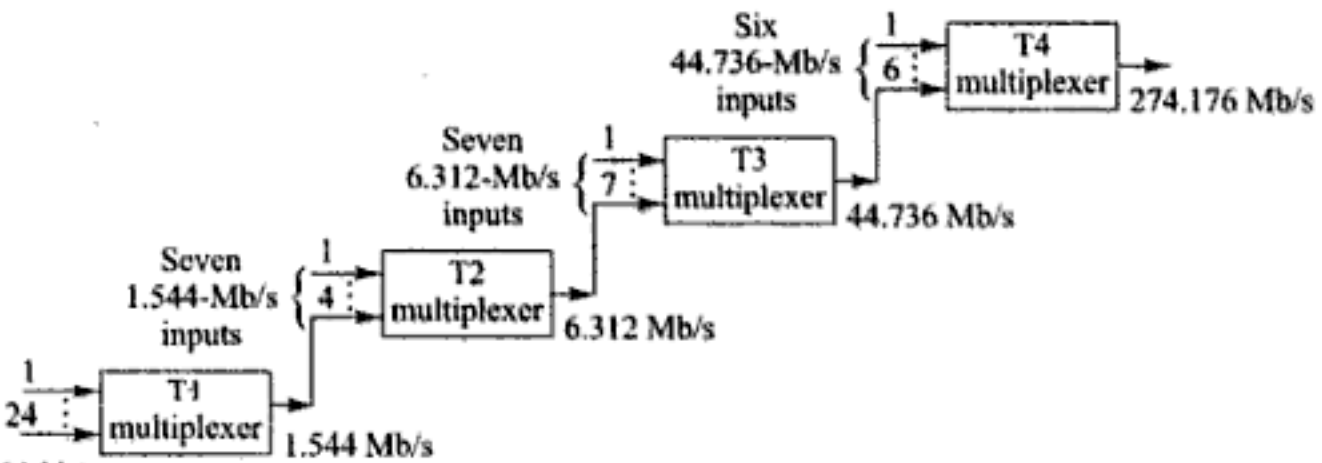

Fig. 1.13 *Digital transmission hierarchy used in the North American telephone network*

DSx* versus *Tx In describing telephone network data rates, one also sees terms such as *T*1, *T*3, and so on. Often the terms *Tx* and *DSx* (e.g., *T*1 and *DS*1 or *T*3 and *DS*3) are used interchangeably. However there is a subtle difference in their meaning. Designations such as *DS*1, *DS*2, and *DS*3 refer to a *service type*, for example, a user who wants to send information at a 1.544 Mb/s rate would subscribe to a *DS*1 service. Abbreviations such as *T*1, *T*2, and *T*3 refer to the data rate which the transmission-line technology uses to deliver that service over a physical link. For example, the *DS*1 service is transported over a physical wire or optical fiber using electrical or optical pulses sent at a *T*1 = 1.544 Mb/s rate.

The TDM scheme is not restricted to multiplexing voice signals. For example, at the *DS*1 level, any 64-kb/s digital signal of the appropriate format could be transmitted as one of the 24 input channels shown in Fig. 1.13. As noted there and in Table 1.5, the main multiplexed rates for North American applications are designated as *DS*1 (1.544 Mb/s), *DS*2 (6.312 Mb/s), and *DS*3 (44.736 Mb/s). European and Japanese networks define similar hierarchies using different bit-rate levels as Table 1.5 shows. In Europe the multiplexing hierarchy is labeled *E*1, *E*2, *E*3, and so on.

Table 1.5 *Digital multiplexing levels used in North America, Europe, and Japan*

Digital multiplexing level	*Number of 64-kb/s channels*	*Bit rate (Mb/s)*		
		North America	*Europe*	*Japan*
*DS*0	1	0.064	0.064	0.064
*DS*1	24	1.544		1.544
	30		2.048	
	48	3.152		3.152
*DS*2	96	6.312		6.312
	120		8.448	
*DS*3	480		34.368	32.064
	672	44.736		
	1344	91.053		
	1440			97.728
*DS*4	1920		139.264	
	4032	274.176		
	5760			397.200

1.4.2 SONET/SDH Multiplexing Hierarchy

With the advent of high-capacity fiber optic transmission lines in the 1980s, service providers established a standard signal format called *synchronous optical network* (SONET) in North America and *synchronous digital hierarchy* (SDH) in other parts of the world.[37, 38] These standards define a synchronous frame structure for sending multiplexed digital traffic over optical fiber trunk lines. The basic building block and first level of the SONET signal hierarchy is called the *Synchronous Transport Signal - Level 1* (STS-1), which has a bit rate of 51.84 Mb/s. Higher-rate SONET signals are obtained by byte-interleaving N of these STS-1 frames, which then are scrambled and converted to an *Optical Carrier - Level N* (OC-N) signal. Thus the OC-N signal will have a line rate exactly N times that of an OC-1 signal. For SDH systems the fundamental building block is the 155.52-Mb/s *Synchronous Transport Module - Level 1* (STM-1). Again, higher-rate information streams are generated by synchronously multiplexing N different STM-1 signals to form the STM-N signal. Table 1.6 shows commonly used SDH and SONET signal levels, the line rate, and the popular numerical name for that rate.

Table 1.6 *Common SDH and SONET line rates and their popular numerical name*

SONET level	*Electrical level*	*SDH level*	*Line rate (Mb/s)*	*Popular rate name*
OC-1	STS-1	—	51.84	—
OC-3	STS-3	STM-1	155.52	155 Mb/s
OC-12	STS-12	STM-4	622.08	622 Mb/s
OC-48	STS-48	STM-16	2488.32	2.5 Gb/s
OC-192	STS-192	STM-64	9953.28	10 Gb/s
OC-768	STS-768	STM-256	39813.12	40 Gb/s

1.5 WDM Concepts

The use of *wavelength division multiplexing* (WDM) offers a further boost in fiber transmission capacity. The basis of WDM is to use multiple sources operating at slightly different wavelengths to transmit several independent information streams simultaneously over the same fiber. Figure 1.14 shows the basic WDM concept. Here N independent optically formatted information streams, each transmitted at a different wavelength, are combined by means of an optical multiplexer and sent over the same fiber. Note that each of these streams could be at a different data rate. Each information stream maintains its individual data rate after being multiplexed with the other traffic streams, and still operates at its unique wavelength. Conceptually, the WDM scheme is the same as frequency division multiplexing (FDM) used in microwave radio and satellite systems.

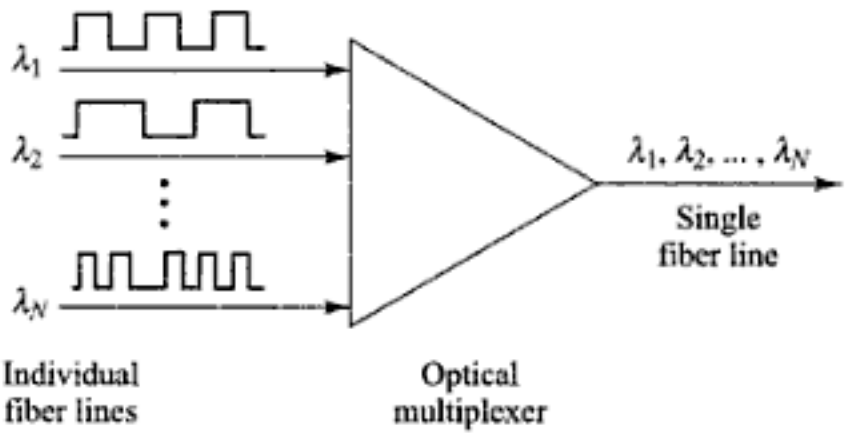

Fig. 1.14 *Basic concept of wavelength division multiplexing*

Although researchers started looking at WDM techniques in the 1970s, during the ensuing years it generally turned out to be easier to transmit only a single wavelength on a fiber using high-speed electronic and optical devices, than to invoke the greater system complexity called for in WDM. However, a dramatic surge in WDM popularity started in the early 1990s owing to several factors. These include new fiber types that provide better performance of multiple-wavelength operation at 1550 nm, advances in producing WDM devices that can separate closely spaced wavelengths, and the development of optical amplifiers that can boost C-band optical signal levels completely in the optical domain.

1.6 Key Elements of Optical Fiber Systems

Similar to electrical communication systems, the basic function of an optical fiber link is to transport a signal from communication equipment (e.g. a computer, telephone, or video device) at one location to corresponding equipment at another location with a high degree of reliability and accuracy. Figure 1.15 shows the main constituents of an optical fiber communications link. The key sections are a transmitter consisting of a light source and its associated drive circuitry, a cable offering mechanical and environmental protection to the optical fibers contained inside, and a receiver consisting of a photodetector plus amplification and signal-restoring circuitry. Additional components include optical amplifiers, connectors, splices, couplers, regenerators (for restoring the signal-shape characteristics), and other passive components and active photonic devices.

1.6.1 Overview of Element Applications

The cabled fiber is one of the most important elements in an optical fiber link. In addition to protecting the glass fibers during installation and service, the cable may contain copper wires for powering optical amplifiers or signal regenerators, which are needed periodically in long-distance links for amplifying and reshaping the signal. A variety of fiber types with different performance characteristics exist for a wide range of applications. To protect the glass fibers during installation and service, there are many different cable configurations depending on whether the cable is to be installed inside a building,

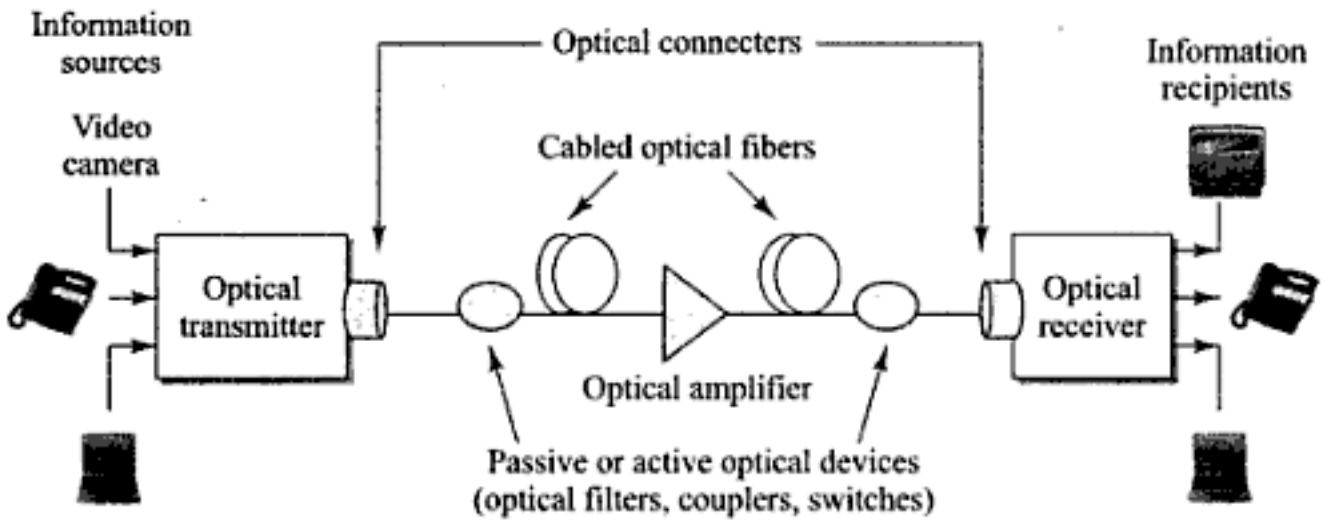

Fig. 1.15 *Main constituents of an optical fiber communications link*

underground in ducts or through direct-burial methods, outside on poles, or under water. Very low-loss optical connectors and splices are needed in all categories of optical fiber networks for joining cables and for attaching one fiber to another.

As a result of installation and/or manufacturing limitations, individual cable lengths will range from several hundred meters to several kilometers. Practical considerations such as reel size and cable weight determine the actual length of a single cable section. The shorter segments tend to be used when the cables are pulled through ducts. Longer lengths are used in aerial, direct-burial, or underwater applications. Transoceanic cable lengths are many hundreds of kilometers long. These cables are assembled in on-shore factories and then loaded into special cable-laying ships. Splicing together individual cable sections forms continuous transmission lines for these long-distance links.

Once the cable is installed, a transmitter can be used to launch a light signal into the fiber. The transmitter consists of a light source that is dimensionally compatible with the fiber core and associated electronic control and modulation circuitry. Semiconductor light-emitting diodes (LEDs) and laser diodes are suitable for this purpose. For these devices the light output can be modulated rapidly by simply varying the input current at the desired transmission rate, thereby producing an optical signal. The electric input signals to the transmitter circuitry for driving the optical source can be either of an analog or digital form. The functions of the associated transmitter electronics are to set and stabilize the source operating point and output power level. For high-rate systems (usually greater than about 2.5 Gb/s), direct modulation of the source can lead to unacceptable optical signal distortion. In this case, an external modulator is used to vary the amplitude of a continuous light output from a laser diode source. In the 770-to-910-nm region the light sources are generally alloys of GaAlAs. At longer wavelengths (1260 to 1675 nm) an InGaAsP alloy is the principal optical source material.

After an optical signal is launched into a fiber, it will become progressively attenuated and distorted with increasing distance because of scattering, absorption, and dispersion mechanisms in the glass material. At the destination of an optical fiber transmission line, there is a receiving device which interprets the information contained in the optical signal. Inside the receiver is a photodiode that detects the weakened and distorted optical signal emerging from the end of an optical fiber and converts it to an electrical signal (referred to as a *photocurrent*). The receiver also contains electronic amplification devices and circuitry to restore signal fidelity. Silicon photodiodes are used in the 770-to-910-nm region. The primary material in the 1260-to-1675-nm region is an InGaAs alloy.

The design of an optical receiver is inherently more complex than that of the transmitter, since it has to interpret the content of the weakened and degraded signal received by the photodetector. The principal

figure of merit for a receiver is the minimum optical power necessary at the desired data rate to attain either a given error probability for digital systems or a specified signal-to-noise ratio for an analog system. The ability of a receiver to achieve a certain performance level depends on the photodetector type, the effects of noise in the system, and the characteristics of the successive amplification stages in the receiver.

Included in any optical fiber link are various passive optical devices that assist in controlling and guiding the light signals. Passive devices are optical components that require no electronic control for their operation. Among these are optical filters that select only a narrow spectrum of desired light, optical splitters that divide the power in an optical signal into a number of different branches, optical multiplexers that combine signals from two or more distinct wavelengths onto the same fiber (or that separate the wavelengths at the receiving end) in multiple-wavelength optical fiber networks, and couplers used to tap off a certain percentage of light, usually for performance monitoring purposes.

In addition, modern sophisticated optical fiber networks contain a wide range of active optical components, which require an electronic control for their operation. These include light signal modulators, tunable (wavelength-selectable) optical filters, reconfigurable elements for adding and dropping wavelengths at intermediate nodes, variable optical attenuators, and optical switches.

After an optical signal has traveled a certain distance along a fiber, it becomes greatly weakened due to power loss along the fiber. Therefore, when setting up an optical link, engineers formulate a power budget and add amplifiers or repeaters when the path loss exceeds the available power margin. The periodically placed amplifiers merely give the optical signal a power boost, whereas a repeater also will attempt to restore the signal to its original shape. Prior to 1990, only repeaters were available for signal amplification. For an incoming optical signal, a repeater performs photon-to-electron conversion, electrical amplification, retiming, pulse shaping, and then electron-to-photon conversion. This process can be fairly complex for high-speed multiwavelength systems. Thus, researchers expended a great deal of effort to develop all-optical amplifiers, which boost the light power level completely in the optical domain. Optical amplification mechanisms for WDM links include the use of devices based on rare-earth-doped lengths of fiber and distributed amplification by means of a stimulated Raman scattering effect.

The installation and operation of an optical fiber communication system require measurement techniques for verifying that the specified performance characteristics of the constituent components are satisfied. In addition to measuring optical fiber parameters, system engineers are interested in knowing the characteristics of passive splitters, connectors, and couplers, and electro-optic components, such as sources, photodetectors, and optical amplifiers. Furthermore, when a link is being installed and tested, operational parameters that should be measured include bit error rate, timing jitter, and signal-to-noise ratio as indicated by the eye pattern. During actual operation, measurements are needed for maintenance and monitoring functions to determine factors such as fault locations in fibers and the status of remotely located optical amplifiers.

1.6.2 Windows and Spectral Bands

Figure 1.16 shows the operating range of optical fiber systems and the characteristics of the four key components of a link: the optical fiber, light sources, photodetectors, and optical amplifiers. Here the dashed vertical lines indicate the centers of the three main traditional operating wavelength bands of optical fiber systems, which are the short-wavelength region, the O-band, and the C-band. One of the principal characteristics of an optical fiber is its attenuation as a function of wavelength, as shown at the top in Fig. 1.16. Early applications in the late 1970s made exclusive use of the 770-to-910-nm wavelength

band where there was a low-loss window and GaAlAs optical sources and silicon photodetectors operating at these wavelengths were available. Originally this region was referred to as the *first window*, since around 1000 nm there was a large attenuation spike due to absorption by water molecules. As a result of this spike, early fibers exhibited a local minimum in the attenuation curve around 850 nm.

By reducing the concentration of hydroxyl ions and metallic impurities in the fiber material, in the 1980s manufacturers could fabricate optical fibers with very low losses in the 1260-to-1675-nm region.

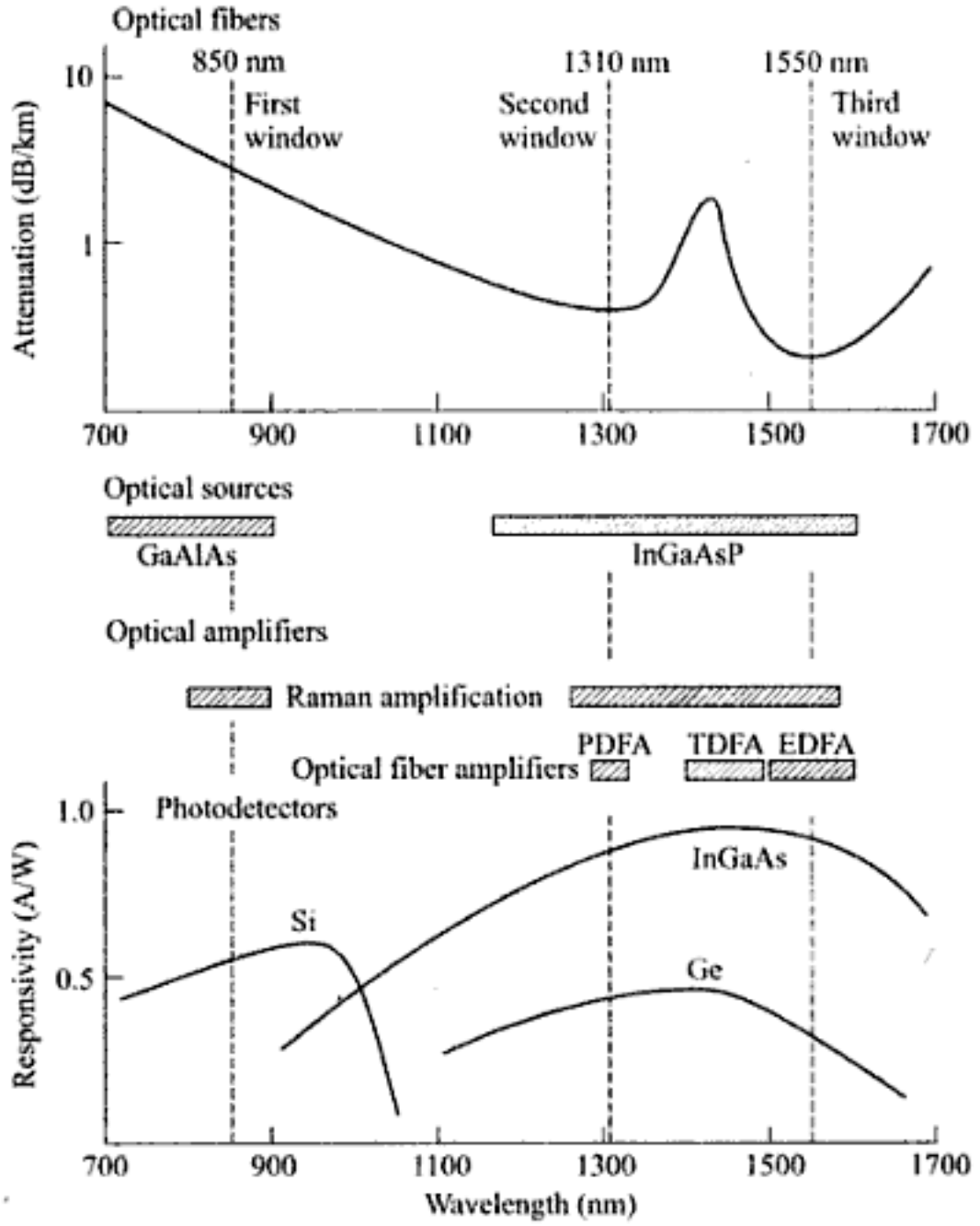

Fig. 1.16 *Characteristics and operating ranges of the four key optical fiber link components*

This spectral band is called the *long-wavelength region*. Since the glass still contained some water molecules, a third-order absorption spike remained around 1400 nm. This spike defined two low-loss windows, these being the *second window* centered at 1310 nm and the *third window* centered at 1550 nm. These two windows now are called the O-band and C-band, respectively. The desire to use the low-loss long-wavelength regions prompted the development of InGaAsP-based light sources and InGaAs photodetectors that can operate at 1310 and 1550 nm. In addition, doping optical fibers with rare-earth

elements such as Pr, Th, and Er creates optical fiber amplifiers (PDFA, TDFA, and EDFA devices). These devices and the use of Raman amplification gave a further capacity boost to long-wavelength WDM systems.

Special material-purification processes can eliminate almost all water molecules from the glass fiber material, thereby dramatically reducing the water-attenuation peak around 1400 nm. This process opens the E-band (1360-to-1460 nm) transmission region to provide around 100 nm more spectral bandwidth in these specially fabricated fibers than in conventional single-mode fibers.

Systems operating at 1550 nm provide the lowest attenuation, but the signal dispersion in a standard silica fiber is larger at 1550 nm than at 1310 nm. Fiber manufacturers overcame this limitation first by creating the dispersion-shifted fibers for single-wavelength operation and then by devising non-zero dispersion-shifted fiber (NZDSF) for use with WDM implementations. The latter fiber type has led to the widespread use of multiple-wavelength S-band and C-band systems for high-capacity, long-span terrestrial and undersea transmission links. These links routinely carry traffic at 10 Gb/s (OC-192/STM-64) over nominally 90-km distances between amplifiers or repeaters. By 2005 links operating at 40 Gb/s were being installed and field trials of 160-Gb/s long-distance transmission systems were tested successfully.[39-42]

1.7 Standards for Optical Fiber Communications

To allow components and equipment from different vendors to interface with one another, numerous international standards have been developed.[43-45] The three basic classes for fiber optics are primary standards, component testing standards, and system standards.

Primary standards refer to measuring and characterizing fundamental physical parameters such as attenuation, bandwidth, operational characteristics of fibers, and optical power levels and spectral widths. In the USA the main organization involved in primary standards is the National Institute of Standards and Technology (NIST). This organization carries out fiber optic and laser standardization work, and it sponsors an annual conference on optical fiber measurements. Other national organizations include the National Physical Laboratory (NPL) in the United Kingdom and the Physikalisch-Technische Bundesanstalt (PTB) in Germany.

Component testing standards define tests for fiber-optic component performance and they establish equipment-calibration procedures. Several different organizations are involved in formulating testing standards, some very active ones being the Telecommunications Industry Association (TIA) in association with the Electronics Industries Alliance (EIA), the Telecommunication Sector of the International Telecommunication Union (ITU-T), and the International Electrotechnical Commission (IEC). The TIA has a list of over 120 fiber optic test standards and specifications under the general designation TIA/EIA-455-XX-YY, where XX refers to a specific measurement technique and YY refers to the publication year. These standards are also called *Fiber Optic Test Procedures* (FOTP), so that TIA/EIA-455-XX becomes FOTP-XX. These include a wide variety of recommended methods for testing the response of fibers, cables, passive devices, and electro-optic components to environmental factors and operational conditions. For example, TIA/EIA-455-60-1997, or FOTP-60, is a method published in 1997 for measuring fiber or cable length.

System standards refer to measurement methods for links and networks. The major organizations are the American National Standards Institute (ANSI), the Institute for Electrical and Electronic Engineers (IEEE), the ITU-T, and Telcordia Technologies. Of particular interest for fiber optics system are test standards and recommendations from the ITU-T. Within the G series (in the number range G.650 and higher) the recommendations relate to fiber cables, optical amplifiers, wavelength multiplexing, optical transport networks (OTN), system reliability and availability, and management and control for passive optical networks (PON). The L series ITU-T recommendations deal with the construction, installation, maintenance support, monitoring, and testing of cable and other elements in the optical fiber outside plant, that is, the fielded cable system. Telcordia Technologies provides a wide range of generic requirements for telecommunication network components and systems. For example, the GR-3120 *Generic Requirements for Hardened Fiber Optic Connectors* document describes the necessary specifications for optical connectors that are environmentally hardened and can be mated in the field.

1.8 Modeling and Simulation Tools

Computer-based simulation and modeling tools that integrate component, link, and network functions can make the design process of complex optical links and networks more efficient, less expensive, and faster.[46-51] The rapid proliferation and increase in capabilities of personal computers led to the development of many sophisticated simulation programs for these machines for predicting photonic component, link, and network performance behavior. These software tools are based on well-established numerical models and can simulate factors such as connector losses due to geometric or position mismatches of fibers, efficiencies of coupling optical power from light sources into fibers, behaviors of passive and active optical components, and the performance of complex optical networks. They also can model many types of passive and active devices, such as waveguide couplers, optical filters, waveguide grating arrays, and optical sources, to a high degree of sophistication.

1.8.1 Simulation Tool Characteristics

Computer-aided design (CAD) tools can offer a powerful method to assist in analyzing the design of an optical component, circuit, or network before costly prototypes are built. Important points to consider, however, are the approximations and modeling assumptions made in the software design. Since most telecommunication systems are designed with several decibels of safety margin, approximations for calculating operating behavior that are reasonably accurate are not only acceptable but in general necessary to allow tractable computation times.

The theoretical models used in computer simulations nominally include the following characteristics:

- Enough detail so that all factors which could influence the performance of the component, circuit, or network can be appropriately evaluated.
- A common set of parameters so that simulated devices can be interconnected with each other to form circuits or networks.
- Interfaces that pass sufficient information between the constituent components so that all possible interactions are identified.
- Computational efficiency that allows a trade-off between accuracy and speed, so that quick estimates of system performance can be made in the early stages of a design.
- The capability to simulate devices over the desired spectral bandwidth.
- The ability to simulate factors such as nonlinear effects, crosstalk between optical channels, distortion in lasers, and dispersion in optical fibers.

To enable a user to visualize and simulate a system quickly, the simulation programs normally have the following features:

- The ability to create a system schematic based on a library of graphical icons and a graphical user interface (GUI). The icons represent various system components (such as optical fibers, filters, amplifiers) and instrumentation, (e.g. data sources, power meters, and spectrum analyzers).
- The ability for the user to interact with the program during a simulation. For example, the user may want to modify a parameter or some operating condition in order to evaluate their effect. This is especially important in the early stages of a design when the operating range of interest is being established.
- A wide range of statistical-analysis, signal-processing, and display tools.
- Common display formats, including time waveforms, electrical and optical spectra, eye diagrams, and error-rate curves.

1.8.2 Graphical Programming

Commercially available simulation tools for lightwave applications are based on well-established graphical-programming languages. In these languages, system components (e.g. lasers, modulators, optical amplifiers, optical fibers), measurement instruments, and plotting tools are represented by a module library of programmed icons that have bidirectional optical and electrical interfaces. Associated with each icon is a menu window where the user specifies the values of the operational parameters of the component and its interface characteristics. In addition to using preprogrammed modules, users can create their own custom devices with either the underlying software code or the graphical programming language.

Using such a set of graphical icons, one can put together a simulation of a complex component, a simple link, or a sophisticated multi-channel transmission path in several minutes. One simply selects the icons representing the desired components and measurement instruments, and connects them together with a wiring tool to create a model of the optical transmission system. When the design is completed, the diagram compiles rapidly and the simulation can be run using control buttons on a tool bar.

Once the icons have been selected and connected together, the complex and challenging part starts for the user. This involves choosing realistic ranges of the parameters of the electrical and optical components and sub-modules. It is important that the parameter values make sense in an actual application. In some cases this may entail examining the specification sheets of vendors.

1.8.3 Example Programs for Student Use

Several commercial vendors offer various suites of software-based modeling-tool modules for optical fiber communication systems.[52–54] These design and planning tools are intended for use across all levels of lightwave network analyses, performance evaluations, and technology comparisons ranging from passive and active components and modules, to complex transmission links, to entire optical networks. Familiar measurement instruments are built into the software to offer a wide range of settable options when displaying data from multiple simulation runs and multidimensional sweeps across a parameter range. Signal-processing modules allow data to be manipulated to mimic any laboratory setup.

Such tools are in use by component and system manufacturers, system integrators, network operators, and access service providers for functions such as capacity planning, comparative assessments of various technologies, optimization of transport and service networks, syntheses and analyses of WDM system and link designs, and component designs. In addition, many universities are using these simulation tools for both research and teaching purposes.

Abbreviated versions of several simulation modules may be downloaded for noncommercial educational use from the websites of the tool vendors. These simplified versions contain predefined component and link configurations that allow interactive concept demonstrations. Among the numerous demonstration setups are optical amplifier structures, simple single-wavelength links, and WDM links. The configurations are fixed, but the reader has the ability to interactively change the operational parameter values of components such as optical fibers, light sources, optical filters, and optical amplifiers. As part of the results that are possible, images of what would appear on the display screen of a standard instrument, such as a spectrum analyzer or an oscilloscope, enable the user to see the effects on link performance when various component values change.

The book website (http://www.mhhe.com/keiser/ofc4e) describes current offerings available on vendor websites of the demonstration modules that the reader may download and learn from.[55]

PROBLEMS

1.1 (*a*) What are the energies in electron volts (eV) of light at wavelengths 850, 1310, 1490, and 1550 nm?

(*b*) Consider a 1-ns pulse with a 100-nW amplitude at each of these wavelengths. How many photons are in such a pulse at each wavelength?

1.2 A WDM optical transmission system is designed so that each channel has a spectral width of 0.8 nm. How many wavelength channels can be used in the C-band?

1.3 Three sine waves have the following periods: 25 μs, 250 ns, 125 ps. What are their frequencies?

1.4 A sine wave is offset 1/6 of a cycle with respect to time zero. What is its phase in degrees and in radians?

1.5 Consider two signals that have the same frequency. When the amplitude of the first signal is at its maximum, the amplitude of the second signal is at half its maximum from the zero level. What is the phase shift between the two signals?

1.6 What is the duration of a bit for each of the following three signals which have bit rates of 64 kb/s, 5 Mb/s, and 10 Gb/s?

1.7 (*a*) Convert the following absolute power gains to decibel power gains: 10^{-3}, 0.3, 1, 4, 10, 100, 500, 2^n.

(*b*) Convert the following decibel power gains to absolute power gains: –30 dB, 0 dB, 13 dB, 30 dB, 10n dB.

1.8 (*a*) Convert the following absolute power levels to dBm values: 1 pW, 1 nW, 1 mW, 10 mW, 50 mW.

(*b*) Convert the following dBm values to power levels in units of mW: –13 dBm, –6 dBm, 6 dBm, 17 dBm.

1.9 A signal travels from point *A* to point *B*. (a) If the signal power is 1.0 mW at point *A* and 0.125 mW at point *B*, what is the attenuation in dB?

(*b*) What is the signal power at point *B* if the attenuation is 15 dB?

1.10 A signal passes through three cascaded amplifiers, each of which has a 5-dB gain. What is the total gain in dB? By what numerical factor is the signal amplified?

1.11 A 50-km long optical fiber has a total attenuation of 24 dB. If 500 μW of optical power get launched into the fiber, what is the output optical power level in dBm and in μW?

1.12 A transmission line has a bandwidth of 2 MHz. If the signal-to-noise ratio at the receiving end is 20 dB, what is the maximum data rate that this line can support?

1.13 (*a*) At the lowest TDM level of the digital service scheme, 24 channels of 64 kb/s each are multiplexed into a 1.544-Mb/s *DS*1 channel. How much is the overhead that is added?

(*b*) The next higher multiplexed level, the *DS*2 rate, is 6.312 Mb/s. How many *DS*1 channels can be accommodated in the *DS*2 rate and what is the overhead?

(*c*) If the *DS*3 rate that is sent over a *T*3 line is 44.376 Mb/s, how many *DS*2 channels can be accommodated on a *T*3 line and what is the overhead?

(d) Using the above results, find how many *DS*0 channels can be sent over a *T*3 line. What is the total added overhead?

1.14 To insert low-speed signals such as 64-kb/s voice channels into a SONET frame, 84 columns in each SPE are divided into seven groups of 12 columns. Each such group is called a *virtual tributary*.

(a) What is the bit rate of such a virtual tributary?

(b) How many 64-kb/s voice channels can a virtual tributary accommodate?

(c) What is the payload efficiency?

REFERENCES

1. S. E. Miller and A. G. Chynoweth, eds., *Optical Fiber Telecommunications*, Academic, New York, 1979. This book and the texts listed in Refs. 2, 3, and 4 contain dozens of topics in all areas of optical fiber technology presented by researchers from AT&T Bell Laboratories over a period of more than twenty years.
2. S. E. Miller and I. P. Kaminow, eds., *Optical Fiber Telecommunications-II*, Academic, New York, 1988.
3. I. P. Kaminow and T.L Koch, eds., *Optical Fiber Telecommunications-III*, vols. A and B, Academic, New York, 1997.
4. I. P. Kaminow and T.Li, eds., *Optical Fiber Telecommunications-IV*, vols. A and B, Academic, New York, 2002.
5. J. M. Senior, *Optical Fiber Communications*, Prentice-Hall, Englewood Cliffs, NJ, 2nd ed., 1992.
6. R. L. Freeman, *Fiber-Optic Systems for Telecommunications*, Wiley, Hoboken, NJ, 2002.
7. G. P. Agrawal, *Fiber Optic Communication Systems*, Wiley, Hoboken, NJ, 3rd ed., 2002.
8. R. Ramaswami and K. N. Sivarajan, *Optical Networks*, Morgan Kaufmann, San Francisco, 2nd ed., 2002.
9. E. Desurvire, *Erbium-Doped Fiber Amplifiers*, Wiley, Hoboken, NJ, 2002.
10. E. Desurvire, D. Bayart, B. Desthieux, and S. Bigo, *Erbium-Doped Fiber Amplifiers: Devices and System Developments*, Wiley, New York, 2002.
11. B. Razavi, *Design of Integrated Circuits for Optical Communications*, McGraw-Hill, New York, 2003.
12. J. A. Buck, *Fundamentals of Optical Fibers*, Wiley, New York, 2004.
13. K.P. Ho, *Phase-Modulated Optical Communication Systems*, Springer, New York, 2005.
14. G. Keiser, *Optical Communications Essentials*, McGraw-Hill, New York, 2003.
15. G. Keiser, *FTTX Concepts and Applications*, Wiley, Hoboken, NJ, 2006.
16. A. Yariv and P. Yeh, *Photonics: Optical Electronics in Modern Communications*, Oxford University Press USA, New York, 6th ed., 2006.
17. B. E. A. Saleh and M. C. Teich, *Fundamentals of Photonics*, Wiley, Hoboken, NJ, 2nd ed., 2007.
18. E. Snitzer, "Cylindrical dielectric waveguide modes," *J. Opt. Soc. Amer.*, vol. 51, pp. 491–498, May 1961.
19. K. C. Kao and G. A. Hockman, "Dielectric-fibre surface waveguides for optical frequencies," *Proceedings IEE*, vol. 113, pp. 1151–1158, July 1966.
20. J. Hecht, *City of Light*, Oxford University Press, New York, 1999.
21. *Optical Fiber Communications (OFC) Conf.* is cosponsored annually by the Optical Society of America (OSA), Washington, DC and the Institute of Electrical and Electronic Engineers (IEEE), New York, NY.
22. *European Conference on Optical Fibre Communications (ECOC)* is held annually in Europe; sponsored by various European engineering organizations.
23. *Photonics West* held in the US and *Asia-Pacific Optical Communications (APOC)* held in Asia are two of a number of annual conferences sponsored by SPIE, Bellingham, WA, USA.

24. Special Issue: "100 years of communication progress," *IEEE Commun. Mag.*, vol. 22, May 1984.
25. A. Leon-Garcia and I. Widjaja, *Communication Networks*, McGraw-Hill, New York, 2nd ed., 2004.
26. J. G. Proakis, *Digital Communications*, McGraw-Hill, New York, 4th ed., 2001.
27. A. B. Carlson, P. Crilly, and J. Rutledge, *Communication Systems*, McGraw-Hill, Burr Ridge, IL, 4th ed., 2002.
28. L. W. Couch II, *Digital and Analog Communication Systems*, Prentice Hall, Upper Saddle River, NJ, 7th ed., 2007.
29. F. P. Kapron, D. B. Keck, and R. D. Maurer, "Radiation losses in glass optical waveguides," *Appl. Phys. Lett.*, vol. 17, pp. 423–425, Nov. 1970.
30. W. A. Gambling, "The rise and rise of optical fibers," *IEEE J. Sel. Topics Quantum Electron.*, vol. 6, no. 6, pp. 1084–1093 Nov./Dec. 2000.
31. B. St. Arnaud, J. Wu, and B. Kalali, "Customer-controlled and -managed optical networks," *J. Lightwave Technology*, vol. 21, pp. 2804–2810, Nov. 2003.
32. D. Simeonidou, R. Nejabati, G. Zervas, D. Klonidis, A. Tzanakaki, M. J. O'Mahony, "Dynamic optical-network architectures and technologies for existing and emerging grid services," *J. Lightwave Technology*, vol. 23, pp. 3347–3357, Oct. 2005.
33. N. Taesombut, F. Uyeda, A. A. Chien, L. Smarr, T. A. DeFanti, P. Papadopoulos, J. Leigh, M. Ellisman, and J. Orcutt, "The OptIPuter: High-performance, QoS-guaranteed network service for emerging e-science applications," *IEEE Commun. Mag.*, vol. 44, pp. 38–45, May 2006.
34. D. H. Rice and G. Keiser, "Applications of fiber optics to tactical communication systems," *IEEE Commun. Mag.*, vol. 23, pp. 46–57, May 1985.
35. ITU-T Recommendation G.Sup39, *Optical System Design and Engineering Considerations*, Feb. 2006.
36. A. J. Jerri, "The Shannon sampling theorem—Its various extensions and applications: A Tutorial Review," *Proc. IEEE*, vol. 65, pp. 1565–1596, Nov. 1977.
37. H. G. Perros, *Connection-Oriented Networks: SONET/SDH, ATM, MPLS and Optical Networks*, Wiley, Hoboken, NJ, 2005.
38. W. Goralski, *SONET/SDH*, McGraw-Hill, New York, 3rd ed., 2003.
39. A. Scavennec and O. Leclerc, "Toward high-speed 40-Gb/s transponders," *Proc. IEEE*, vol. 94, pp. 986–996, May 2006.
40. J.X. Cai, C. R. Davidson, M. Nissov, H. Li, W. T. Anderson, Y. Cai, L. Liu, A. N. Pilipetskii, D. G. Foursa, W. W. Patterson, P. C. Corbett, A. J. Lucero, and N. S. Bergano, "Transmission of 40-Gb/s WDM signals over transoceanic distance using conventional NZ-DSF with receiver dispersion slope compensation," *J. Lightwave Technology*, vol. 24, pp. 191–200, Jan. 2006.
41. E. Le Rouzic and S. Gosselin, "160-Gb/s optical networking: A prospective techno-economical analysis," *J. Lightwave Technology*, vol. 23, pp. 3024–3033, Oct. 2005.
42. M. Schneiders, S. Vorbeck, R. Leppla, E. Lach, M. Schmidt, S. B. Papernyi, and K. Sanapi, "Field transmission of 8 × 170 Gb/s over high-loss SSMF link using third-order distributed Raman amplification," *J. Lightwave Technology*, vol. 24, pp. 175–182, Jan. 2006.
43. M. L. Jones, "Optical networking standards," *J. Lightwave Technology*, vol. 22, pp. 275–280, Jan. 2004.
44. Telecommunications Sector—International Telecommunication Union (ITU-T), various G.600 Series Recommendations for all aspects of optical fiber communications.
45. Special issue on "Standards activities: Addressing the challenges of next-generation optical networks," K. Kazi, guest editor, *Optical Networks Magazine*, vol. 4, issue 1, Jan./Feb. 2003.
46. J. Piprek, ed., *Optoelectronic Devices: Advanced Simulation and Analysis*, Springer, New York, 2005.
47. K. Kawano and T. Kitoh, *Introduction to Optical Waveguide Analysis: Solving Maxwell's Equation and the Schrödinger Equation*, Wiley, Hoboken, NJ, 2002.

48. A. J. Lowery, "Photonic simulation tools," in I. Kaminow and T. Li, eds., *Optical Fiber Telecommunications IV-B: Systems and Impairments*, Academic, 2002.
49. A. J. Lowery, "WDM systems simulations," in A. Gumaste and T. Anthony, eds., *DWDM Network Designs and Engineering Solutions*, Cisco Press, 2003.
50. G. Guekos, ed., *Photonic Devices for Telecommunications: How to Model and Measure*, Springer, New York, 1998.
51. N. Antoniades, I. Roudas, G. Ellinas, and V. Grigoryan, *Modeling and Computer-Aided Design of Optical Communications Systems and Networks*, Springer, New York, 2007.
52. VPIsystems, Inc., Holmdel, New Jersey, USA, www.vpisystems.com.
53. RSoft Design Group, Inc., Ossining, New York, USA, www.rsoftdesign.com.
54. Optiwave Systems, Inc., Toronto, Ontario, Canada, www.optiwave.com.
55. The book website can be found at http://www.mhhe.com/keiser/ofc4e.

CHAPTER 2

Optical Fibers: Structures, Waveguiding, and Fabrication

One of the most important components in any optical fiber system is the optical fiber itself, since its transmission characteristics play a major role in determining the performance of the entire system. Some of the questions that arise concerning optical fibers are

1. What is the structure of an optical fiber?
2. How does light propagate along a fiber?
3. Of what materials are fibers made?
4. How is the fiber fabricated?
5. How are fibers incorporated into cable structures?
6. What is the signal loss or attenuation mechanism in a fiber?
7. Why and to what degree does a signal get distorted as it travels along a fiber?

The purpose of this chapter is to present some of the fundamental answers to the first five questions in order to attain a good understanding of the physical structure and waveguiding properties of optical fibers. Questions 6 and 7 are answered in Chapter 3. The discussions address both conventional silica and photonic crystal fibers.

Since fiber optics technology involves the emission, transmission and detection of light, we begin our discussion by first considering the nature of light and then we shall review a few basic laws and definitions of optics.[1] Following a description of the structure of optical fibers, two methods are used to describe how an optical fiber guides light. The first approach uses the geometrical or ray optics concept of light reflection and refraction to provide an intuitive picture of the propagation mechanisms. In the second approach, light is treated as an electromagnetic wave which propagates along the optical fiber waveguide. This involves solving Maxwell's equations subject to the cylindrical boundary conditions of the fiber.

2.1 The Nature of Light

The concepts concerning the nature of light have undergone several variations during the history of physics. Until the early seventeenth century, it was generally believed that light consisted of a stream of

minute particles that were emitted by luminous sources. These particles were pictured as travelling in straight lines, and it was assumed that they could penetrate transparent materials but were reflected from opaque ones. This theory adequately described certain large-scale optical effects, such as reflection and refraction, but failed to explain finer-scale phenomena, such as interference and diffraction.

The correct explanation of diffraction was given by Fresnel in 1815. Fresnel showed that the approximately rectilinear propagation character of light could be interpreted on the assumption that light is a wave motion, and that the diffraction fringes could thus be accounted for in detail. Later, the work of Maxwell in 1864 theorized that light waves must be electromagnetic in nature. Furthermore, observation of polarization effects indicated that light waves are transverse (i.e., the wave motion is perpendicular to the direction in which the wave travels). In this *wave* or *physical optics viewpoint,* the electromagnetic waves radiated by a small optical source can be represented by a train of spherical wave fronts with the source at the center as shown in Fig. 2.1. A *wave front* is defined as the locus of all points in the wave train which have the same phase. Generally, one draws wave fronts passing through either the maxima or the minima of the wave, such as the peak or trough of a sine wave, for example. Thus, the wave fronts (also called *phase fronts)* are separated by one wavelength.

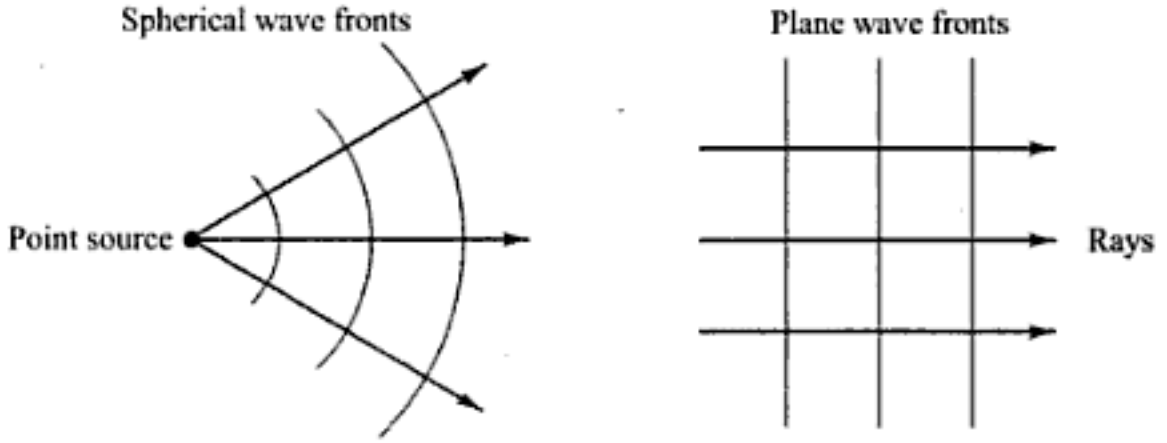

Fig. 2.1 *Representations of spherical and plane wave fronts and their associated rays*

When the wavelength of the light is much smaller than the object (or opening) which it encounters, the wave fronts appear as straight lines to this object or opening. In this case, the light wave can be represented as a *plane wave,* and its direction of travel can be indicated by a *light ray* which is drawn perpendicular to the phase front. The light-ray concept allows large-scale optical effects such as reflection and refraction to be analyzed by the simple geometrical process of *ray tracing.* This view of optics is referred to as *ray* or *geometrical optics.* The concept of light rays is very useful because the rays show the direction of energy flow in the light beam.

2.1.1 Linear Polarization

The electric or magnetic field of a train *of plane linearly polarized waves* traveling in a direction **k** can be represented in the general form

$$\mathbf{A}(\mathbf{x}, t) = \mathbf{e}_i A_0 \exp[j(\omega t - \mathbf{k} \cdot \mathbf{x})] \tag{2.1}$$

with $\mathbf{x} = x\mathbf{e}_x + y\mathbf{e}_y + z\mathbf{e}_z$ representing a general position vector and $\mathbf{k} = k_x\mathbf{e}_x + k_y\mathbf{e}_y + k_z\mathbf{e}_z$ representing the wave propagation vector.

Here, A_0 is the maximum amplitude of the wave, $\omega = 2\pi\nu$, where ν is the frequency of the light; the magnitude of the wavevector **k** is $k = 2\pi/\lambda$, which is known as the *wave propagation constant,* with λ being the wavelength of the light; and $\mathbf{e}_i$ is a unit vector lying parallel to an axis designated by i.

Note that the components of the actual (measurable) electromagnetic field represented by Eq. (2.1) are obtained by taking the real part of this equation. For example, if $\mathbf{k} = k\mathbf{e}_z$, and if $\mathbf{A}$ denotes the electric field $\mathbf{E}$ with the coordinate axes chosen such that $\mathbf{e}_i = \mathbf{e}_x$, then the real measurable electric field is given by

$$\mathbf{E}_x(z, t) = \text{Re}(\mathbf{E}) = \mathbf{e}_x E_{0x} \cos(\omega t - kz) \tag{2.2}$$

which represents a plane wave that varies harmonically as it travels in the z direction. The reason for using the exponential form is that it is more easily handled mathematically than equivalent expressions given in terms of sine and cosine. In addition, the rationale for using harmonic functions is that any waveform can be expressed in terms of sinusoidal waves using Fourier techniques.

The electric and magnetic field distributions in a train of plane electromagnetic waves at a given instant in time are shown in Fig. 2.2. The waves are moving in the direction indicated by the vector $\mathbf{k}$. Based on Maxwell's equations, it can be shown[2] that $\mathbf{E}$ and $\mathbf{H}$ are both perpendicular to the direction of propagation. This condition defines a *plane wave*, that is, the vibrations in the electric field are parallel to each other at all points in the wave. Thus, the electric field forms a plane called the *plane of vibration*. Likewise all points in the magnetic field component of the wave lie in another plane of vibration. Furthermore, $\mathbf{E}$ and $\mathbf{H}$ are mutually perpendicular, so that $\mathbf{E}$, $\mathbf{H}$, and $\mathbf{k}$ form a set of orthogonal vectors.

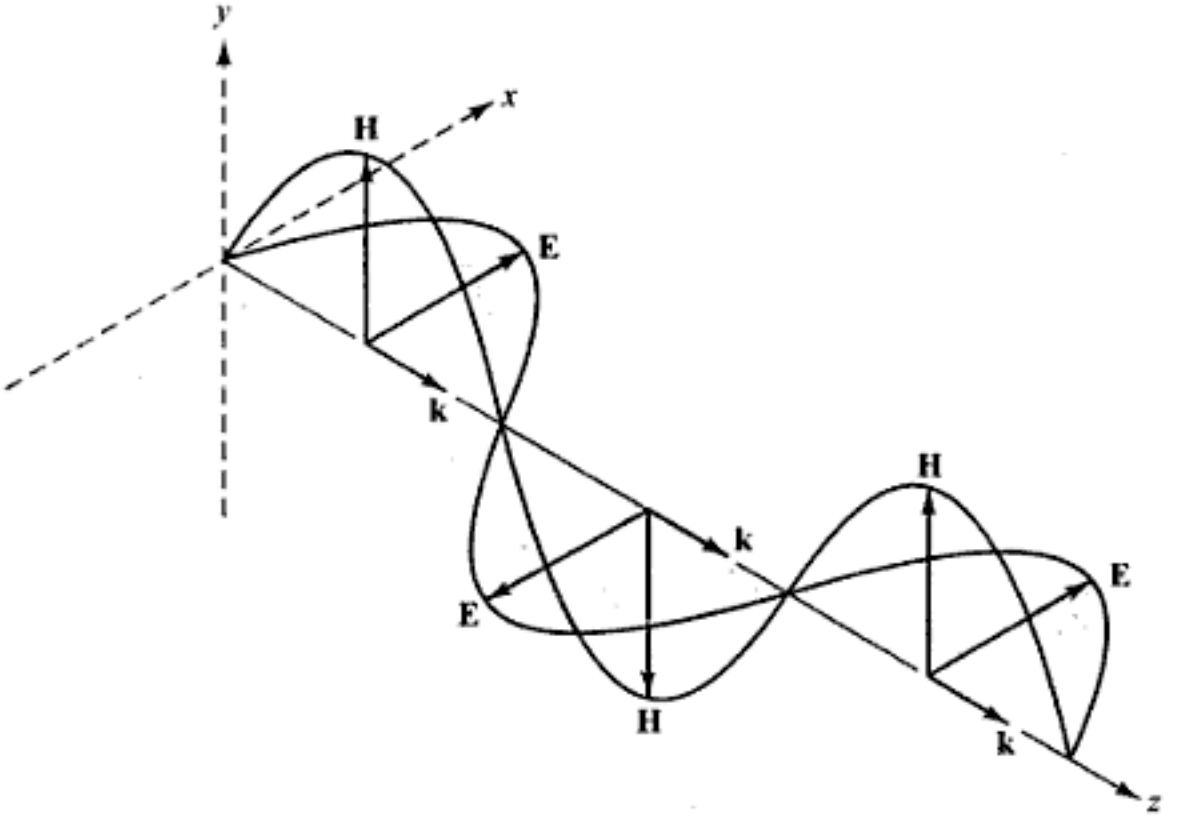

Fig. 2.2 *Electric and magnetic field distributions in a train of plane electromagnetic waves at a given instant in time*

The plane wave example given by Eq. (2.2) has its electric field vector always pointing in the $\mathbf{e}_x$ direction. Such a wave is *linearly polarized* with polarization vector $\mathbf{e}_x$. A general state of polarization is described by considering another linearly polarized wave which is independent of the first wave and orthogonal to it. Let this wave be

$$\mathbf{E}_y(z, t) = \mathbf{e}_y E_{0y} \cos(\omega t - kz + \delta) \tag{2.3}$$

where δ is the relative phase difference between the waves. The resultant wave is

$$\mathbf{E}(z, t) = \mathbf{E}_x(z, t) + \mathbf{E}_y(z, t) \tag{2.4}$$

If δ is zero or an integer multiple of 2π, the waves are in phase. Equation (2.4) is then also a linearly polarized wave with a polarization vector making an angle

$$\theta = \arctan \frac{E_{0y}}{E_{0x}} \tag{2.5}$$

with respect to $\mathbf{e}_x$ and having a magnitude

$$E = \left(E_{0x}^2 + E_{0y}^2\right)^{1/2} \tag{2.6}$$

This case is shown schematically in Fig. 2.3. Conversely, just as any two orthogonal plane waves can be combined into a linearly polarized wave, an arbitrary linearly polarized wave can be resolved into two independent orthogonal plane waves that are in phase.

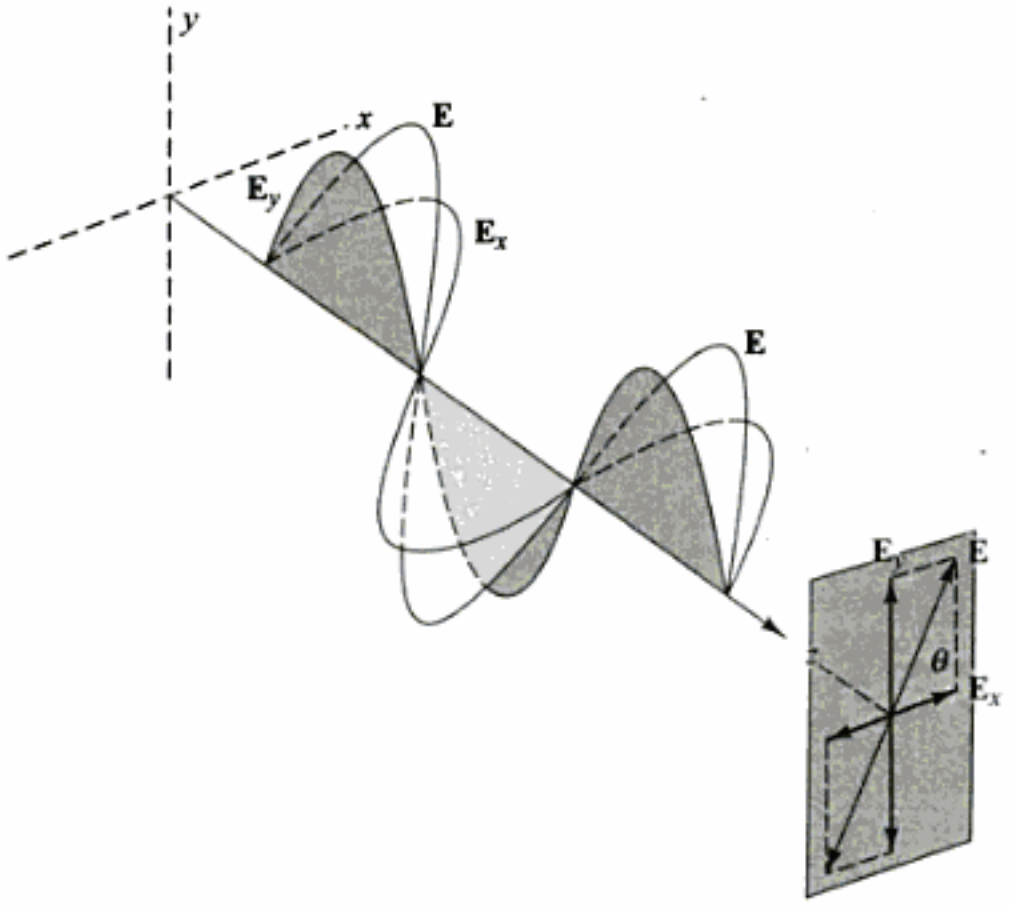

Fig. 2.3 *Addition of two linearly polarized waves having a zero relative phase between them*

2.1.2 Elliptical and Circular Polarization

For general values of δ the wave given by Eq. (2.4) is *elliptically polarized.* The resultant field vector **E** will both rotate and change its magnitude as a function of the angular frequency ω. From Eqs. (2.2) and (2.3) we can show that (see Prob. 2.4) for a general value of δ,

$$\left(\frac{E_x}{E_{0x}}\right)^2 + \left(\frac{E_y}{E_{0y}}\right)^2 - 2\left(\frac{E_x}{E_{0x}}\right)\left(\frac{E_y}{E_{0y}}\right)\cos\delta = \sin^2\delta \tag{2.7}$$

which is the general equation of an ellipse. Thus, as Fig. 2.4 shows, the endpoint of **E** will trace out an ellipse at a given point in space. The axis of the ellipse makes an angle α relative to the x axis given by

$$\tan 2\alpha = \frac{2E_{0x}E_{0y}\cos\delta}{E_{0x}^2 - E_{0y}^2} \tag{2.8}$$

To get a better picture of Eq. (2.7), let us align the principal axis of the ellipse with the x axis. Then $\alpha = 0$, or, equivalently, $\delta = \pm\pi/2, \pm 3\pi/2, \ldots$, so that Eq. (2.7) becomes

$$\left(\frac{E_x}{E_{0x}}\right)^2 + \left(\frac{E_y}{E_{0y}}\right)^2 = 1 \tag{2.9}$$

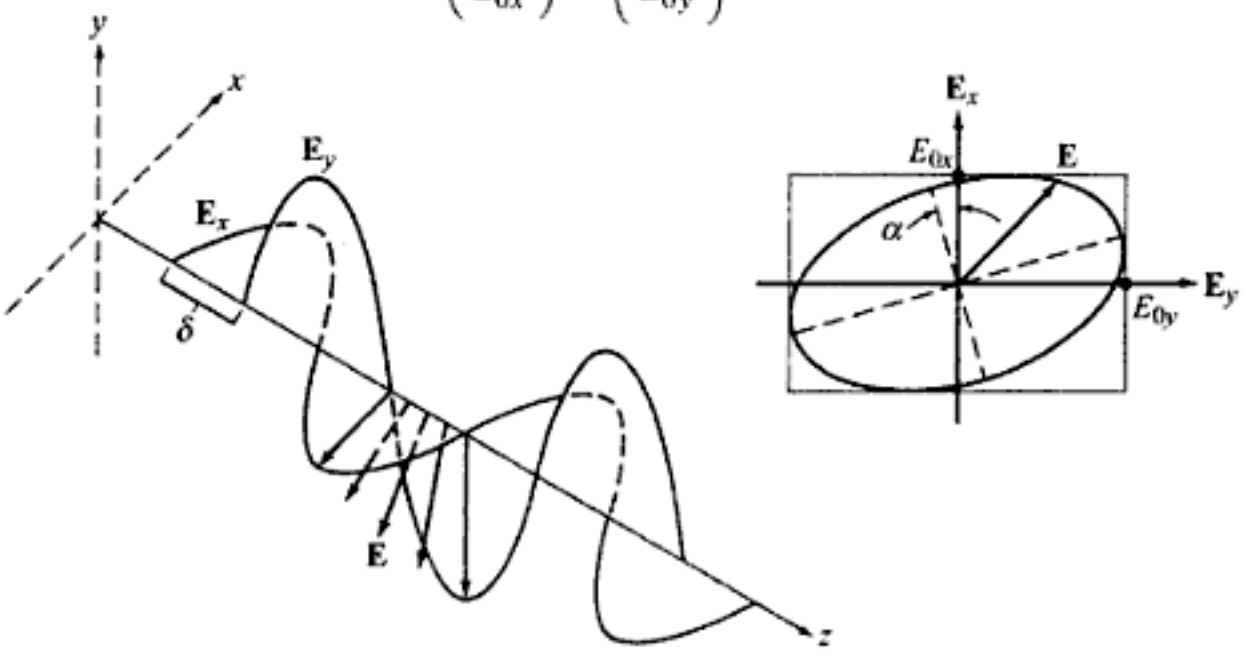

Fig. 2.4 *Elliptically polarized light results from the addition of two linearly polarized waves of unequal amplitude having a nonzero phase difference δ between them*

This is the familiar equation of an ellipse with the origin at the center and semi-axes E_{0x} and E_{0y}.

When $E_{0x} = E_{0y} = E_0$ and the relative phase difference $\delta = \pm\pi/2 + 2m\pi$, where $m = 0, \pm 1, \pm 2, \ldots$, then we have *circularly polarized* light. In this case, Eq. (2.9) reduces to

$$E_x^2 + E_y^2 = E_0^2 \tag{2.10}$$

which defines a circle. Choosing the positive sign for δ, Eqs (2.2) and (2.3) become

$$\mathbf{E}_x(z, t) = \mathbf{e}_x E_0 \cos(\omega t - kz) \tag{2.11}$$

$$\mathbf{E}_y(z, t) = -\mathbf{e}_y E_0 \sin(\omega t - kz) \tag{2.12}$$

In this case, the endpoint of **E** will trace out a circle at a given point in space, as Fig. 2.5 illustrates. To see this, consider an observer located at some arbitrary point z_{ref} toward whom the wave is moving. For convenience, we will pick this point at $z = \pi/k$ at $t = 0$. Then, from Eqs (2.11) and (2.12) we have

$$\mathbf{E}_x(z, t) = -\mathbf{e}_x E_0 \quad \text{and} \quad \mathbf{E}_y(z, t) = 0$$

so that **E** lies along the negative x axis as Fig. 2.5 shows. At a later time, say $t = \pi/2\omega$, the electric field vector has rotated through 90° and now lies along the positive y axis at z_{ref}. Thus, as the wave moves toward the observer with increasing time, the resultant electric field vector **E** rotates *clockwise* at an

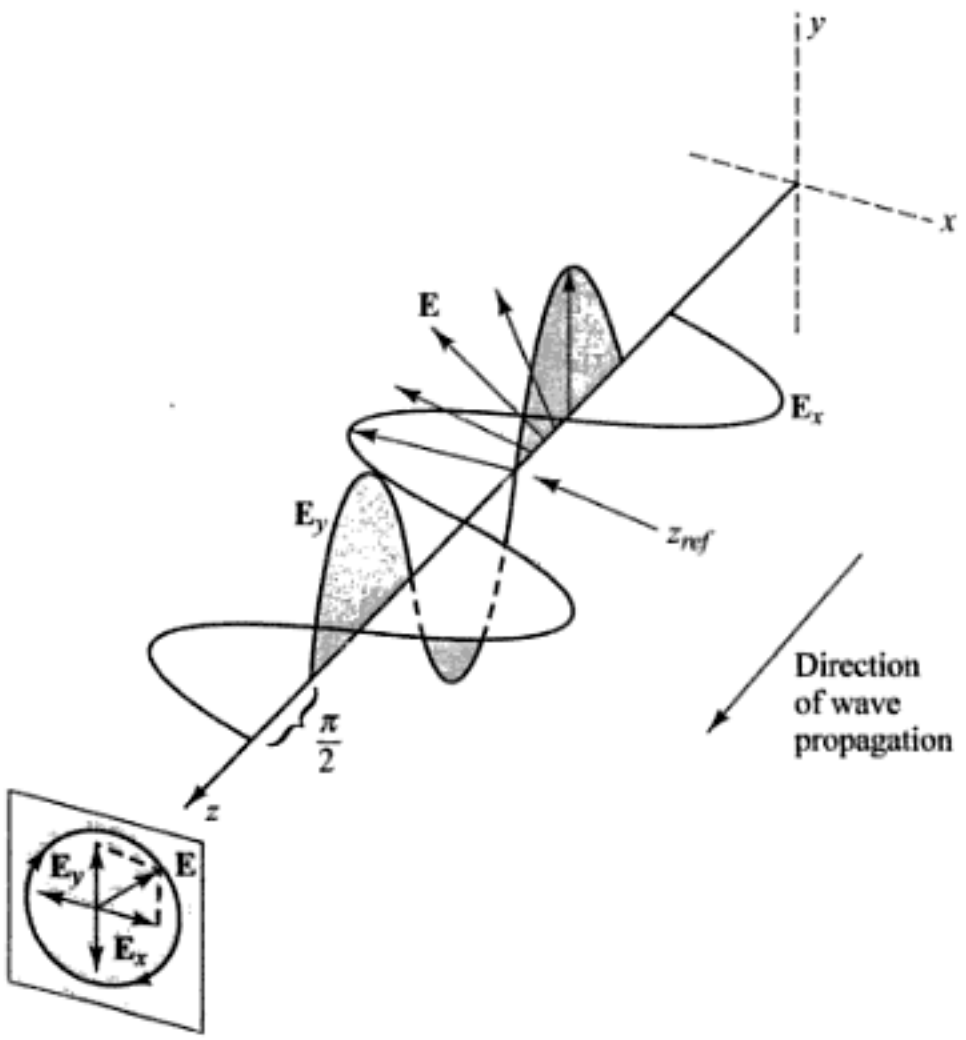

Fig. 2.5 *Addition of two equal-amplitude linearly polarized waves with a relative phase difference $\delta = \pi/2 + 2m\pi$ results in a right circularly polarized wave*

angular frequency ω. It makes one complete rotation as the wave advances through one wavelength. Such a light wave is *right circularly polarized.*

If we choose the negative sign for δ, then the electric field vector is given by

$$\mathbf{E} = E_0[\mathbf{e}_x \cos(\omega t - kz) + \mathbf{e}_y \sin(\omega t - kz)] \tag{2.13}$$

Now **E** rotates *counterclockwise* and the wave is *left circularly polarized.*

2.1.3 The Quantum Nature of Light

The wave theory of light adequately accounts for all phenomena involving the transmission of light. However, in dealing with the interaction of light and matter, such as occurs in dispersion and in the emission and absorption of light, neither the particle theory nor the wave theory of light is appropriate. Instead, we must turn to quantum theory, which indicates that optical radiation has particle as well as wave properties. The particle nature arises from the observation that light energy is always emitted or absorbed in discrete units called *quanta* or *photons.* In all experiments used to show the existence of photons, the photon energy is found to depend only on the frequency ν. This frequency, in turn, must be measured by observing a wave property of light.

The relationship between the energy E and the frequency ν of a photon is given by

$$E = h\nu \tag{2.14}$$

where $h = 6.625 \times 10^{-34}$ J·s is Planck's constant. When light is incident on an atom, a photon can transfer its energy to an electron within this atom, thereby exciting it to a higher energy level. In this process either all or none of the photon energy is imparted to the electron. The energy absorbed by the electron must be exactly equal to that required to excite the electron to a higher energy level. Conversely, an electron in an excited state can drop to a lower state separated from it by an energy $h\nu$ by emitting a photon of exactly this energy.

2.2 Basic Optical Laws and Definitions

This section reviews some of the basic optics laws and definitions relevant to optical fiber transmission technology. These include Snell's law, the definition of the refractive index of a material, and the concepts of reflection, refraction, and polarization.

2.2.1 Refractive Index

A fundamental optical parameter of a material is the *refractive index* (or *index of refraction*). In free space a light wave travels at a speed $c = 3 \times 10^8$ m/s. The speed of light is related to the frequency ν and the wavelength λ by $c = \nu\lambda$. Upon entering a dielectric or nonconducting medium the wave now travels at a speed v, which is characteristic of the material and is less than c. The ratio of the speed of light in a vacuum to that in matter is the index of refraction n of the material and is given by

$$n = \frac{c}{v} \tag{2.15}$$

Typical values of n are 1.00 for air, 1.33 for water, 1.45 for silica glass, and 2.42 for diamond.

2.2.2 Reflection and Refraction

The concepts of reflection and refraction can be interpreted most easily by considering the behavior of light rays associated with plane waves traveling in a dielectric material. When a light ray encounters a boundary separating two different media, part of the ray is reflected back into the first medium and the remainder is bent (or refracted) as it enters the second material. This is shown in Fig. 2.6 where $n_2 < n_1$. The bending or refraction of the light ray at the interface is a result of the difference in the speed of light in two materials that have different refractive indices. The relationship at the interface is known as Snell's law and is given by

$$n_1 \sin \phi_1 = n_2 \sin \phi_2 \tag{2.16}$$

or, equivalently, as

$$n_1 \cos \theta_1 = n_2 \cos \theta_2 \tag{2.17}$$

where the angles are defined in Fig. 2.6. The angle ϕ_1 between the incident ray and the normal to the surface is known as the *angle of incidence*.

According to the law of reflection, the angle θ_1 at which the incident ray strikes the interface is exactly equal to the angle that the reflected ray makes with the same interface. In addition, the incident ray, the normal to the interface, and the reflected ray all lie in the same plane, which is perpendicular to the interface plane between the two materials. This plane is called the *plane of incidence*. When light traveling in a certain medium is reflected off an optically denser material (one with a higher refractive index), the process is referred to as *external reflection*. Conversely, the reflection of light off of less optically dense material (such as light traveling in glass being reflected at a glass–air interface) is called *internal reflection*.

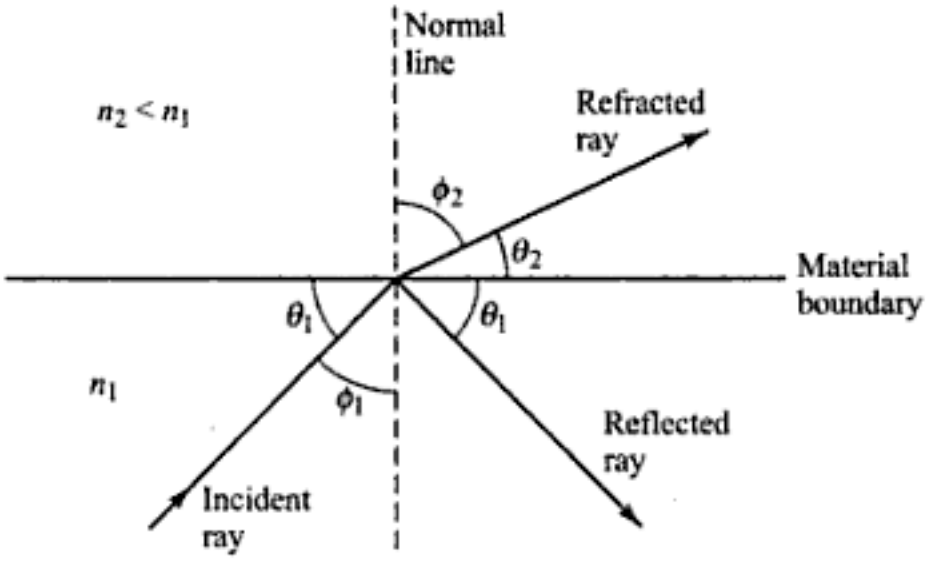

Fig. 2.6 *Refraction and reflection of a light ray at a material boundary*

As the angle of incidence ϕ_1 in an optically denser material becomes larger, the refracted angle ϕ_2 approaches $\pi/2$. Beyond this point no refraction is possible and the light rays become *totally internally reflected.* The conditions required for total internal reflection can be determined by using Snell's law [Eq. (2.16)]. Consider Fig. 2.7, which shows a glass surface in air. A light ray gets bent toward the glass surface as it leaves the glass in accordance with Snell's law. If the angle of incidence ϕ_1 is increased, a point will eventually be reached where the light ray in air is parallel to the glass surface. This point is known as the *critical angle of incidence* ϕ_c. When the incidence angle ϕ_1 is greater than the critical angle, the condition for total internal reflection is satisfied; that is, the light is totally reflected back into the glass with no light escaping from the glass surface. (This is an idealized situation. In practice, there is always some tunneling of optical energy through the interface. This can be explained in terms of the electromagnetic wave theory of light, which is presented in Sec. 2.4.)

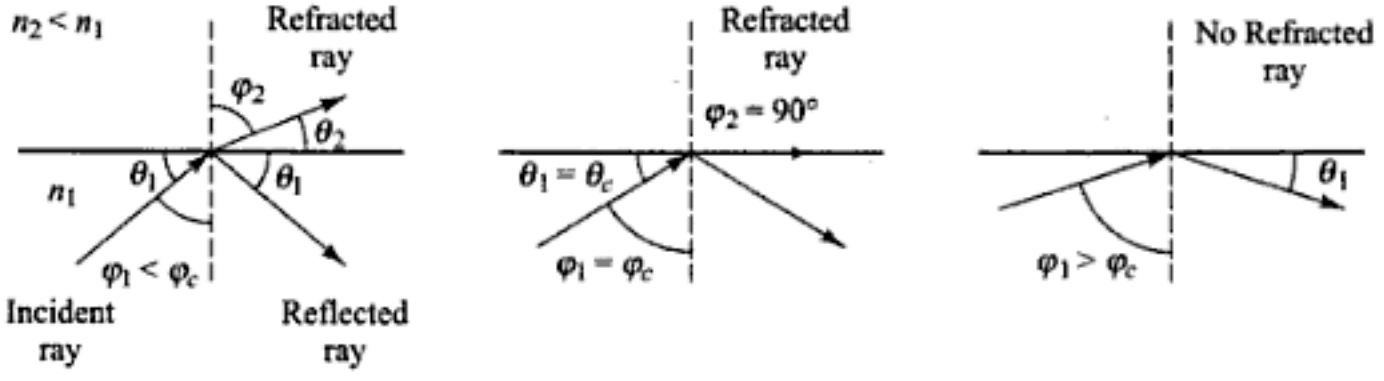

Fig. 2.7 *Representation of the critical angle and total internal reflection at a glass-air interface*

As an example, consider the glass–air interface shown in Fig. 2.7. When the light ray in air is parallel to the glass surface, then $\phi_2 = 90°$ so that $\sin \phi_2 = 1$. The critical angle in the glass is thus

$$\sin \phi_c = \frac{n_2}{n_1} \tag{2.18}$$

Example 2.1 Using $n_1 = 1.48$ for glass and $n_2 = 1.00$ for air, ϕ_c is about 42.5° Any light in the glass incident on the interface at an angle ϕ_1 greater than 42.5° is totally reflected back into the glass.

In addition, when light is totally internally reflected, a phase change δ occurs in the reflected wave. This phase change depends on the angle $\theta_1 < \pi/2 - \phi_c$ according to the relationships[1]

$$\tan \frac{\delta_N}{2} = \frac{\sqrt{n^2 \cos^2 \theta_1 - 1}}{n \sin \theta_1} \qquad (2.19a)$$

$$\tan \frac{\delta_p}{2} = n \frac{\sqrt{n^2 \cos^2 \theta_1 - 1}}{\sin \theta_1} \qquad (2.19b)$$

Here, δ_N and δ_p are the phase shifts of the electric-field wave components normal and parallel to the plane of incidence, respectively, and $n = n_1/n_2$. These phase shifts are shown in Fig. 2.8 for a glass–air interface ($n = 1.5$ and $\phi_c = 42.5°$). The values range from zero immediately at the critical angle to $\pi/2 - \phi_c$ when $\phi_c = 90°$.

These basic optical principles will now be used to illustrate how optical power is transmitted along a fiber.

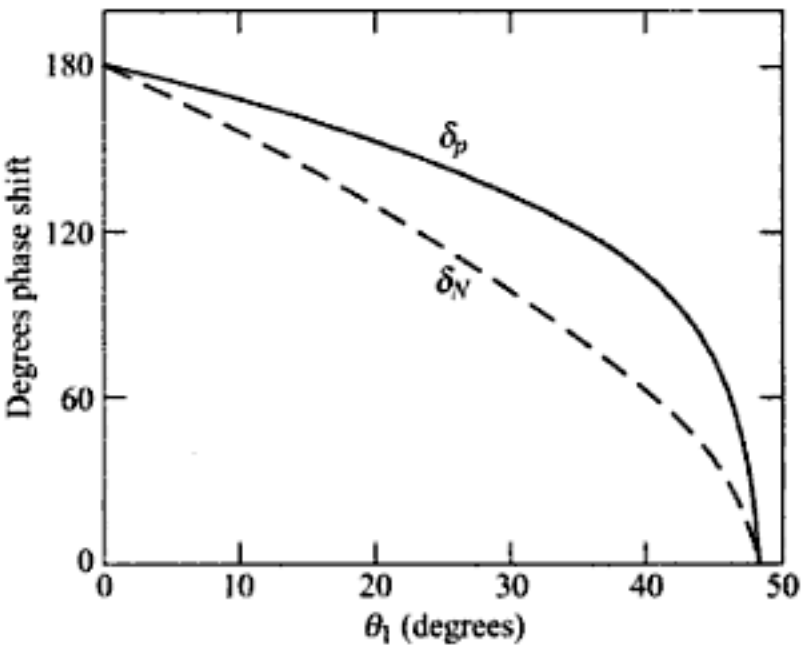

Fig. 2.8 *Phase shifts occurring from the reflection of wave components normal (δ_N) and parallel (δ_p) to the plane of incidence*

2.2.3 Polarization Components of Light

An ordinary lightwave consists of many transverse electromagnetic waves that vibrate in a variety of directions (i.e., in more than one plane) and is called *unpolarized light*. However, one can represent any arbitrary direction of vibration as a combination of a parallel vibration and a perpendicular vibration, as shown in Fig. 2.9. Therefore, one can consider unpolarized light as consisting of two orthogonal plane

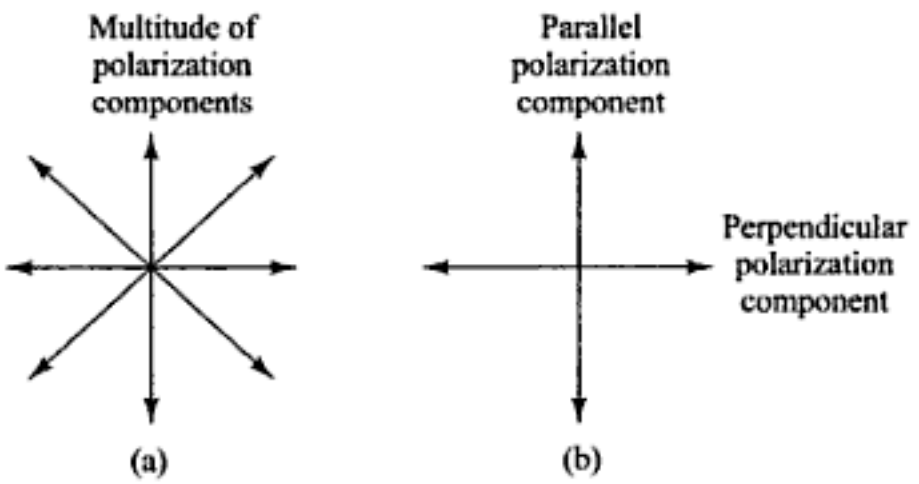

Fig. 2.9 *Polarization represented as a combination of a parallel vibration and a perpendicular vibration*

polarization components, one that lies in the plane of incidence (the plane containing the incident and reflected rays) and the other of which lies in a plane perpendicular to the plane of incidence. These are the *parallel polarization* and the *perpendicular polarization* components, respectively. In the case when all the electric field planes of the different transverse waves are aligned parallel to each other, then the lightwave is linearly polarized. This is the simplest type of polarization, as Sec. 2.1.1 describes.

Unpolarized light can be split into separate polarization components either by reflection off of a nonmetallic surface or by refraction when the light passes from one material to another. As noted in Fig. 2.6, when an unpolarized light beam travelling in air impinges on a nonmetallic surface such as glass, part of the beam is reflected and part is refracted into the glass. A circled dot and an arrow designate the parallel and perpendicular polarization components, respectively, in Fig. 2.10. The reflected beam is partially polarized and at a specific angle (known as the *Brewster's angle*) the reflected light is completely perpendicularly polarized. The parallel component of the refracted beam is transmitted entirely into the glass, whereas the perpendicular component is only partially refracted. How much of the refracted light is polarized depends on the angle at which the light approaches the surface and on the material composition.

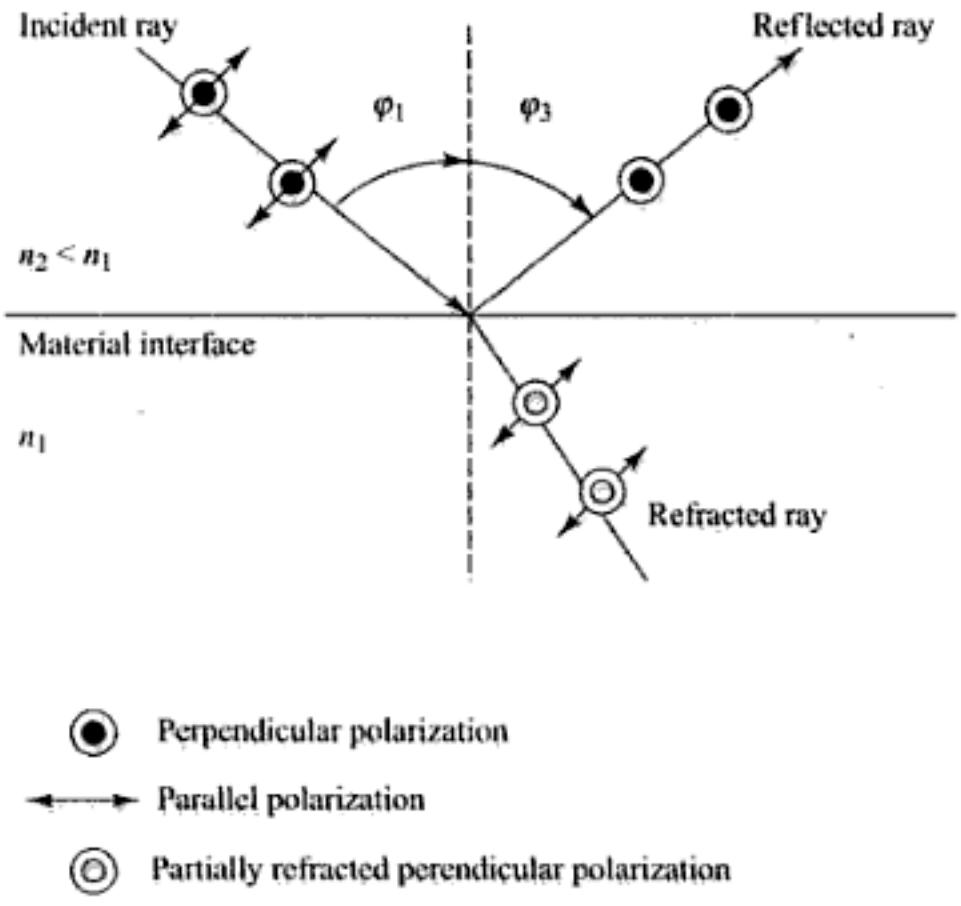

Fig. 2.10 *Behavior of an unpolarized light beam at the interface between air and a nonmetallic surface*

2.2.4 Polarization-Sensitive Materials

The polarization characteristics of light are important when examining the behavior of components such as optical isolators and light filters. Here we look at three polarization-sensitive materials or devices that are used in such components. These are polarizers, Faraday rotators, and birefringent crystals.

A *polarizer* is a material or device that transmits only one polarization component and blocks the other. For example, in the case when unpolarized light enters a polarizer that has a vertical transmission axis as shown in Fig. 2.11, only the vertical polarization component passes through the device. A familiar example of this concept is the use of polarizing sunglasses to reduce the glare of partially polarized sunlight reflections from road or water surfaces. To see the polarization property of the sunglasses, a number of glare spots will appear when users tilt their head sideways. The polarization filters in the sunglasses block out the polarized light coming from these glare spots when the head is held normally.

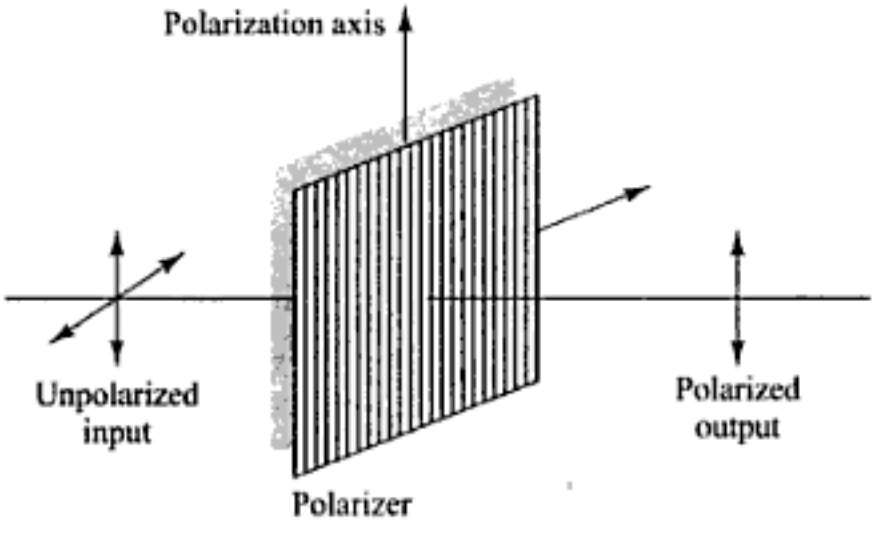

Fig. 2.11 *Only the vertical polarization component passes through a vertically oriented polarizer*

A *Faraday rotator* is a device that rotates the *state of polarization* (SOP) of light passing through it by a specific amount. For example a popular device rotates the SOP clockwise by 45° or a quarter of a wavelength, as shown in Fig. 2.12.

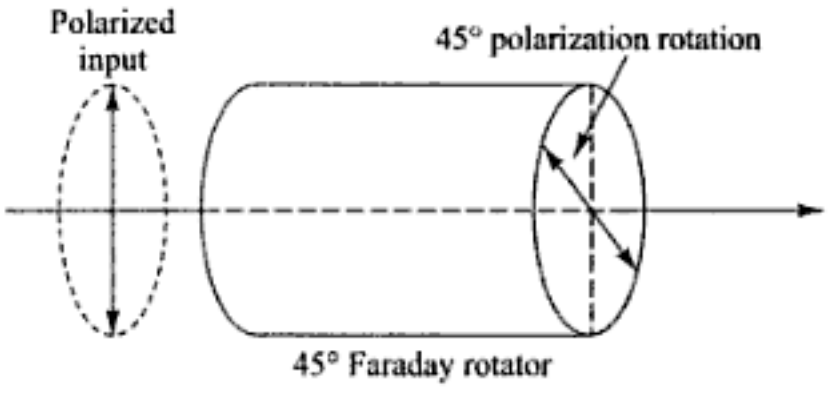

Fig. 2.12 *A Faraday rotator is a device that rotates the state of polarization clockwise by 45° or a quarter of a wavelength*

This rotation is independent of the SOP of input light, but the rotation angle is different depending on the direction in which the light passes through the device. That is, the rotation process is not reciprocal. In this process, the SOP of the input light is maintained after the rotation. For example, if the input light to a 45° Faraday rotator is linearly polarized in a vertical direction, then the rotated light exiting the crystal also is linearly polarized at a 45° angle. The Faraday rotator material usually is an asymmetric crystal such as yttrium iron garnet (YIG) and the degree of angular rotation is proportional to the thickness of the device.

Birefringent or *double-refractive crystals* have a property called *double refraction*. This means that the indices of refraction are slightly different along two perpendicular axes of the crystal as shown in Fig. 2.13. A device made from such materials is known as a *spatial walk-off polarizer* (SWP). The SWP

splits the light signal entering it into two orthogonally (perpendicularly) polarized beams. One of the beams is called an *ordinary ray* or o-ray, since it obeys Snell's law of refraction at the crystal surface. The second beam is called the *extraordinary ray* or e-ray, since it refracts at an angle that deviates from the prediction of the standard form of Snell's law. Each of the two orthogonal polarization components thus is refracted at a different angle as shown in Fig. 2.13. For example, if the incident unpolarized light arrives at an angle perpendicular to the surface of the device, the o-ray can pass straight through the device whereas the e-ray component is deflected at a slight angle so it follows a different path through the material.

Table 2.1 lists the ordinary index n_o and the extra-ordinary index n_e of some common birefringent crystals that are used in optical communication components and gives some of their applications.

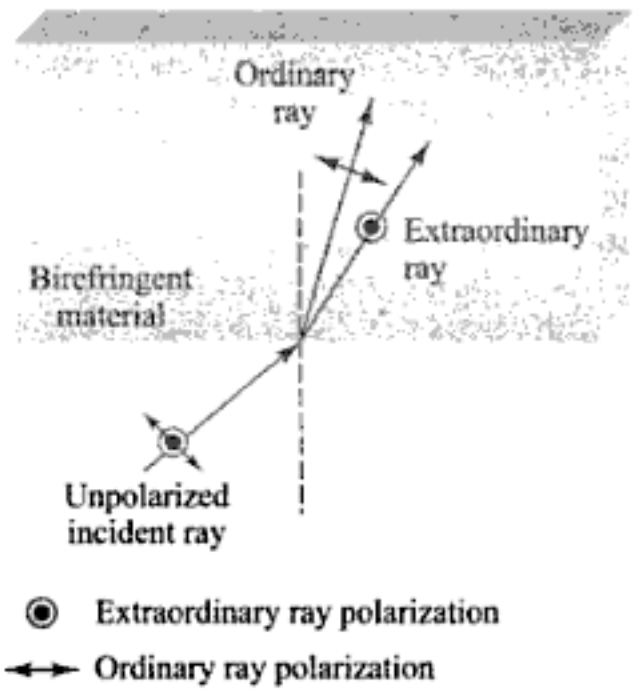

Fig. 2.13 *A birefringent crystal splits the light signal entering it into two perpendicularly polarized beams*

Table 2.1 *Common birefringent crystals and some applications*

Crystal name	*Symbol*	n_o	n_e	*Applications*
Calcite	$CaCO_3$	1.658	1.486	Polarization controllers and beamsplitters
Lithium niobate	$LiNbO_3$	2.286	2.200	Light signal modulators
Rutile	TiO_2	2.616	2.903	Optical isolators and circulators
Yttrium vanadate	YVO_4	1.945	2.149	Optical isolators, circulators, and beam displacers

2.3 Optical Fiber Modes and Configurations

Before going into details on optical fiber characteristics, this section first presents a brief overview of the underlying concepts of optical fiber modes and optical fiber configurations. The discussions in Sec. 2.3 through 2.7 address conventional optical fibers, which consist of solid dielectric structures. Section 2.8 describes the structure of photonic crystal fibers, which can be created to have a variety of internal microstructures. Chapter 3 describes the operational characteristics of both categories of fibers.

2.3.1 Fiber Types

An optical fiber is a dielectric waveguide that operates at optical frequencies. This fiber waveguide is normally cylindrical in form. It confines electromagnetic energy in the form of light to within its surfaces and guides the light in a direction parallel to its axis. The transmission properties of an optical waveguide

are dictated by its structural characteristics, which have a major effect in determining how an optical signal is affected as it propagates along the fiber. The structure basically establishes the information-carrying capacity of the fiber and also influences the response of the waveguide to environmental perturbations.

The propagation of light along a waveguide can be described in terms of a set of guided electromagnetic waves called the *modes* of the waveguide. These guided modes are referred to as the *bound* or *trapped* modes of the waveguide. Each guided mode is a pattern of electric and magnetic field distributions that is repeated along the fiber at equal intervals. Only a certain discrete number of modes are capable of propagating along the guide. As will be seen in Sec. 2.4, these modes are those electromagnetic waves that satisfy the homogeneous wave equation in the fiber and the boundary condition at the waveguide surfaces.

Although many different configurations of the optical waveguide have been discussed in the literature,[3] the most widely accepted structure is the single solid dielectric cylinder of radius a and index of refraction n_1 shown in Fig. 2.14. This cylinder is known as the *core* of the fiber. The core is surrounded by a solid dielectric *cladding* which has a refractive index n_2 that is less than n_1. Although, in principle, a cladding is not necessary for light to propagate along the core of the fiber, it serves several purposes. The cladding reduces scattering loss that results from dielectric discontinuities at the core surface, it adds mechanical strength to the fiber, and it protects the core from absorbing surface contaminants with which it could come in contact.

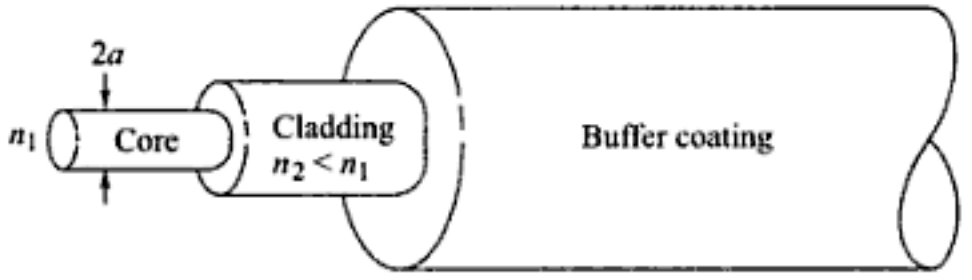

Fig. 2.14 *Schematic of a conventional silica fiber structure. A circular solid core of refractive index n_1 is surrounded by a cladding having a refractive index $n_2 < n_1$. An elastic plastic buffer encapsulates the fiber*

In standard optical fibers the core material is highly pure silica glass (SiO_2) and is surrounded by a glass cladding. Higher-loss plastic-core fibres with plastic claddings are also widely in use. In addition, most fibers are encapsulated in an elastic, abrasion-resistant plastic material. This material adds further strength to the fiber and mechanically isolates or buffers the fibers from small geometrical irregularities, distortions, or roughnesses of adjacent surfaces. These perturbations could otherwise cause scattering losses induced by random microscopic bends that can arise when the fibers are incorporated into cables or supported by other structures.

Variations in the material composition of the core give rise to the two commonly used fiber types shown in Fig. 2.15. In the first case, the refractive index of the core is uniform throughout and undergoes an abrupt change (or step) at the cladding boundary. This is called a *step-index fiber.* In the second case, the core refractive index is made to vary as a function of the radial distance from the center of the fiber. This type is a *graded-index fiber.*

Both the step- and the graded-index fibers can be further divided into single-mode and multimode classes. As the name implies, a single-mode fiber sustains only one mode of propagation, whereas multimode fibers contain many hundreds of modes. A few typical sizes of single- and multimode fibers

are given in Fig. 2.15 to provide an idea of the dimensional scale. Multimode fibers offer several advantages compared with single-mode fibers. As we shall see in Chapter 5, the larger core radii of multimode fibers make it easier to launch optical power into the fiber and facilitate the connecting together of similar fibers. Another advantage is that light can be launched into a multimode fiber using a light-emitting-diode (LED) source, whereas single-mode fibers must generally be excited with laser diodes. Although LEDs have less optical output power than laser diodes (as we shall discuss in Chapter 4), they are easier to make, are less expensive, require less complex circuitry, and have longer lifetimes than laser diodes, thus making them more desirable in certain applications.

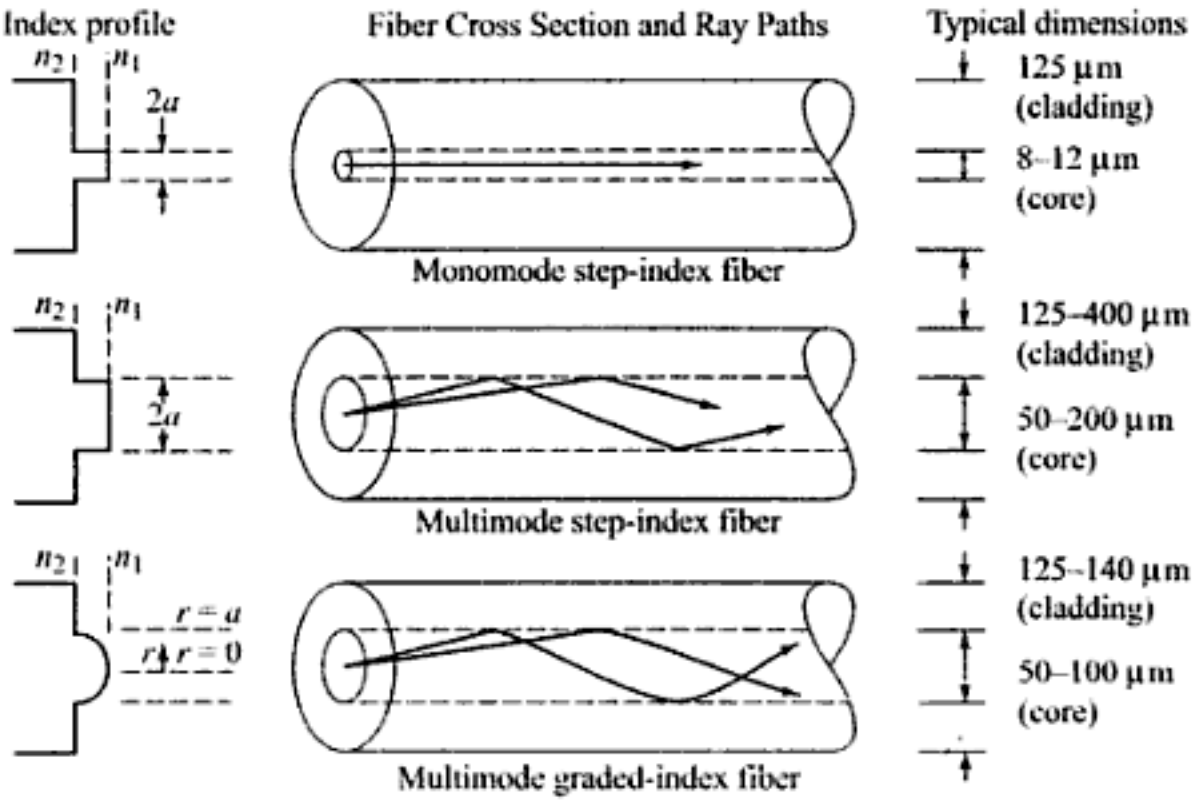

Fig. 2.15 *Comparison of conventional single-mode and multimode step-index and graded-index optical fibers*

A disadvantage of multimode fibers is that they suffer from intermodal dispersion. We shall describe this effect in detail in Chapter 3. Briefly, intermodal dispersion can be described as follows. When an optical pulse is launched into a fiber, the optical power in the pulse is distributed over all (or most) of the modes of the fiber. Each of the modes that can propagate in a multimode fiber travels at a slightly different velocity. This means that the modes in a given optical pulse arrive at the fiber end at slightly different times, thus causing the pulse to spread out in time as it travels along the fiber. This effect, which is known as *intermodal dispersion* or *intermodal distortion,* can be reduced by using a graded-index profile in a fiber core. This allows graded-index fibers to have much larger bandwidths (data rate transmission capabilities) then step-index fibers. Even higher band-widths are possible in single-mode fibers, where intermodal dispersion effects are not present.

2.3.2 Rays and Modes

The electromagnetic light field that is guided along an optical fiber can be represented by a superposition of bound or trapped modes. Each of these guided modes consists of a set of simple electromagnetic field

configurations. For monochromatic light fields of radian frequency ω, a mode traveling in the positive z direction (i.e., along the fiber axis) has a time and z dependence given by

$$e^{j(\omega t-\beta z)}$$

The factor β is the z component of the wave propagation constant $k = 2\pi/\lambda$ and is the main parameter of interest in describing fiber modes. For guided modes, β can assume only certain discrete values, which are determined from the requirement that the mode field must satisfy Maxwell's equations and the electric and magnetic field boundary conditions at the core-cladding interface. This is described in detail in Sec. 2.4.

Another method for theoretically studying the propagation characteristics of light in an optical fiber is the geometrical optics or ray-tracing approach. This method provides a good approximation to the light acceptance and guiding properties of optical fibers when the ratio of the fiber radius to the wavelength is large. This is known as the *small-wavelength limit*. Although the ray approach is strictly valid only in the zero-wavelength limit, it is still relatively accurate and extremely valuable for nonzero wavelengths when the number of guided modes is large; that is, for multimode fibers. The advantage of the ray approach is that, compared with the exact electromagnetic wave (modal) analysis, it gives a more direct physical interpretation of the light propagation characteristics in an optical fiber.

Since the concept of a light ray is very different from that of a mode, let us see qualitatively what the relationship is between them. (The mathematical details of this relationship are beyond the scope of this book but can be found in the literature.[4-6]) A guided mode traveling in the z direction (along the fiber axis) can be decomposed into a family of superimposed plane waves that collectively form a standing-wave pattern in the direction transverse to the fiber axis. That is, the phases of the plane waves are such that the envelope of the collective set of waves remains stationary. Since with any plane wave we can associate a light ray that is perpendicular to the phase front of the wave, the family of plane waves corresponding to a particular mode forms a set of rays called a *ray congruence*. Each ray of this particular set travels in the fiber at the same angle relative to the fiber axis. We note here that, since only a certain number M of discrete guided modes exist in a fiber, the possible angles of the ray congruences corresponding to these modes are also limited to the same number M. Although a simple ray picture appears to allow rays at any angle greater than the critical angle to propagate in a fiber, the allowable quantized propagation angles result when the phase condition for standing waves is introduced into the ray picture. This is discussed further in Sec. 2.3.5.

Despite the usefulness of the approximate geometrical optics method, a number of limitations and discrepancies exist between it and the exact modal analysis. An important case is the analysis of single-mode or few-mode fibers, which must be dealt with by using electromagnetic theory. Problems involving coherence or interference phenomena must also be solved with an electromagnetic approach. In addition, a modal analysis is necessary when a knowledge of the field distribution of individual modes is required. This arises, for example, when analyzing the excitation of an individual mode or when analyzing the coupling of power between modes at waveguide imperfections (which we shall discuss in Chapter 3).

Another discrepancy between the ray optics approach and the modal analysis occurs when an optical fiber is uniformly bent with a constant radius of curvature. As shown in Chapter 3, wave optics correctly predicts that every mode of the curved fiber experiences some radiation loss. Ray optics, on the other hand, erroneously predicts that some ray congruences can undergo total internal reflection at the curve and, consequently, can remain guided without loss.

2.3.3 Step-Index Fiber Structure

We begin our discussion of light propagation in an optical waveguide by considering the step-index fiber. In practical step-index fibers the core of radius a has a refractive index n_1 which is typically equal to 1.48. This is surrounded by a cladding of slightly lower index n_2, where

$$n_2 = n_1(1 - \Delta) \tag{2.20}$$

The parameter Δ is called the *core-cladding index difference* or simply the *index difference.* Values of n_2 are chosen such that Δ is nominally 0.01. Typical values range from 1 to 3 percent for multimode fibers and from 0.2 to 1.0 percent for single-mode fibers. Since the core refractive index is larger than the cladding index, electromagnetic energy at optical frequencies is made to propagate along the fiber waveguide through internal reflection at the core–cladding interface.

2.3.4 Ray Optics Representation

Since the core size of multimode fibers is much larger than the wavelength of the light we are interested in (which is approximately 1 μm), an intuitive picture of the propagation mechanism in an ideal multimode step-index optical waveguide is most easily seen by a simple ray (geometrical) optics representation.[6-11] For simplicity, in this analysis we shall consider only a particular ray belonging to a ray congruence which represents a fiber mode. The two types of rays that can propagate in a fiber are meridional rays and skew rays. *Meridional rays* are confined to the meridian planes of the fiber, which are the planes that contain the axis of symmetry of the fiber (the core axis). Since a given meridional ray lies in a single plane, its path is easy to track as it travels along the fiber. Meridional rays can be divided into two general classes: bound rays that are trapped in the core and propagate along the fiber axis according to the laws of geometrical optics, and unbound rays that are refracted out of the fiber core.

Skew rays are not confined to a single plane, but instead tend to follow a helical-type path along the fiber as shown in Fig. 2.16. These rays are more difficult to track as they travel along the fiber, since they do not lie in a single plane. Although skew rays constitute a major portion of the total number of guided rays, their analysis is not necessary to obtain a general picture of rays propagating in a fiber. The examination of meridional rays will suffice for this purpose. However, a detailed inclusion of skew rays will change such expressions as the light-acceptance ability of the fiber and power losses of light traveling along a waveguide.[6, 10]

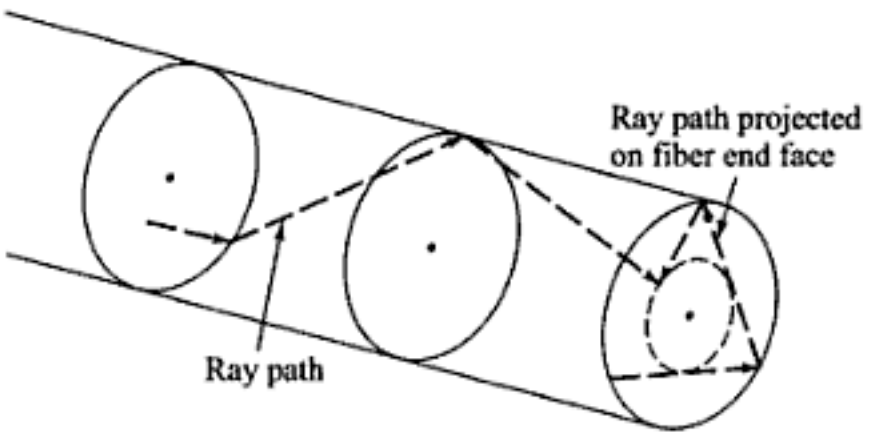

Fig. 2.16 *Ray optics representation of skew rays traveling in a step-index optical fiber core*

A greater power loss arises when skew rays are included in the analyses, since many of the skew rays that geometric optics predicts to be trapped in the fiber are actually leaky rays.[5, 12, 13] These leaky rays are only partially confined to the core of the circular optical fiber and attenuate as the light travels along the optical waveguide. This partial reflection of leaky rays cannot be described by pure ray theory alone. Instead, the analysis of radiation loss arising from these types of rays must be described by mode theory. This is explained further in Sec. 2.4.

The meridional ray is shown in Fig. 2.17 for a step-index fiber. The light ray enters the fiber core from a medium of refractive index n at an angle θ_0 with respect to the fiber axis and strikes the core–cladding interface at a normal angle ϕ. If it strikes this interface at such an angle that it is totally internally reflected, then the meridional ray follows a zigzag path along the fiber core, passing through the axis of the guide after each reflection.

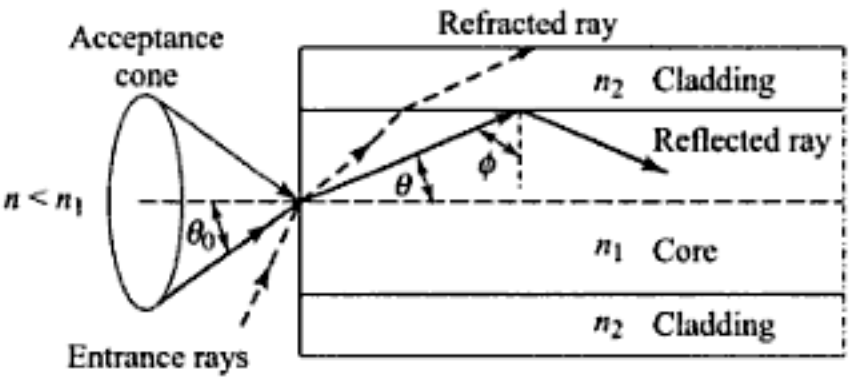

Fig. 2.17 *Meridional ray optics representation of the propagation mechanism in an ideal step-index optical waveguide*

From Snell's law, the minimum angle ϕ_{min} that supports total internal reflection for the meridional ray is given by

$$\sin \phi_{min} = \frac{n_2}{n_1} \tag{2.21}$$

Rays striking the core–cladding interface at angles less than ϕ_{min} will refract out of the core and be lost in the cladding. By applying Snell's law to the air-fiber face boundary, the condition of Eq. (2.21) can be related to the maximum entrance angle $\theta_{0,\,max}$ through the relationship

$$n \sin \theta_{0,\,max} = n_1 \sin \theta_c = \left(n_1^2 - n_2^2\right)^{1/2} \tag{2.22}$$

where $\theta_c = \pi/2 - \phi_c$. Thus, those rays having entrance angles θ_0 less than $\theta_{0,\,max}$ will be totally internally reflected at the core-cladding interface.

Equation (2.22) also defines the *numerical aperture* (NA) of a step-index fiber for meridional rays:

$$\text{NA} = n \sin \theta_{0,\,max} = \left(n_1^2 - n_2^2\right)^{1/2} \approx n_1\sqrt{2\Delta} \tag{2.23}$$

The approximation on the right-hand side is valid for the typical case where Δ, as defined by Eq. (2.20), is much less than 1. Since the numerical aperture is related to the maximum acceptance angle, it is commonly used to describe the light acceptance or gathering capability of a fiber and to calculate source-to-fiber optical power coupling efficiencies. This is detailed in Chapter 5. The numerical aperture is a dimensionless quantity which is less than unity, with values normally ranging from 0.14 to 0.50.

Example 2.2 Consider a multimode silica fiber that has a core refractive index $n_1 = 1.48$ and a cladding index $n_2 = 1.46$.

(a) From Eq. (2.21) the critical angle is given by

$$\varphi_c = \sin^{-1}\frac{n_2}{n_1} = \sin^{-1}\frac{1.46}{1.48} = 80.5°$$

(b) From Eq. (2.23) the numerical aperture is NA = 0.242

(c) From Eq. (2.22) the acceptance angle in air is

$$\theta_{0,\,max} = \sin^{-1}\text{NA} = \sin^{-1}0.242 = 14°$$

2.3.5 Wave Representation in a Dielectric Slab Waveguide

Referring to Fig. 2.17, the ray theory appears to allow rays at any angle ϕ greater than the critical angle ϕ_c to propagate along the fiber. However, when the interference effect due to the phase of the plane wave associated with the ray is taken into account, it is seen that only waves at certain discrete angles greater than or equal to ϕ_c are capable of propagating along the fiber.

To see this, let us consider wave propagation in an infinite dielectric slab waveguide of thickness d. Its refractive index n_1 is greater than the index n_2 of the material above and below the slab. A wave will thus propagate in this guide through multiple reflections, provided that the angle of incidence with respect to the upper and lower surfaces satisfies the condition given in Eq. (2.22).

Figure 2.18 shows the geometry of the waves reflecting at the material interfaces. Here, we consider two rays, designated ray 1 and ray 2, associated with the same wave. The rays are incident on the material interface at an angle $\theta < \theta_c = \pi/2 - \phi_c$. The ray paths in Fig. 2.18 are denoted by solid lines and their associated constant-phase fronts by dashed lines.

The condition required for wave propagation in the dielectric slab is that all points on the same phase front of a plane wave must be in phase. This means that the phase change occurring in ray 1 when travelling from point A to point B minus the phase change in ray 2 between points C and D must differ by an integer multiple of 2π. As the wave travels through the material, it undergoes a phase shift Δ given by

$$\Delta = k_1 s = n_1 k s = n_1 2\pi s/\lambda$$

where k_1 = the propagation constant in the medium of refractive index n_1
$k = k_1/n_1$ is the free-space propagation constant
s = the distance the wave has traveled in the material

The phase of the wave changes not only as the wave travels but also upon reflection from a dielectric interface, as described in Sec. 2.2.

In going from point A to point B, ray 1 travels a distance $s_1 = d/\sin\theta$ in the material, and undergoes two phase changes δ at the reflection points. Ray 2 does not incur any reflections in going from point C to point D. To determine its phase change, first note that the distance from point A to point D is $\overline{AD} = (d/\tan\theta) - d\tan\theta$. Thus, the distance between points C and D is

$$s_2 = \overline{AD}\cos\theta = (\cos^2\theta - \sin^2\theta)\, d/\sin\theta$$

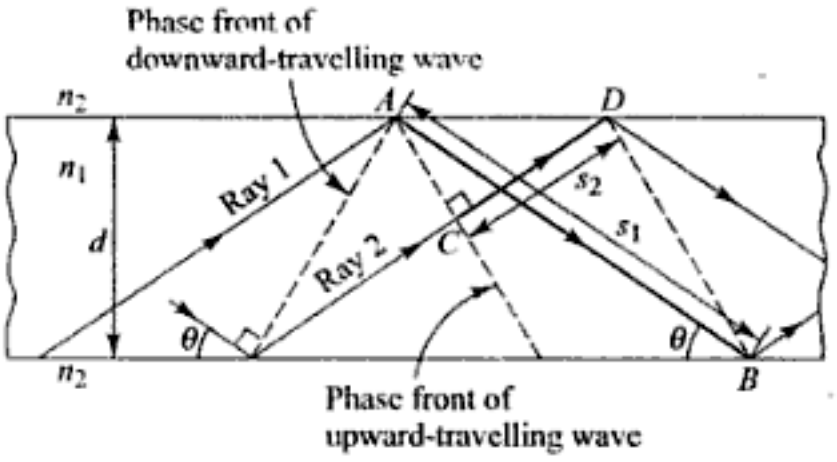

Fig. 2.18 *Light wave propagating along a fiber waveguide. Phase changes occur both as the wave travels through the fiber medium and at the reflection points*

The requirement for wave propagation can then be written as

$$\frac{2\pi n_1}{\lambda}(s_1 - s_2) + 2\delta = 2\pi m \tag{2.24a}$$

where $m = 0, 1, 2, 3, \ldots$. Substituting the expressions for s_1 and s_2 into Eq. (2.24*a*) then yields

$$\frac{2\pi n_1}{\lambda}\left\{\frac{d}{\sin\theta} - \left[\frac{(\cos^2\theta - \sin^2\theta)d}{\sin\theta}\right]\right\} + 2\delta = 2\pi m \tag{2.24b}$$

which can be reduced to

$$\frac{2\pi n_1 d \sin\theta}{\lambda} + \delta = \pi m \tag{2.24c}$$

Considering only electric waves with components normal to the plane of incidence, we have from Eq. (2.19*a*) that the phase shift upon reflection is

$$\delta = -2\arctan\left[\frac{\sqrt{\cos^2\theta - \left(n_2^2/n_1^2\right)}}{\sin\theta}\right] \tag{2.25}$$

The negative sign is needed here since the wave in the medium must be a decaying and not a growing wave. Substituting this expression into Eq. (2.24c) yields

$$\frac{2\pi n_1 d \sin\theta}{\lambda} - \pi m = 2\arctan\left[\frac{\sqrt{\cos^2\theta - \left(n_2^2/n_1^2\right)}}{\sin\theta}\right] \tag{2.26a}$$

or

$$\tan\left(\frac{\pi n_1 d \sin\theta}{\lambda} - \frac{\pi m}{2}\right) = \left[\frac{\sqrt{n_1^2\cos^2\theta - n_2^2}}{n_1 \sin\theta}\right] \tag{2.26b}$$

Thus, only waves that have those angles θ which satisfy the condition in Eq. (2.26) will propagate in the dielectric slab waveguide (see Prob. 2.13).

2.4 Mode Theory for Circular Waveguides

To attain a more detailed understanding of the optical power propagation mechanism in a fiber, it is necessary to solve Maxwell's equations subject to the cylindrical boundary conditions at the interface between the core and the cladding of the fiber. This has been done in extensive detail in a number of works.[7, 10, 14–18] Since a complete treatment is beyond the scope of this book, only a general outline of a simplified (but still complex) analysis will be given here.

Before presenting the basic mode theory in circular optical fibers, in Sec. 2.4.1 we first give a qualitative overview of the concepts of modes in a waveguide. Next, Sec. 2.4.2 presents a brief summary of the fundamental results obtained from the analyses in Secs. 2.4.3 through 2.4.9, so that those who are not familiar with Maxwell's equations can skip over those sections designated by a star (*) without loss of continuity.

When solving Maxwell's equations for hollow metallic waveguides, only transverse electric (TE) modes and transverse magnetic (TM) modes are found. However, in optical fibers the core–cladding boundary conditions lead to a coupling between the electric and magnetic field components. This gives rise to hybrid modes, which makes optical waveguide analysis more complex than metallic waveguide analysis. The hybrid modes are designated as HE or EH modes, depending on whether the transverse electric field (the E field) or the transverse magnetic field (the H field) is larger for that mode. The two lowest-order modes are designated by HE_{11} and TE_{01}, where the subscripts refer to possible modes of propagation of the optical field.

Although the theory of light propagation in optical fibers is well understood, a complete description of the guided and radiation modes is rather complex since it involves six-component hybrid electromagnetic fields that have very involved mathematical expressions. A simplification[19–23] of these expressions can be carried out, in practice, since fibers usually are constructed so that the difference in the core and cladding indices of refraction is very small; that is, $n_1 - n_2 \ll 1$. With this assumption, only four field components need to be considered and their expressions become significantly simpler. The field components are called *linearly polarized* (LP) modes and are labeled LP_{jm} where j and m are integers designating mode solutions. In this scheme for the lowest-order modes, each LP_{0m} mode is derived from an HE_{1m} mode and each LP_{1m} mode comes from TE_{0m}, TM_{0m}, and HE_{0m} modes. Thus, the fundamental LP_{01} mode corresponds to an HE_{11} mode.

Although the analysis required for even these simplifications is still fairly involved, this material is key to understanding the principles of optical fiber operation. In Secs. 2.4.3 through 2.4.9 we first will solve Maxwell's equations for a circular step-index waveguide and then will describe the resulting solutions for some of the lower-order modes.

2.4.1 Overview of Modes

Before we progress with a discussion of mode theory in circular optical fibers, let us qualitatively examine the appearance of modal fields in the planar dielectric slab waveguide shown in Fig. 2.19. The core of this waveguide is a dielectric slab of index n_1 that is sandwiched between two dielectric layers which have refractive indices $n_2 < n_1$. These surrounding layers are called the *cladding*. This represents the simplest form of an optical waveguide and can serve as a model to gain an understanding of wave propagation in optical fibers. In fact, a cross-sectional view of the slab waveguide looks the same as the cross sectional view of an optical fiber cut along its axis. Figure 2.19 shows the field patterns of several of the lower-order transverse electric (TE) modes (which are solutions of Maxwell's equations for the slab waveguide[7–10]). The *order* of a mode is equal to the number of field zeros across the guide. The order of the mode is also related to the angle that the ray congruence corresponding to this mode makes with the plane of the waveguide (or the axis of a fiber); that is, the steeper the angle, the higher the order of the mode. The plots show that the electric fields of the guided modes are not completely confined to the central dielectric slab (i.e., they do not go to zero at the guide–cladding interface), but, instead, they extend partially into the cladding. The fields vary harmonically in the guiding region of refractive index n_1 and decay exponentially outside of this region. For low-order modes the fields are tightly concentrated near the center of the slab (or the axis of an optical fiber), with little penetration into the cladding region. On the other hand, for higher-order modes the fields are distributed more toward the edges of the guide and penetrate farther into the cladding region.

Solving Maxwell's equations shows that, in addition to supporting a finite number of guided modes, the optical fiber waveguide has an infinite continuum of *radiation modes* that are not trapped in the core and guided by the fiber but are still solutions of the same boundary-value problem. The radiation field

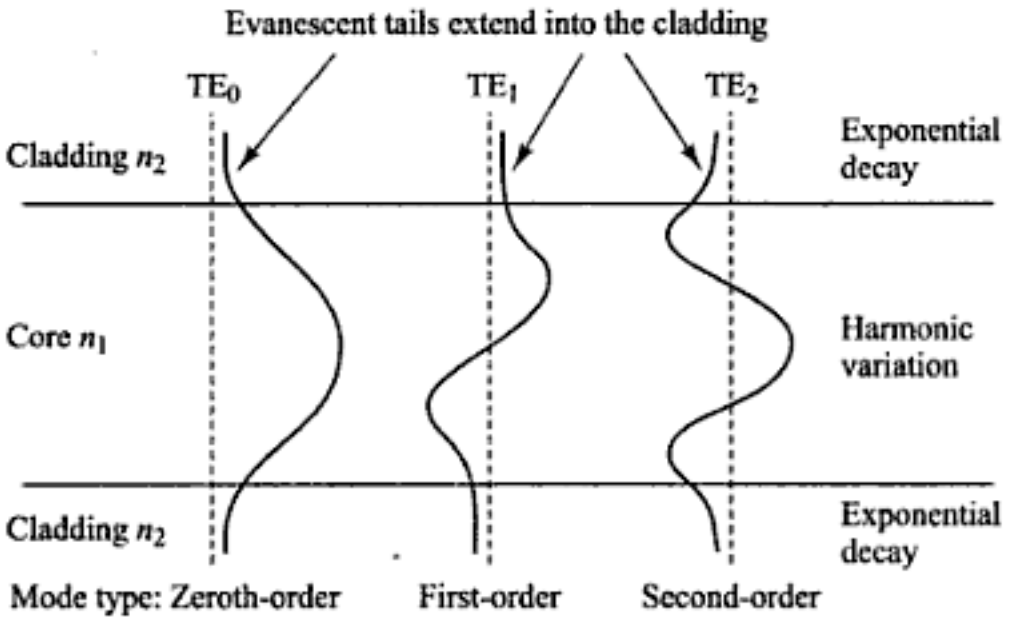

Fig. 2.19 *Electric field distributions for several of the lower-order guided modes in a symmetrical-slab waveguide*

basically results from the optical power that is outside the fiber acceptance angle being refracted out of the core. Because of the finite radius of the cladding, some of this radiation gets trapped in the cladding, thereby causing cladding modes to appear. As the core and cladding modes propagate along the fiber, mode coupling occurs between the cladding modes and the higher-order core modes. This coupling occurs because the electric fields of the guided core modes are not completely confined to the core but extend partially into the cladding (see Fig. 2.19) and likewise for the cladding modes. A diffusion of power back and forth between the core and cladding modes thus occurs; this generally results in a loss of power from the core modes. In practice, the cladding modes will be suppressed by a lossy coating which covers the fiber or they will scatter out of the fiber after traveling a certain distance because of roughness on the cladding surface.

In addition to bound and refracted modes, a third category of modes called *leaky* modes[5, 6, 8, 12, 13] is present in optical fibers. These leaky modes are only partially confined to the core region, and attenuate by continuously radiating their power out of the core as they propagate along the fiber. This power radiation out of the waveguide results from a quantum mechanical phenomenon known as the *tunnel effect*. Its analysis is fairly lengthy and beyond the scope of this book. However, it is essentially based on the upper and lower bounds that the boundary conditions for the solutions of Maxwell's equations impose on the propagation factor β. A mode remains guided as long as β satisfies the condition

$$n_2 k < \beta < n_1 k$$

where n_1 and n_2 are the refractive indices of the core and cladding, respectively, and $k = 2\pi/\lambda$. The boundary between truly guided modes and leaky modes is defined by the *cutoff condition* $\beta = n_2 k$. As soon as β becomes smaller than $n_2 k$, power leaks out of the core into the cladding region. Leaky modes can carry significant amounts of optical power in short fibers. Most of these modes disappear after a few centimeters, but a few have sufficiently low losses to persist in fiber lengths of a kilometer.

2.4.2 Summary of Key Modal Concepts

An important parameter connected with the cutoff condition is the *V number* defined by

$$V = \frac{2\pi a}{\lambda}\left(n_1^2 - n_2^2\right)^{1/2} = \frac{2\pi a}{\lambda}\mathrm{NA} \tag{2.27}$$

This is a dimensionless number that determines how many modes a fiber can support. Except for the lowest-order HE_{11} mode, each mode can exist only for values of V that exceed a certain limiting value (with each mode having a different V limit). The modes are cut off when $\beta = n_2 k$. This occurs when $V \leq 2.405$. The HE_{11} mode has no cutoff and ceases to exist only when the core diameter is zero. This is the principle on which single-mode fibers are based. The details for these and other modes are given in Sec. 2.4.7.

The V number also can be used to express the number of modes M in a multimode fiber when V is large. For this case, an estimate of the total number of modes supported in a fiber is

$$M \approx \frac{1}{2}\left(\frac{2\pi a}{\lambda}\right)^2 (n_1^2 - n_2^2) = \frac{V^2}{2} \tag{2.28}$$

Since the field of a guided mode extends partly into the cladding, as shown in Fig. 2.19, a final quantity of interest for a step-index fiber is the fractional power flow in the core and cladding for a given mode. As the V number approaches cutoff for any particular mode, more of the power of that mode is in the cladding. At the cutoff point, the mode becomes radiative with all the optical power of the mode residing in the cladding. Far from cutoff—that is, for large values of V—the fraction of the average optical power residing in the cladding can be estimated by

$$\frac{P_{\text{clad}}}{P} \approx \frac{4}{3\sqrt{M}} \tag{2.29}$$

where P is the total optical power in the fiber. The details for the power distribution between the core and the cladding of various LP_{jm} modes are given in Sec. 2.4.9. Note that since M is proportional to V^2, the power flow in the cladding decreases as V increases. However, this increases the number of modes in the fiber, which is not desirable for a high-bandwidth capability.

2.4.3 Maxwell's Equations*

To analyze the optical waveguide we need to consider Maxwell's equations that give the relationships between the electric and magnetic fields. Assuming a linear, isotropic dielectric material having no currents and free charges, these equations take the form[2]

$$\nabla \times \mathbf{E} = -\frac{\partial \mathbf{B}}{\partial t} \tag{2.30a}$$

$$\nabla \times \mathbf{H} = \frac{\partial \mathbf{D}}{\partial t} \tag{2.30b}$$

$$\nabla \cdot \mathbf{D} = 0 \tag{2.30c}$$

$$\nabla \cdot \mathbf{B} = 0 \tag{2.30d}$$

where $\mathbf{D} = \epsilon \mathbf{E}$ and $\mathbf{B} = \mu \mathbf{H}$. The parameter ϵ is the permittivity (or dielectric constant) and μ is permeability of the medium.

A relationship defining the wave phenomena of the electromagnetic fields can be derived from Maxwell's equations. Taking the curl of Eq. (2.30a) and making use of Eq. (2.30b) yields

$$\nabla \times (\nabla \times \mathbf{E}) = -\mu \frac{\partial}{\partial t}(\nabla \times \mathbf{H}) = -\epsilon \mu \frac{\partial^2 \mathbf{E}}{\partial t^2} \tag{2.31a}$$

Using the vector identity (see App. B),

$$\nabla \times (\nabla \times \mathbf{E}) = \nabla(\nabla \cdot \mathbf{E}) - \nabla^2 \mathbf{E}$$

and using Eq. (2.30*c*) (i.e., $\nabla \cdot \mathbf{E} = 0$), Eq. (2.31*a*) becomes

$$\nabla^2 \mathbf{E} = \epsilon \mu \frac{\partial^2 \mathbf{E}}{\partial t^2} \tag{2.31b}$$

Similarly, by taking the curl of Eq. (2.30*b*), it can be shown that

$$\nabla^2 \mathbf{H} = \epsilon \mu \frac{\partial^2 \mathbf{H}}{\partial t^2} \tag{2.31c}$$

Equations (2.31*b*) and (2.31*c*) are the standard *wave equations.*

2.4.4 Waveguide Equations*

Consider electromagnetic waves propagating along the cylindrical fiber shown in Fig. 2.20. For this fiber, a cylindrical coordinate system $\{r, \phi, z\}$ is defined with the z axis lying along the axis of the waveguide. If the electromagnetic waves are to propagate along the z axis, they will have a functional dependence of the form

$$\mathbf{E} = \mathbf{E}_0(r, \phi)\, e^{j(\omega t - \beta z)} \tag{2.32a}$$

$$\mathbf{H} = \mathbf{H}_0(r, \phi)\, e^{j(\omega t - \beta z)} \tag{2.32b}$$

which are harmonic in time t and coordinate z. The parameter β is the z component of the propagation vector and will be determined by the boundary conditions on the electromagnetic fields at the core-cladding interface described in Sec. 2.4.6. When Eqs (2.32*a*) and (2.32*b*) are substituted into Maxwell's curl equations, we have, from Eq. (2.30*a*)

$$\frac{1}{r}\left(\frac{\partial E_z}{\partial \phi} + jr\beta E_\phi\right) = -j\omega\mu H_r \tag{2.33a}$$

$$j\beta E_r + \frac{\partial E_z}{\partial r} = j\omega\mu H_\phi \tag{2.33b}$$

$$\frac{1}{r}\left(\frac{\partial}{\partial r}(rE_\phi) - \frac{\partial E_r}{\partial \phi}\right) = -j\mu\omega H_z \tag{2.33c}$$

and, from Eq. (2.30*b*),

$$\frac{1}{r}\left(\frac{\partial H_z}{\partial \phi} + jr\beta H_\phi\right) = j\epsilon\omega E_r \tag{2.34a}$$

$$j\beta H_r + \frac{\partial H_z}{\partial r} = -j\epsilon\omega E_\phi \tag{2.34b}$$

$$\frac{1}{r}\left[\frac{\partial}{\partial r}(rH_\phi) - \frac{\partial H_r}{\partial \phi}\right] = j\epsilon\omega E_z \tag{2.34c}$$

By eliminating variables these equations can be rewritten such that, when E_z and H_z are known, the remaining transverse components E_r, E_ϕ, H_r, and H_ϕ can be determined. For example, E_ϕ or H_r can be eliminated from Eqs (2.33*a*) and (2.34*b*) so that the component H_ϕ or E_r, respectively, can be found in terms of E_z or H_z. Doing so yields

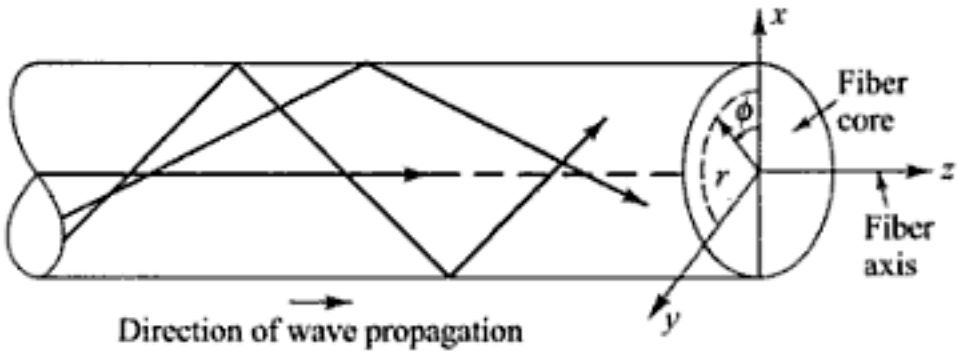

Fig. 2.20 *Cylindrical coordinate system used for analyzing electromagnetic wave propagation in an optical fiber*

$$E_r = -\frac{j}{q^2}\left(\beta\frac{\partial E_z}{\partial r} + \frac{\mu\omega}{r}\frac{\partial H_z}{\partial \phi}\right) \tag{2.35a}$$

$$E_\phi = -\frac{j}{q^2}\left(\frac{\beta}{r}\frac{\partial E_z}{\partial \phi} - \mu\omega\frac{\partial H_z}{\partial r}\right) \tag{2.35b}$$

$$H_r = \frac{-j}{q^2}\left(\beta\frac{\partial H_z}{\partial r} - \frac{\omega\epsilon}{r}\frac{\partial E_z}{\partial \phi}\right) \tag{2.35c}$$

$$H_\phi = -\frac{-j}{q^2}\left(\frac{\beta}{r}\frac{\partial H_z}{\partial \phi} + \omega\epsilon\frac{\partial E_z}{\partial r}\right) \tag{2.35d}$$

where $q^2 = \omega^2\epsilon\mu - \beta^2 = k^2 - \beta^2$.

Substitution of Eqs (2.35*c*) and (2.35*d*) into Eq. (2.34*c*) results in the wave equation in cylindrical coordinates,

$$\frac{\partial^2 E_z}{\partial r^2} + \frac{1}{r}\frac{\partial E_z}{\partial r} + \frac{1}{r^2}\frac{\partial^2 E_z}{\partial \phi^2} + q^2 E_z = 0 \tag{2.36}$$

and substitution of Eqs (2.35*a*) and (2.35*b*) into Eq. (2.33*c*) leads to

$$\frac{\partial^2 H_z}{\partial r^2} + \frac{1}{r}\frac{\partial H_z}{\partial r} + \frac{1}{r^2}\frac{\partial^2 H_z}{\partial \phi^2} + q^2 H_z = 0 \tag{2.37}$$

It is interesting to note that Eqs. (2.36) and (2.37) each contain either only E_z or only H_z. This appears to imply that the longitudinal components of **E** and **H** are uncoupled and can be chosen arbitrarily provided that they satisfy Eqs (2.36) and (2.37). However, in general, coupling of E_z and H_z is required by the boundary conditions of the electromagnetic field components described in Sec. 2.4.6. If the boundary conditions do not lead to coupling between the field components, mode solutions can be obtained in which either $E_z = 0$ or $H_z = 0$. When $E_z = 0$ the modes are called *transverse electric* or TE modes, and when $H_z = 0$ they are called *transverse magnetic* or TM modes. *Hybrid* modes exist if both E_z and H_z are nonzero. These are designated as HE or EH modes, depending on whether H_z or E_z, respectively, makes a larger contribution to the transverse field. The fact that the hybrid modes are present in optical waveguides makes their analysis more complex than in the simpler case of hollow metallic waveguides where only TE and TM modes are found.

2.4.5 Wave Equations for Step-Index Fibers*

We now use the above results to find the guided modes in a step-index fiber. A standard mathematical procedure for solving equations such as Eq. (2.36) is to use the separation-of-variables method, which assumes a solution of the form

$$E_z = AF_1(r)F_2(\phi)F_3(z)F_4(t) \tag{2.38}$$

As was already assumed, the time- and z-dependent factors are given by

$$F_3(z)F_4(t) = e^{j(\omega t-\beta z)} \tag{2.39}$$

since the wave is sinusoidal in time and propagates in the z direction. In addition, because of the circular symmetry of the waveguide, each field component must not change when the coordinate ϕ is increased by 2π. We thus assume a periodic function of the form

$$F_2(\phi) = e^{j\nu\phi} \tag{2.40}$$

The constant ν can be positive or negative, but it must be an integer since the fields must be periodic in ϕ with a period of 2π.

Substituting Eq. (2.40) into Eq. (2.38), the wave equation for E_z [Eq. 2.36)] becomes

$$\frac{\partial^2 F_1}{\partial r^2} + \frac{1}{r}\frac{\partial F_1}{\partial r} + \left(q^2 - \frac{\nu^2}{r^2}\right)F_1 = 0 \tag{2.41}$$

which is a well-known differential equation for Bessel functions.[24–26] An exactly identical equation can be derived for H_z.

For the configuration of the step-index fiber we consider a homogeneous core of refractive index n_1 and radius a, which is surrounded by an infinite cladding of index n_2. The reason for assuming an infinitely thick cladding is that the guided modes in the core have exponentially decaying fields outside the core and these must have insignificant values at the outer boundary of the cladding. In practice, optical fibers are designed with claddings that are sufficiently thick so that the guided-mode field does not reach the outer boundary of the cladding. To get an idea of the field patterns, the electric field distributions for several of the lower-order guided modes in a symmetrical-slab waveguide were shown in Fig. 2.14. The fields vary harmonically in the guiding region of refractive index n_1 and decay exponentially outside of this region.

Equation (2.41) must now be solved for the regions inside and outside the core. For the inside region the solutions for the guided modes must remain finite as $r \to 0$, whereas on the outside the solutions must decay to zero as $r \to \infty$. Thus, for $r < a$ the solutions are Bessel functions of the first kind of order ν. For these functions we use the common designation $J_\nu(ur)$. Here, $u^2 = k_1^2 - \beta^2$ with $k_1 = 2\pi n_1/\lambda$. The expressions for E_z and H_z inside the core are thus

$$E_z(r < a) = AJ_\nu(ur)\, e^{j\nu\phi}e^{j(\omega t-\beta z)} \tag{2.42}$$

$$H_z(r < a) = BJ_\nu(ur)\, e^{j\nu\phi}e^{j(\omega t-\beta z)} \tag{2.43}$$

where A and B are arbitrary constants.

Outside of the core the solutions to Eq. (2.41) are given by modified Bessel functions of the second kind, $K_\nu(wr)$, where $w^2 = \beta^2 - k_2^2$ with $k_2 = 2\pi n_2/\lambda$. The expressions for E_z and H_z outside the core are therefore

$$E_z(r > a) = CK_\nu(wr)\, e^{j\nu\phi}e^{j(\omega t-\beta z)} \tag{2.44}$$

$$H_z(r > a) = DK_\nu(wr)\, e^{j\nu\phi}e^{j(\omega t-\beta z)} \tag{2.45}$$

with C and D being arbitrary constants.

The definitions of $J_\nu(ur)$ and $K_\nu(wr)$ and various recursion relations are given in App. C. From the definition of the modified Bessel function, it is seen that $K_\nu(wr) \to e^{-wr}$ as $wr \to \infty$. Since $K_\nu(wr)$ must go to zero as $r \to \infty$, it follows that $w > 0$. This, in turn, implies that $\beta \geq k_2$, which represents a cutoff condition. The *cutoff condition* is the point at which a mode is no longer bound to the core region. A second condition on β can be deduced from the behavior of $J_\nu(ur)$. Inside the core the parameter u must be real for F_1 to be real, from which it follows that $k_1 \geq \beta$. The permissible range of β for bound solutions is therefore

$$n_2 k = k_2 \leq \beta \leq k_1 = n_1 k \tag{2.46}$$

where $k = 2\pi/\lambda$ is the free-space propagation constant.

2.4.6 Modal Equation*

The solutions for β must be determined from the boundary conditions. The boundary conditions require that the tangential components E_ϕ and E_z of **E** inside and outside of the dielectric interface at $r = a$ must be the same, and similarly for the tangential components H_ϕ and H_z. Consider first the tangential components of **E**. For the z component we have, from Eq. (2.42) at the inner core-cladding boundary ($E_z = E_{z1}$) and from Eq. (2.44) at the outside of the boundary ($E_z = E_{z2}$), that

$$E_{z1} - E_{z2} = AJ_\nu(ua) - CK_\nu(wa) = 0 \tag{2.47}$$

The ϕ component is found from Eq. (2.35*b*). Inside the core the factor q^2 is given by

$$q^2 = u^2 = k_1^2 - \beta^2 \tag{2.48}$$

where $k_1 = 2\pi n_1/\lambda = \omega\sqrt{\epsilon_1 \mu}$, while outside the core

$$w^2 = \beta^2 - k_2^2 \tag{2.49}$$

with $k_2 = 2\pi n_2/\lambda = \omega\sqrt{\epsilon_2 \mu}$. Substituting Eqs (2.42) and (2.43) into Eq. (2.35*b*) to find $E_{\phi 1}$, and, similarly, using Eqs. (2.44) and (2.45) to determine $E_{\phi 2}$, yields, at $r = a$,

$$\begin{aligned} E_{\phi 1} - E_{\phi 2} &= -\frac{j}{u^2}\left[A\frac{j\nu\beta}{a}J_\nu(ua) - B\omega\mu u J_\nu'(ua)\right] \\ -\frac{j}{w^2}&\left[C\frac{j\nu\beta}{a}K_\nu(wa) - D\omega\mu w K_\nu'(wa)\right] = 0 \end{aligned} \tag{2.50}$$

where the prime indicates differentiation with respect to the argument.

Similarly, for the tangential components of **H** it is readily shown that, at $r = a$,

$$H_{z1} - H_{z2} = BJ_\nu(ua) - DK_\nu(wa) = 0 \tag{2.51}$$

and

$$\begin{aligned} H_{\phi 1} - H_{\phi 2} &= -\frac{j}{u^2}\left[B\frac{j\nu\beta}{a}J_\nu(ua) + A\omega\epsilon_1 u J_\nu'(ua)\right] \\ -\frac{j}{w^2}&\left[D\frac{j\nu\beta}{a}K_\nu(wa) + C\omega\epsilon_2 w K_\nu'(wa)\right] = 0 \end{aligned} \tag{2.52}$$

Equations (2.47), (2.50), (2.51), and (2.52) are a set of four equations with four unknown coefficients, *A*, *B*, *C*, and *D*. A solution to these equations exists only if the determinant of these coefficients is zero:

$$\begin{vmatrix} J_\nu(ua) & 0 & -K_\nu(wa) & 0 \\ \frac{\beta\nu}{au^2}J_\nu(ua) & \frac{j\omega\mu}{u}J'_\nu(ua) & \frac{\beta\nu}{aw^2}K_\nu(wa) & \frac{j\omega\mu}{w}K'_\nu(wa) \\ 0 & J_\nu(ua) & 0 & -K_\nu(wa) \\ -\frac{j\omega\varepsilon_1}{u}J'_\nu(ua) & \frac{\beta\nu}{au^2}J_\nu(ua) & -\frac{j\omega\varepsilon_2}{w}K'_\nu(wa) & \frac{\beta\nu}{aw^2}K_\nu(wa) \end{vmatrix} \tag{2.53}$$

Evaluation of this determinant yields the following eigenvalue equation for β:

$$(\mathcal{J}_\nu + \mathcal{K}_\nu)(k_1^2\mathcal{J}_\nu + k_2^2\mathcal{K}_\nu) = \left(\frac{\beta\nu}{a}\right)\left(\frac{1}{u^2}+\frac{1}{w^2}\right) \tag{2.54}$$

where

$$\mathcal{J}_\nu = \frac{J'_\nu(ua)}{uJ_\nu(ua)} \quad \text{and} \quad \mathcal{K}_\nu = \frac{K'_\nu(wa)}{wK_\nu(wa)}$$

Upon solving Eq. (2.54) for β, it will be found that only discrete values restricted to the range given by Eq. (2.46) will be allowed. Although Eq. (2.54) is a complicated transcendental equation which is generally solved by numerical techniques, its solution for any particular mode will provide all the characteristics of that mode. We shall now consider this equation for some of the lowest-order modes of a step-index waveguide.

2.4.7 Modes in Step-Index Fibers*

To help describe the modes, we shall first examine the behavior of the J-type Bessel functions. These are plotted in Fig. 2.21 for the first three orders. The J-type Bessel functions are similar to harmonic functions since they exhibit oscillatory behavior for real k, as is the case for sinusoidal functions. Because of the oscillatory behavior of J_ν, there will be m roots of Eq. (2.54) for a given ν value. These roots will be designated by $\beta_{\nu m}$, and the corresponding modes are either $TE_{\nu m}$, $TM_{\nu m}$, $EH_{\nu m}$, or $HE_{\nu m}$. Schematics of the transverse electric field patterns for the four lowest-order modes over the cross section of a step-index fiber are shown in Fig. 2.22.

For the dielectric fiber waveguide, all modes are hybrid modes except those for which $\nu = 0$. When $\nu = 0$ the right-hand side of Eq. (2.54) vanishes and two different eigenvalue equations result. These are

$$\mathcal{J}_0 + \mathcal{K}_0 = 0 \tag{2.55a}$$

or, using the relations for J'_ν and K'_ν in App. C,

$$\frac{J_1(ua)}{uJ_0(ua)} + \frac{K_1(wa)}{wK_0(wa)} = 0 \tag{2.55b}$$

which corresponds to TE_{0m} modes ($E_z = 0$), and

$$k_1^2\mathcal{J}_0 + k_2^2\mathcal{K}_0 = 0 \tag{2.56a}$$

or

$$\frac{k_1^2 J_1(ua)}{uJ_0(ua)} + \frac{k_2^2 K_1(wa)}{wK_0(wa)} = 0 \tag{2.56b}$$

which corresponds to TM_{0m} modes ($H_z = 0$). The proof of this is left as an exercise (see Prob. 2.16).

When $v \neq 0$ the situation is more complex and numerical methods are needed to solve Eq. (2.54) exactly. However, simplified and highly accurate approximations based on the principle that the core and cladding refractive indices are nearly the same have been derived[19, 20, 27]. The condition that $n_1 - n_2 \ll 1$ was referred to by Gloge as giving rise to *weakly guided* modes. A treatment of these derivations is given in Sec. 2.4.8.

Let us examine the cutoff conditions for fiber modes. As was mentioned in relation to Eq. (2.46), a mode is referred to as being cut off when it is no longer bound to the core of the fiber, so that its field no longer decays on the outside of the core. The cutoffs for the various modes are found by solving Eq. (2.54) in the limit $w^2 \to 0$. This is, in general, fairly complex, so that only the results,[14, 16] which are listed in Table 2.2, will be given here.

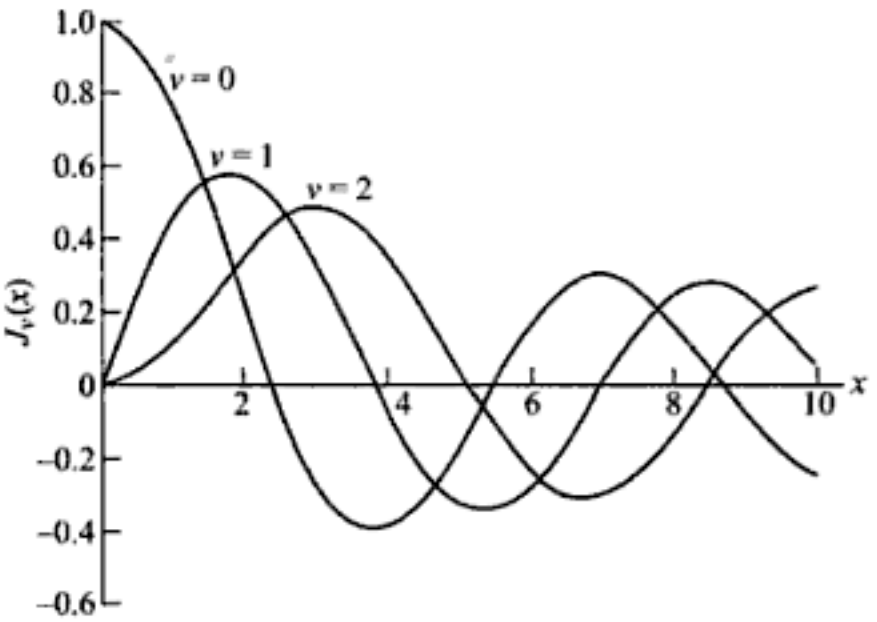

Fig. 2.21 *Variation of the Bessel function $J_v(x)$ for the first three orders (v = 0, 1, 2) plotted as a function of x*

An important parameter connected with the cutoff condition is the *normalized frequency* V (also called the *V number* or *V parameter)* defined by

$$V^2 = (u^2 + w^2)a^2 = \left(\frac{2\pi a}{\lambda}\right)^2 (n_1^2 - n_2^2) = \left(\frac{2\pi a}{\lambda}\right)^2 \mathrm{NA}^2 \tag{2.57}$$

which is a dimensionless number that determines how many modes a fiber can support. The number of modes that can exist in a waveguide as a function of V may be conveniently represented in terms of a *normalized propagation constant* b defined by[20]

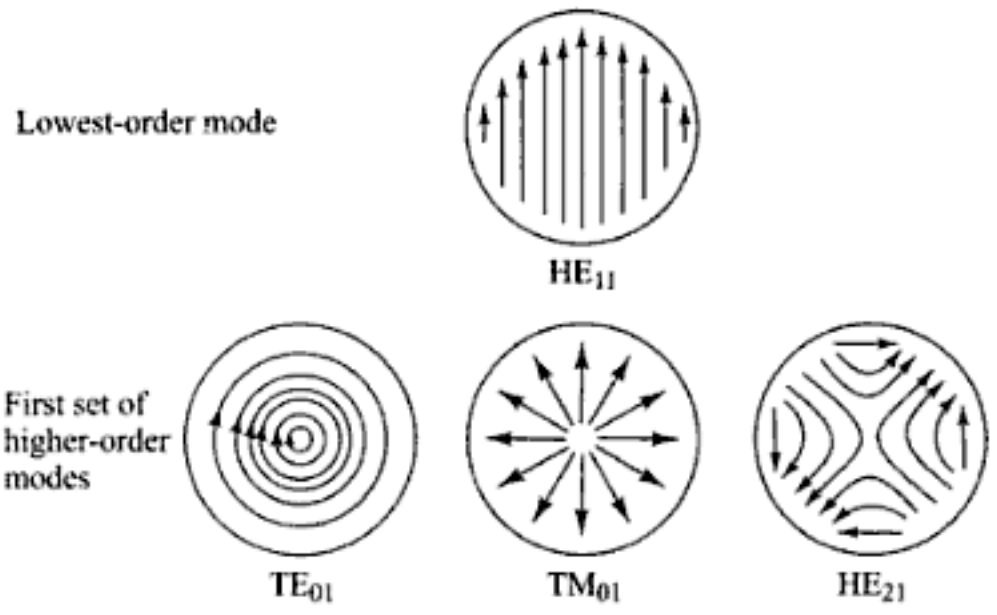

Fig. 2.22 *Fiber end views of the transverse electric field vectors for the four lowest-order modes in a step-index fiber*

Table 2.2 *Cutoff conditions for some lower-order modes*

v	*Mode*	*Cutoff condition*
0	TE_{0m}, TM_{0m}	$J_0(ua) = 0$
1	HE_{1m}, EH_{1m}	$J_1(ua) = 0$
≥ 2	EH_{vm}	$J_v(ua) = 0$
	HE_{vm}	$\left(\frac{n_1^2}{n_2^2} + 1\right) J_{v-1}(ua) = \frac{ua}{v-1} J_v(ua)$

$$b = \frac{a^2 w^2}{V^2} = \frac{(\beta/k)^2 - n_2^2}{n_1^2 - n_2^2}$$

A plot of b (in terms of β/k) as a function of V is shown in Fig. 2.33 for a few of the low-order modes. This figure shows that each mode can exist only for values of V that exceed a certain limiting value. The modes are cut off when $\beta/k = n_2$. The HE_{11} mode has no cutoff and ceases to exist only when the core diameter is zero. This is the principle on which the single-mode fiber is based. By appropriately choosing a, n_1, and n_2 so that

$$V = \frac{2\pi a}{\lambda}(n_1^2 - n_2^2)^{1/2} \leq 2.405 \tag{2.58}$$

which is the value at which the lowest-order Bessel function $J_0 = 0$ (see Fig. 2.21), all modes except the HE_{11} mode are cut off.

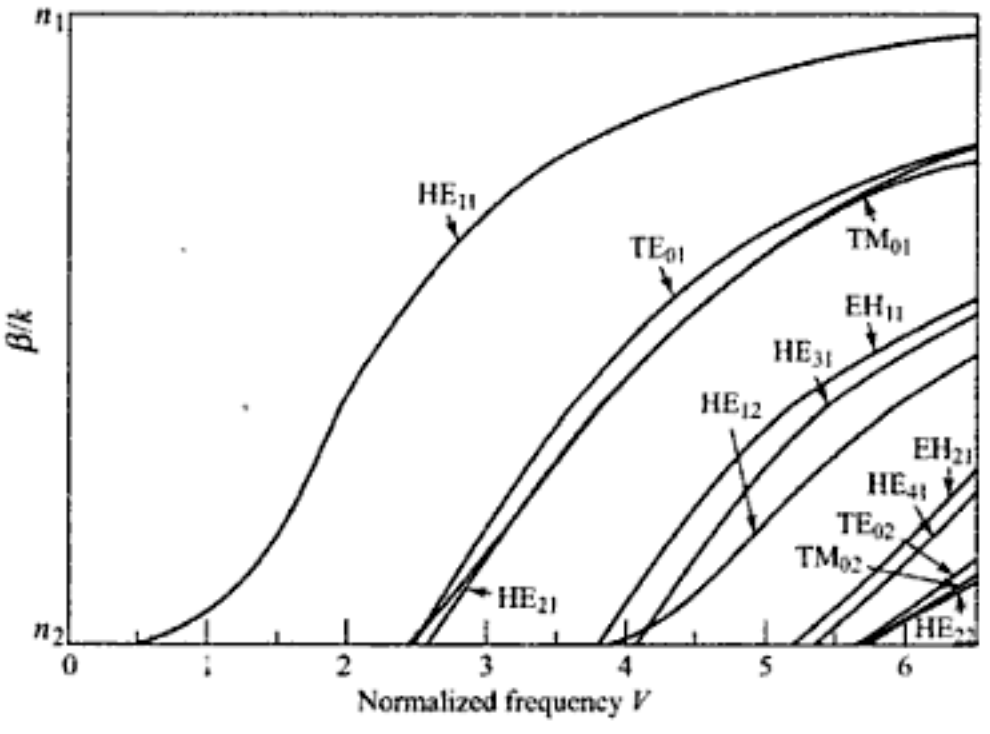

Fig. 2.23 *Plots of the propagation constant (in terms of β/k) as a function of V for a few of the lowest-order modes (Modified with permission from Gloge[20])*

Example 2.3 A step-index fiber has a normalized frequency $V = 26.6$ at a 1300-nm wavelength. If the core radius is 25 μm, let us find the numerical aperture. From Eq. (2.57) we have

$$\text{NA} = V\frac{\lambda}{2\pi a} = 26.6\frac{1.3}{2\pi(25)} = 0.22$$

The parameter V can also be related to the number of modes M in a multi-mode fiber when M is large. An approximate relationship for step-index fibers can be derived from ray theory. A ray congruence will be accepted by the fiber if it lies within an angle θ defined by the numerical aperture as given in Eq. (2.23):

$$\text{NA} = \sin\theta = (n_1^2 - n_2^2)^{1/2} \tag{2.59}$$

For practical numerical apertures, $\sin\theta$ is small so that $\sin\theta \simeq \theta$. The solid acceptance angle for the fiber is therefore

$$\Omega = \pi\theta^2 = \pi(n_1^2 - n_2^2) \tag{2.60}$$

For electromagnetic radiation of wavelength λ emanating from a laser or a waveguide, the number of modes per unit solid angle is given by $2A/\lambda^2$, where A is the area the mode is leaving or entering.[28] The area A in this case is the core cross section πa^2. The factor 2 comes from the fact that the plane wave can have two polarization orientations. The total number of modes M entering the fiber is thus given by

$$M \simeq \frac{2A}{\lambda^2}\Omega = \frac{2\pi^2 a^2}{\lambda^2}(n_1^2 - n_2^2) = \frac{V^2}{2} \tag{2.61}$$

2.4.8 Linearly Polarized Modes*

The exact analysis for the modes of a fiber is mathematically complex. However, a simpler but highly accurate approximation can be used, based on the principle that in a typical step-index fiber the difference between the indices of refraction of the core and cladding is very small; that is, $\Delta \ll 1$. This is the basis of the *weakly guiding fiber approximation*.[7, 19, 20, 27] In this approximation the electromagnetic field patterns and the propagation constants of the mode pairs $\text{HE}_{\nu+1,m}$ and $\text{EH}_{\nu-1,m}$ are very similar. This holds likewise for the three modes TE_{0m}, TM_{0m}, and HE_{2m}. This can be seen from Fig. 2.23 with $(\nu, m) = (0, 1)$ and (2, 1) for the mode groupings $\{\text{HE}_{11}\}$, $\{\text{TE}_{01}, \text{TM}_{01}, \text{HE}_{21}\}$, $\{\text{HE}_{31}, \text{EH}_{11}\}$, $\{\text{HE}_{12}\}$, $\{\text{HE}_{41}, \text{EH}_{21}\}$, and $\{\text{TE}_{02}, \text{TM}_{02}, \text{HE}_{22}\}$. The result is that only four field components need to be considered instead of six, and the field description is further simplified by the use of caretesian instead of cylindrical coordinates.

When $\Delta \ll 1$ we have that $k_1^2 \simeq k_2^2 \simeq \beta^2$. Using these approximations, Eq. (2.54) becomes

$$\mathcal{J}_\nu + \cdot\mathcal{K}_\nu = \pm\frac{\nu}{a}\left(\frac{1}{u^2} + \frac{1}{w^2}\right). \tag{2.62}$$

Thus, Eq. (2.55*b*) for TE_{0m} modes is the same as Eq. (2.56*b*) for TM_{0m} modes. Using the recurrence relations for J_ν' and K_ν' given in App. C, we get two sets of equations for Eq. (2.62) for the positive and negative signs. The positive sign yields

$$\frac{J_{\nu+1}(ua)}{uJ_\nu(ua)} + \frac{K_{\nu+1}(wa)}{wK_\nu(wa)} = 0 \tag{2.63}$$

The solution of this equation gives a set of modes called the EH modes. For the negative sign in Eq. (2.62) we get

$$\frac{J_{\nu-1}(ua)}{uJ_{\nu}(ua)} - \frac{K_{\nu-1}(wa)}{wK_{\nu}(wa)} = 0 \tag{2.64a}$$

or, alternatively, taking the inverse of Eq. (2.64*a*) and using the first expressions for $J_\nu(ua)$ and $K_\nu(wa)$ from Sec. C.1.2 and Sec. C.2.2,

$$-\frac{uJ_{\nu-2}(ua)}{J_{\nu-1}(ua)} = \frac{wK_{\nu-2}(wa)}{wK_{\nu-1}(wa)} \tag{2.64b}$$

This results in a set of modes called the HE modes.

If we define a new parameter

$$j = \begin{cases} 1 & \text{for TE and TM modes} \\ \nu+1 & \text{for EH modes} \\ \nu-1 & \text{for HE modes} \end{cases} \tag{2.65}$$

then Eqs (2.55*b*) (2.63), and (2.64*b*) can be written in the unified form

$$\frac{uJ_{j-1}(ua)}{J_j(ua)} = -\frac{wK_{j-1}(wa)}{K_j(wa)} \tag{2.66}$$

Equations (2.65) and (2.66) show that within the weakly guiding approximation all modes characterized by a common set of j and m satisfy the same characteristic equation. This means that these modes are degenerate. Thus, if an $HE_{\nu+1,m}$ mode is degenerate with an $EH_{\nu-1,m}$ mode (i.e., if HE and EH modes of corresponding radial order m and equal circumferential order ν form degenerate pairs), then any combination of an $HE_{\nu+1,m}$ mode with an $EH_{\nu-1,m}$ mode will likewise constitute a guided mode of the fiber.

Such degenerate modes are called *linearly polarized* (LP) modes, and are designated LP_{jm} modes regardless of their TM, TE, EH, or HE field configuration[20]. The normalized propagation constant b as a function of V is given for various LP_{jm} modes in Fig. 2.24 general, we have the following:

1. Each LP_{0m} mode is derived from an HE_{1m} mode.
2. Each LP_{1m} mode comes from TE_{0m}, TM_{0m}, and HE_{2m} modes.
3. Each $LP_{\nu m}$ mode ($\nu \geq 2$) is from an $HE_{\nu+1,m}$ and an $EH_{\nu-1,m}$ mode.

The correspondence between the ten lowest LP modes (i.e., those having the lowest cutoff frequencies) and the traditional TM, TE, EH, and HE modes is given in Table 2.3. This table also shows the number of degenerate modes.

A very useful feature of the LP-mode designation is the ability to readily visualize a mode. In a complete set of modes only one electric and one magnetic field component are significant. The electric field vector **E** can be chosen to lie along an arbitrary axis, with the magnetic field vector **H** being perpendicular to it. In addition, there are equivalent solutions with the field polarities reversed. Since each of the two possible polarization directions can be coupled with either a $\cos j\phi$ or a $\sin j\phi$ azimuthal dependence, four discrete mode patterns can be obtained from a single LP_{jm} label. As an example, the four possible electric and magnetic field directions and the corresponding intensity distributions for the LP_{11} mode are shown Fig. 2.25. Figure 2.26*a* and 2.26*b* illustrate how two LP_{11} modes are composed from the exact HE_{21} plus TE_{01} and the exact HE_{21} plus TM_{01} modes, respectively.

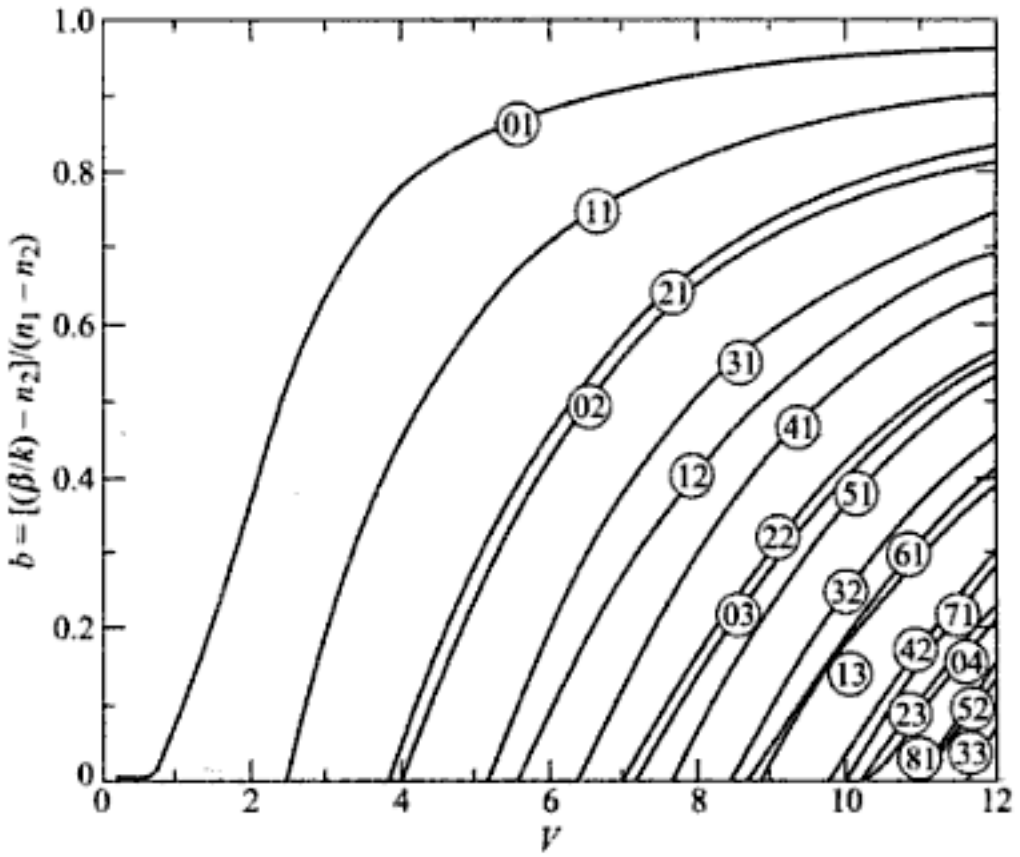

Fig. 2.24 *Plots of the propagation constant b as a function of V for various LP_{jm} modes. (Reproduced with permission from Gloge[20])*

Table 2.3 *Composition of the lower-order linearly polarized modes*

LP-mode designation	*Traditional-mode designation and number of modes*	*Number of degenerate modes*
LP_{01}	$HE_{11} \times 2$	2
LP_{11}	TE_{01}, TM_{01}, $HE_{21} \times 2$	4
LP_{21}	$EH_{11} \times 2$, $HE_{31} \times 2$	4
LP_{02}	$HE_{12} \times 2$	2
LP_{31}	$EH_{21} \times 2$, $HE_{41} \times 2$	4
LP_{12}	TE_{02}, TM_{02}, $HE_{22} \times 2$	4
LP_{41}	$EH_{31} \times 2$, $HE_{51} \times 2$	4
LP_{22}	$EH_{12} \times 2$, $HE_{32} \times 2$	4
LP_{03}	$HE_{13} \times 2$	2
LP_{51}	$EH_{41} \times 2$, $HE_{61} \times 2$	4

2.4.9 Power Flow in Step-Index Fibers*

A final quantity of interest for step-index fibers is the fractional power flow in the core and cladding for a given mode. As illustrated in Fig. 2.19, the electromagnetic field for a given mode does not go to zero at the core-cladding interface, but changes from an oscillating form in the core to an exponential decay in the cladding. Thus, the electromagnetic energy of a guided mode is carried partly in the core and partly in the cladding. The further away a mode is from its cutoff frequency, the more concentrated its energy is in the core. As cutoff is approached, the field penetrates farther into the cladding region and a greater percentage of the energy travels in the cladding. At cutoff the field no longer decays outside the core and the mode now becomes a fully radiating mode.

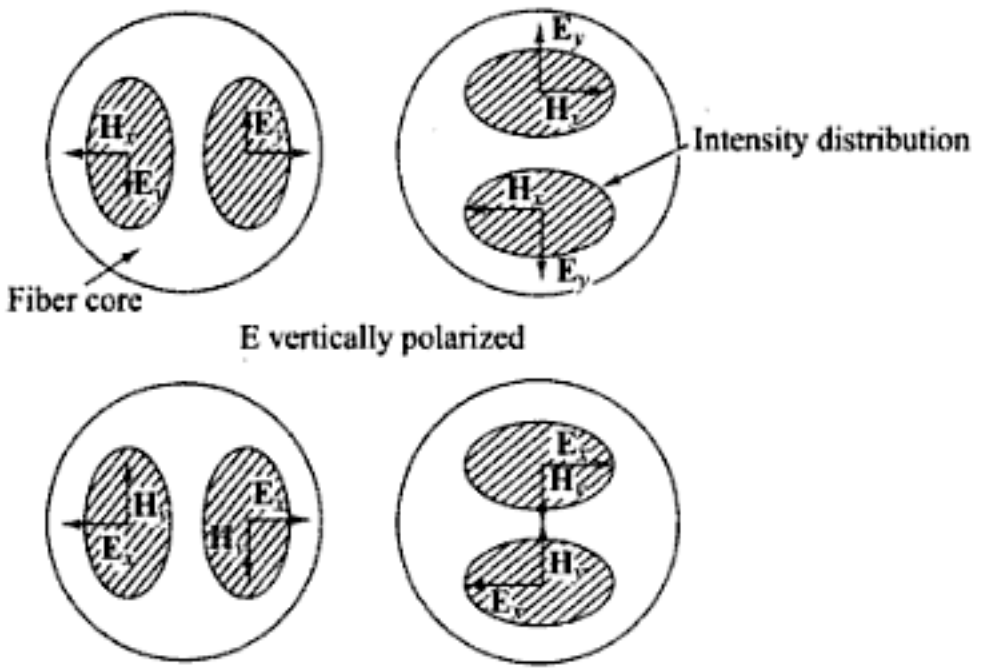

Fig. 2.25 *The four possible transverse electric field and magnetic field directions and the corresponding intensity distributions for the LP_{11} mode*

The relative amounts of power flowing in the core and the cladding can be obtained by integrating the Poynting vector in the axial direction,

$$S_z = \frac{1}{2}\,\mathrm{Re}(\mathbf{E} \times \mathbf{H}^*) \cdot \mathbf{e}_z \tag{2.67}$$

over the fiber cross section. Thus, the powers in the core and cladding, respectively, are given by

$$P_{\text{core}} = \frac{1}{2}\int_0^a \int_0^{2\pi} r(E_x H_y^* - E_y H_x^*)\, d\phi\, dr \tag{2.68}$$

$$P_{\text{clad}} = \frac{1}{2}\int_a^\infty \int_0^{2\pi} r(E_x H_y^* - E_y H_x^*)\, d\phi\, dr \tag{2.69}$$

where the asterisk denotes the complex conjugate. Based on the weakly guided mode approximation, which has an accuracy on the order of the index difference Δ between the core and cladding, the relative core and cladding powers for a particular mode v are given by[20, 29]

$$\frac{P_{\text{core}}}{P} = \left(1 - \frac{u^2}{V^2}\right)\left[1 - \frac{J_v^2(ua)}{J_{v+1}(ua)\,J_{v-1}(ua)}\right] \tag{2.70}$$

and

$$\frac{P_{\text{clad}}}{P} = 1 - \frac{P_{\text{core}}}{P} \tag{2.71}$$

where P is the total power in the mode v. The relationships between P_{core} and P_{clad} are plotted in Fig. 2.27 in terms of the fractional powers P_{core}/P and P_{clad}/P for various LP_{jm} modes. In addition, far from cutoff the average total power in the cladding has been derived for fibers in which many modes can propagate. Because of this large number of modes, those few modes that are appreciably close to cutoff can be ignored to a reasonable approximation. The derivation assumes an incoherent source, such as a tungsten filament lamp or a light-emitting diode, which, in general, excites every fiber mode with the same amount of power. The total average cladding power is thus approximated by[20]

$$\left(\frac{P_{\text{clad}}}{P}\right)_{\text{total}} = \frac{4}{3}M^{-1/2} \tag{2.72}$$

where, from Eq. (2.61), M is the total number of modes entering the fiber. From Fig. 2.27 and Eq. (2.72) it can be seen that, since M is proportional to V^2, the power flow in the cladding decreases as V increases.

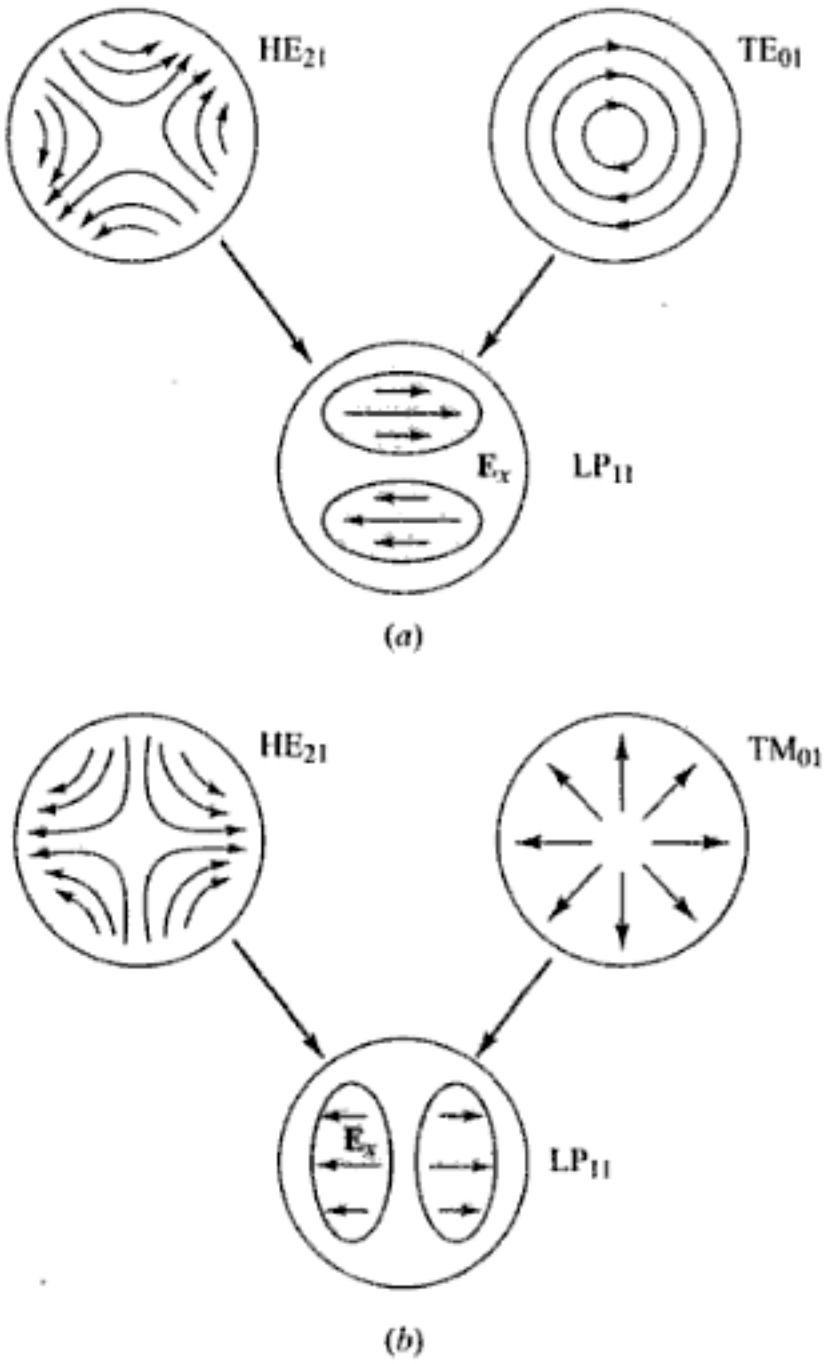

Fig. 2.26 *Composition of two LP_{11} modes from exact modes and their transverse electric field and intensity distributions*

Example 2.4 As an example, consider a fiber having a core radius of 25 μm, a core index of 1.48, and $\Delta = 0.01$. At an operating wavelength of 0.84 μm the value of V is 39 and there are 760 modes in the fiber. From Eq. (2.72), approximately 5 percent of the power propagates in the cladding. If Δ is decreased to, say, 0.003 in order to decrease signal dispersion (see Chapter 3), then 242 modes propagate in the fiber and about 9 percent of the power resides in the cladding. For the case of the single-mode fiber, considering the LP_{01} mode (the HE_{11} mode) in Fig. 2.27, it is seen that for $V = 1$ about 70 percent of the power propagates in the cladding, whereas for $V = 2.405$, which is where the LP_{11} mode (the TE_{01} mode) begins, approximately 84 percent of the power is now within the core.

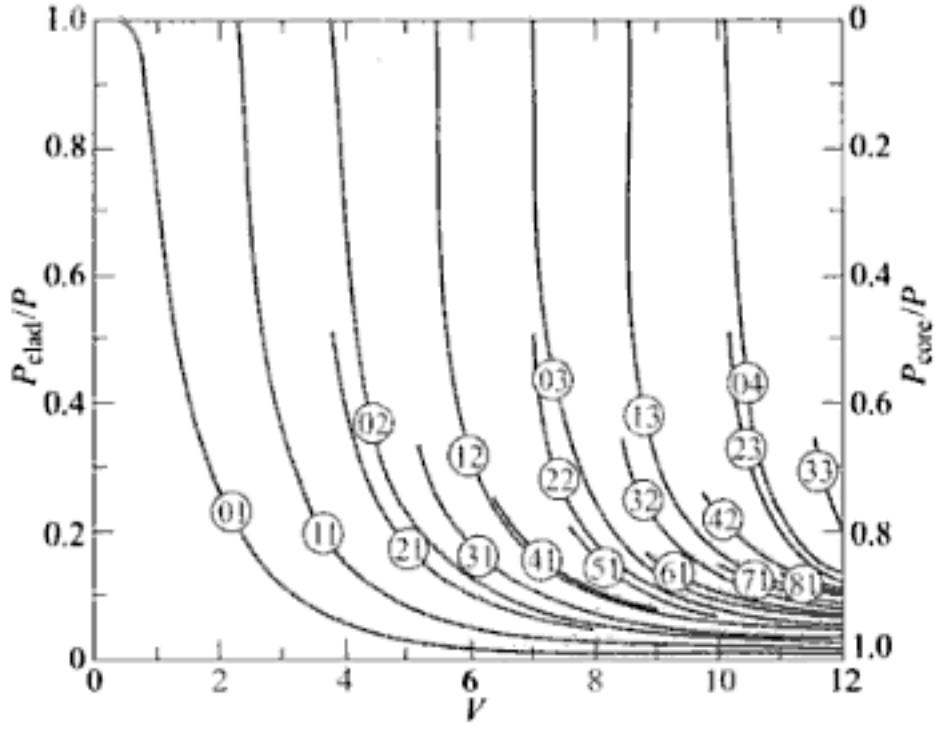

Fig. 2.27 *Fractional power flow in the cladding of a step-index optical fiber as a function of V. When $v \neq 1$, the curve numbers vm designate the $HE_{v+1,m}$ and $EH_{v-1,m}$ modes. For $v = 1$, the curve numbers vm give the HE_{2m}, TE_{0m}, and TM_{0m} modes (Reproduced with permission from Gloge[20])*

2.5 Single-mode Fibers

Single-mode fibers are constructed by letting the dimensions of the core diameter be a few wavelengths (usually 8-12) and by having small index differences between the core and the cladding. From Eq. (2.27) or (2.58) with $V = 2.4$, it can be seen that single-mode propagation is possible for fairly large variations in values of the physical core size a and the core–cladding index differences Δ. However, in practical designs of single-mode fibers,[27] the core–cladding index difference varies between 0.2 and 1.0 percent, and the core diameter should be chosen to be just below the cutoff of the first higher-order mode; that is, for V slightly less than 2.4. For example, a typical single-mode fiber may have a core radius of 3 μm and a numerical aperture of 0.1 at a wavelength of 0.8 µm. From Eqs (2.23) and (2.57) [or Eq. (2.27)], this yields $V = 2.356$.

2.5.1 Mode Field Diameter

For multimode fibers the core diameter and numerical aperture are key parameters for describing the signal transmission properties. In single-mode fibers the geometric distribution of light in the propagating mode is what is needed when predicting the performance characteristics of these fibers. Thus a fundamental parameter of a single-mode fiber is the *mode-field diameter* (MFD). This parameter can be determined from the mode-field distribution of the fundamental fiber mode, and is a function of the optical source wavelength, the core radius, and the refractive index profile of the fiber. The mode-field diameter is analogous to the core diameter in multimode fibers, except that in single-mode fibers not all the light that propagates through the fiber is carried in the core (see Sec. 2.4). Figure 2.28 illustrates this effect.

For example, at $V = 2$ only 75 percent of the optical power is confined to the core. This percentage increases for larger values of V and is less for smaller V values.

The MFD is an important parameter for single-mode fiber, since it is used to predict fiber properties such as splice loss, bending loss, cut-off wavelength, and waveguide dispersion. Chapters 3 and 5 describe these parameters and their effects on fiber performance. A variety of models have been proposed for characterizing and measuring the MFD.[30-35] These include far-field scanning, near-field scanning, transverse offset, variable aperture in the far field, knife-edge, and mask methods.[30] The main consideration of all these methods is how to approximate the optical power distribution.

A standard technique to find the MFD is to measure the far-field intensity distribution $E^2(r)$ and then calculate the MFD using the Petermann II equation[32]

$$\text{MFD} = 2W_0 = 2\left[\frac{2\int_0^{\infty} E^2(r)\, r^3\, dr}{\int_0^{\infty} E^2(r)\, r\, dr}\right]^{1/2} \tag{2.73}$$

where $2W_0$ (called the *spot size)* is the full width of the far-field distribution. For calculation simplicity the exact field distribution can be fitted to a Gaussian function[21]

$$E(r) = E_0 \exp\left(r^2/W_0^2\right) \tag{2.74}$$

where r is the radius and E_0 is the field at zero radius, as shown in Fig. 2.28. Then the MFD is given by the $1/e^2$ width of the optical power.

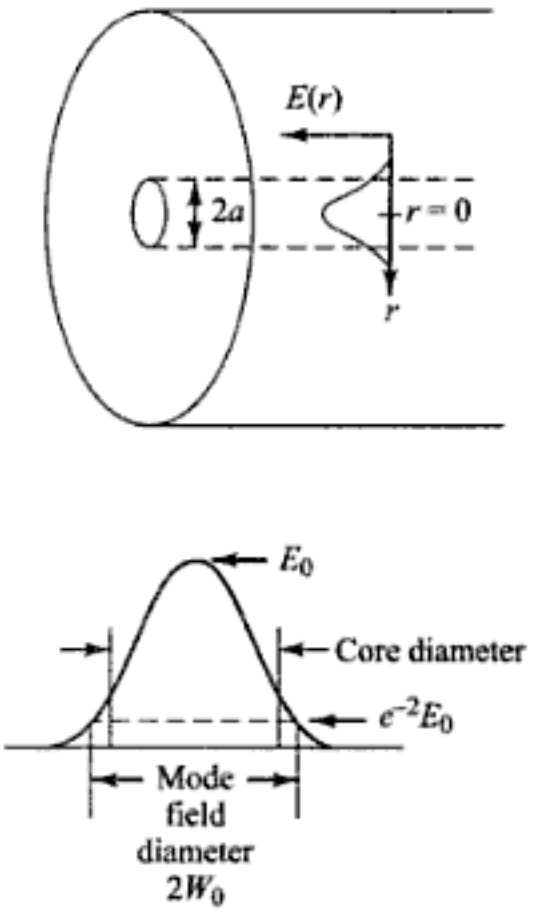

Fig. 2.28 *Distribution of light in a single-mode fiber above its cutoff wavelength. For a Gaussian distribution the MFD is given by the $1/e^2$ width of the optical power*

2.5.2 Propagation Modes in Single-Mode Fibers

As described in Sec. 2.4.8, in any ordinary single-mode fiber there are actually two independent, degenerate propagation modes[36–39]. These modes are very similar but their polarization planes are orthogonal. These may be chosen arbitrarily as the horizontal (H) and the vertical (V) polarizations as shown in Fig. 2.29. Either one of these two polarization modes constitutes the fundamental HE_{11} mode. In general, the electric field of the light propagating along the fiber is a linear superposition of these two polarization modes and depends on the polarization of the light at the launching point into the fiber.

Suppose we arbitrarily choose one of the modes to have its transverse electric field polarized along the x direction and the other independent orthogonal, mode to be polarized in the y direction as shown in Fig. 2.29. In ideal fibers with perfect rotational symmetry, the two modes are degenerate with equal propagation constants ($k_x = k_y$), and any polarization state injected into the fiber will propagate unchanged. In actual fibers there are imperfections, such as asymmetrical lateral stresses, noncircular cores, and variations in refractive-index profiles. These imperfections break the circular symmetry of the ideal fiber and lift the degeneracy of the two modes. The modes propagate with different phase velocities, and the difference between their effective refractive indices is called the fiber *birefringence,*

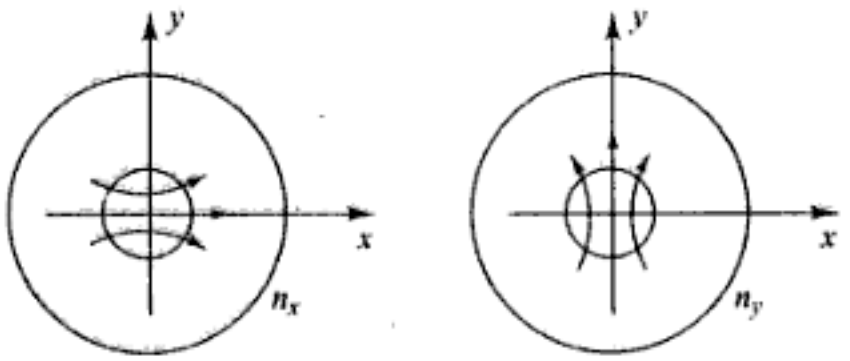

Fig. 2.29 *Two polarizations of the fundamental HE_{11} mode in a single-mode fiber*

$$B_f = n_y - n_x \tag{2.75}$$

Equivalently, we may define the birefringence as

$$\beta = k_0(n_y - n_x) \tag{2.76}$$

where $k_0 = 2\pi/\lambda$ is the free-space propagation constant.

If light is injected into the fiber so that both modes are excited, then one will be delayed in phase relative to the other as they propagate. When this phase difference is an integral multiple of 2π, the two modes will beat at this point and the input polarization state will be reproduced. The length over which this beating occurs is the *fiber beat length*,

$$L_p = 2\pi/\beta \tag{2.77}$$

Example 2.5 A single mode optical fiber has a beat length of 8 cm at 1300 nm. From Eqs. (2.75) to (2.77) we have that the modal birefringence is

$$B_f = n_y - n_x = \frac{\lambda}{L_p} = \frac{1.3\times10^{-6}\text{m}}{8\times10^{-2}\text{ m}} = 1.63\times10^{-5}$$

or, alternatively,

$$\beta = \frac{2\pi}{L_p} = \frac{2\pi}{0.08\text{ m}} = 78.5\text{ m}^{-1}$$

This indicates an intermediate-type fiber, since birefringences can vary from $B_f = 1\times10^{-3}$ (a typical high-birefringence fiber) to $B_f = 1\times10^{-8}$ (a typical low-birefringence fiber).

2.6 Graded-index Fiber Structure

In the graded-index fiber design the core refractive index decreases continuously with increasing radial distance r from the center of the fiber, but is generally constant in the cladding. The most commonly used construction for the refractive-index variation in the core is the power law relationship

$$n(r) = \begin{cases} n_1\left[1-2\Delta\left(\dfrac{r}{a}\right)^{\alpha}\right]^{1/2} & \text{for} \quad 0\le r\le 0 \\ n_1(1-2\Delta)^{1/2} \cong n_1(1-\Delta) = n_2 & \text{for} \quad r\ge a \end{cases} \tag{2.78}$$

Here, r is the radial distance from the fiber axis, a is the core radius, n_1 is the refractive index at the core axis, n_2 is the refractive index of the cladding, and the dimensionless parameter α defines the shape of the index profile. The index difference Δ for the graded-index fiber is given by

$$\Delta = \frac{n_1^2 - n_2^2}{2n_1^2} \simeq \frac{n_1 - n_2}{n_1} \tag{2.79}$$

The approximation on the right-hand side of this equation reduces the expression for Δ to that of the step-index fiber given by Eq. (2.20). Thus, the same symbol is used in both cases. For $\alpha = \infty$, Eq. (2.78) reduces to the step-index profile $n(r) = n_1$.

Determining the NA for graded-index fibers is more complex than for step-index fibers, since it is a function of position across the core end face. This is in contrast to the step-index fiber, where the NA is constant across the core. Geometrical optics considerations show that light incident on the fiber core at position r will propagate as a guided mode only if it is within the local numerical aperture NA(r) at that point. The local numerical aperture is defined as[40]

$$\text{NA}(r) = \begin{cases} [n^2(r) - n_2^2]^{1/2} \simeq \text{NA}(0)\sqrt{1-(r/a)^\alpha} & \text{for} \quad r \le a \\ 0 & \text{for} \quad r > 0 \end{cases} \tag{2.80a}$$

where the axial numerical aperture is defined as

$$\text{NA}(0) = [n^2(0) - n_2^2]^{1/2} = (n_1^2 - n_2^2)^{1/2} \simeq n_1\sqrt{2\Delta} \tag{2.80b}$$

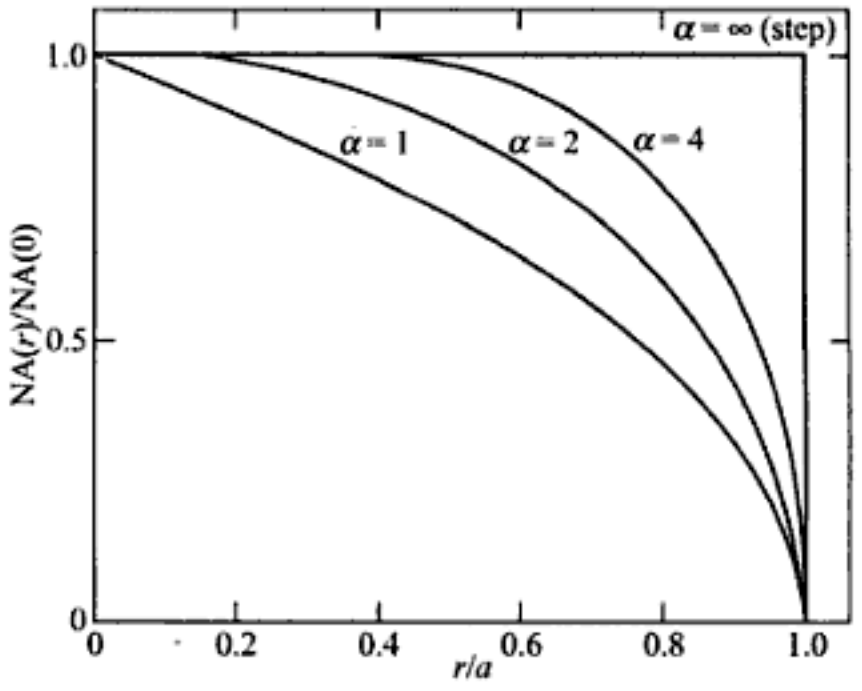

Fig. 2.30 *A comparison of the numerical apertures for fibers having various core index profiles*

Thus, the NA of a graded-index fiber decreases from NA(0) to zero as r moves from the fiber axis to the core–cladding boundary. A comparison of the numerical apertures for fibers having various α profiles is shown in Fig. 2.30. The number of bound modes in a graded-index fiber is[40-41]

$$M_g = \frac{\alpha}{\alpha+2} a^2 k^2 n_1^2 \Delta \simeq \frac{\alpha}{\alpha+2} \frac{V^2}{2} \tag{2.81}$$

where $k = 2\pi/\lambda$ and the right-hand approximation is derived using Eqs (2.23) and (2.27). As Sec. 3.4 describes, fiber manufacturers typically choose a *parabolic refractive index profile* given by $\alpha = 2.0$. In

this case, $M_g = V^2/4$, which is half the number of modes supported by a step-index fiber (for which $\alpha = \infty$) that has the same V value, as Eq. (2.61) shows.

2.7 Fiber Materials

In selecting materials for optical fibers, a number of requirements must be satisfied. For example:

1. It must be possible to make long, thin, flexible fibers from the material.
2. The material must be transparent at a particular optical wavelength in order for the fiber to guide light efficiently.
3. Physically compatible materials that have slightly different refractive indices for the core and cladding must be available.

Materials that satisfy these requirements are glasses and plastics.

The majority of fibers are made of glass consisting of either silica (SiO_2) or a silicate. The variety of available glass fibers ranges from moderate-loss fibers with large cores used for short-transmission distances to very transparent (low-loss) fibers employed in long-haul applications. Plastic fibers are less widely used because of their substantially higher attenuation than glass fibers. The main use of plastic fibers is in short-distance applications (several hundred meters) and in abusive environments, where the greater mechanical strength of plastic fibers offers an advantage over the use of glass fibers.

2.7.1 Glass Fibers

Glass is made by fusing mixtures of metal oxides, sulfides, or selenides.[42–44] The resulting material is a randomly connected molecular network rather than a well-defined ordered structure as found in crystalline materials. A consequence of this random order is that glasses do not have well-defined melting points. When glass is heated up from room temperature, it remains a hard solid up to several hundred degrees centigrade. As the temperature increases further, the glass gradually begins to soften until at very high temperatures it becomes a viscous liquid. The expression "melting temperature" is commonly used in glass manufacture. This term refers only to an extended temperature range in which the glass becomes fluid enough to free itself fairly quickly of gas bubbles.

The largest category of optically transparent glasses from which optical fibers are made consists of the oxide glasses. Of these, the most common is silica (SiO_2), which has a refractive index of 1.458 at 850 nm. To produce two similar materials that have slightly different indices of refraction for the core and cladding, either fluorine or various oxides (referred to as *dopants*), such as B_2O_3, GeO_2, or P_2O_5, are added to the silica. As shown in Fig. 2.31 the addition of GeO_2 or P_2O_5 increases the refractive index, whereas doping the silica with fluorine or B_2O_3 decreases it. Since the cladding must have a lower index than the core, examples of fiber compositions are

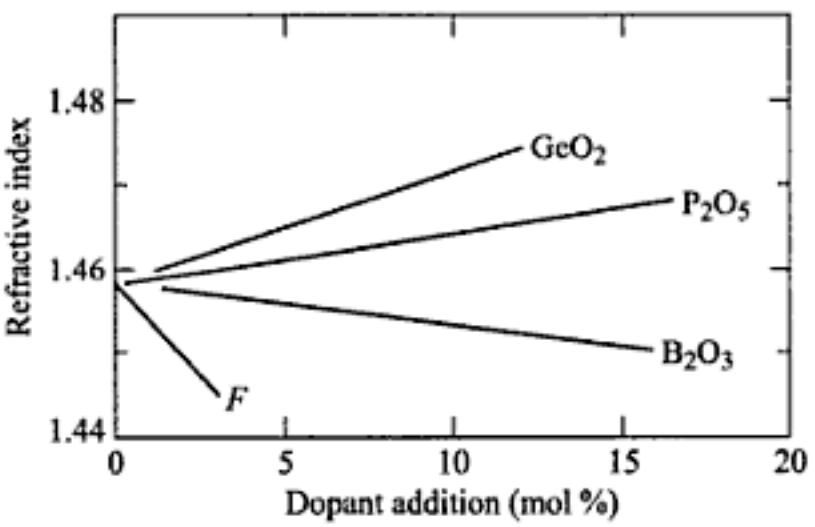

Fig. 2.31 *Variation in refractive index as a function of doping concentration in silica glass*

1. GeO_2–SiO_2 core; SiO_2 cladding
2. P_2O_5–SiO_2 core; SiO_2 cladding
3. SiO_2 core; B_2O_3–SiO_2 cladding
4. GeO_2–B_2O_3–SiO_2 core; B_2O_3–SiO_2 cladding

Here, the notation GeO_2–SiO_2, for example, denotes a GeO_2-doped silica glass.

The principal raw material for silica is high-purity sand. Glass composed of pure silica is referred to as either *silica glass, fused silica,* or *vitreous silica.* Some of its desirable properties are a resistance to deformation at temperatures as high as 1000°C, a high resistance to breakage from thermal shock because of its low thermal expansion, good chemical durability, and high transparency in both the visible and infrared regions of interest to fiber optic communication systems. Its high melting temperature is a disadvantage if the glass is prepared from a molten state. However, this problem is partially avoided when using vapor deposition techniques.

2.7.2 Active Glass Fibers

Incorporating rare-earth elements (atomic numbers 57–71) into a normally passive glass gives the resulting material new optical and magnetic properties. These new properties allow the material to perform amplification, attenuation, and phase retardation on the light passing through it.[45–47] Doping can be carried out for silica, tellurite, and halide glasses.

Two commonly used materials for fiber lasers are erbium and neodymium. The ionic concentrations of the rare-earth elements are low (on the order of 0.005–0.05 mole percent) to avoid clustering effects. By examining the absorption and fluorescence spectra of these materials, one can use an optical source which emits at an absorption wavelength to excite electrons to higher energy levels in the rare-earth dopants. When these excited electrons are stimulated by a photon to drop to lower energy levels, they emit light in a narrow optical spectrum at the fluorescence wavelength. Chapter 11 discusses the applications of fibers doped with rare-earth elements to create optical amplifiers.

Table 2.4 *Sample characteristics of PMMA and PF polymer optical fibers*

Characteristic	*PMMA POF*	*PF POF*
Core diameter	0.4 mm	0.125–0.30 mm
Cladding diameter	1.0 mm	0.25–0.60 mm
Numerical aperture	0.25	0.20
Attenuation	150 dB/km at 650 nm	< 40 dB/km at 650–1300 nm
Bandwidth	2.5 Gb/s over 200 m	2.5 Gb/s over 550 m

2.7.3 Plastic Optical Fibers

The growing demand for delivering high-speed services directly to the workstation has led fiber developers to create high-bandwidth graded-index polymer (plastic) optical fibers (POF) for use in a customer premises.[48, 49] The core of these fibers is either polymethylmethacrylate or a perfluorinated polymer. These fibers are hence referred to as PMMA POF and PF POF, respectively. Although they exhibit considerably greater optical signal attenuations than glass fibers, they are tough and durable. For example, since the modulus of these polymers is nearly two orders of magnitude lower than that of silica, even a

1-mm-diameter graded-index POF is sufficiently flexible to be installed in conventional fiber cable routes. Compared with silica fibers, the core diameters of plastic fibers are 10–20 times larger, which allows a relaxation of connector tolerances without sacrificing optical coupling efficiencies. Thus, inexpensive plastic injection-molding technologies can be used to fabricate connectors, splices, and transceivers.

Table 2.4 gives sample characteristics of PMMA and PF polymer optical fibers.

2.8 Photonic Crystal Fibers

In the early 1990s researchers envisioned and demonstrated a new optical fiber structure. Initially this was called a *holey fiber* and later became known as a *photonic crystal fiber* (PCF) or a *microstructured* fiber.[50–54] The difference between this new structure and that of a conventional fiber is that the cladding and, in some cases, the core regions of a PCF contain air holes, which run along the entire length of the fiber. Whereas the material properties of the core and cladding define the light-transmission characteristics of conventional fibers, the structural arrangement in a PCF creates an internal microstructure, which offers another dimension of light control in the fiber.

The size and spacing (known as the *pitch*) of the holes in the microstructure and the refractive index of its constituent material determine the light-guiding characteristics of photonic crystal fibers. The two basic PCF categories are index-guiding fibers and photonic bandgap fibers. The light transmission mechanism in an *index-guiding fiber* is similar to that in a conventional fiber, since it has a high-index core surrounded by a lower-index cladding. However, for a PCF the effective refractive index of the cladding depends on the wavelength and the size and pitch of the holes. In contrast, a *photonic bandgap fiber* has a hollow core which is surrounded by a micro structured cladding. This class of fibers guides light by means of a photonic bandgap effect.

2.8.1 Index-Guiding PCF

Figure 2.32 shows a two-dimensional cross-sectional end view of the structure of an index-guiding PCF. The fiber has a solid core that is surrounded by a cladding region which contains air holes running along the length of the fiber. The holes have a diameter d and a pitch Λ. Although the core and the cladding are made of the same material (for example, pure silica), the air holes lower the effective index of refraction in the cladding region, since $n = 1$ for air and 1.45 for silica. Consequently, the microstructure arrangement creates a step-index optical fiber.

The fact that the core can be made of pure silica, gives the PCF a number of operational advantages over conventional fibers, which typically have a germanium-doped silica core. These include very low

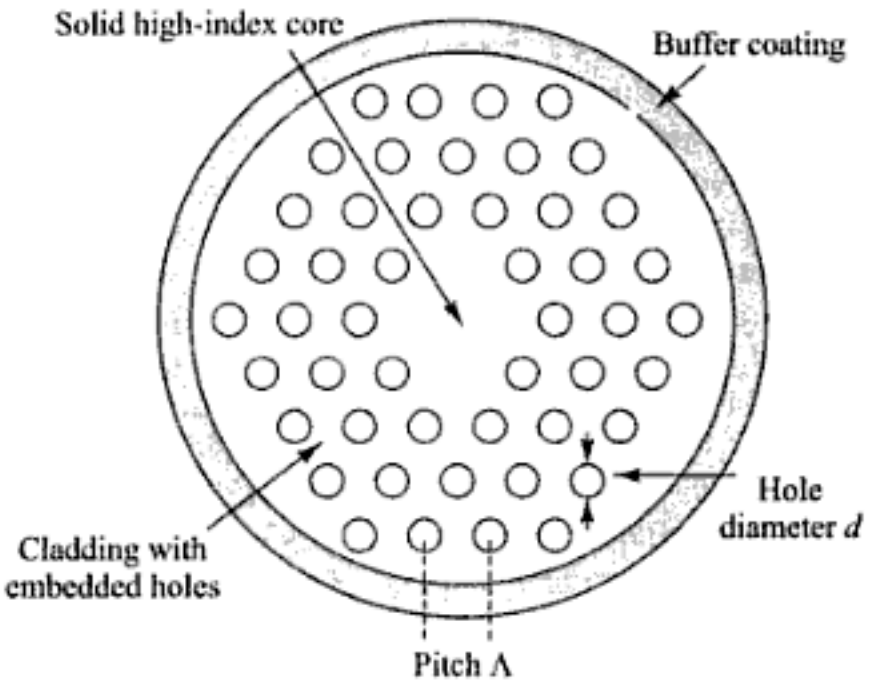

Fig. 2.32 *Cross-sectional end view of the structure of an index-guiding photonic crystal fiber*

losses, the ability to transmit high optical power levels, and a high resistance to darkening effects from nuclear radiation. The fibers can support single-mode operation over wavelengths ranging from 300 nm to more than 2000 nm. The mode field area of a PCF can be greater than 300 μm^2 compared to the 80 μm^2 area of conventional single-mode fibers. This allows the PCF to transmit high optical power levels without encountering the nonlinear effects exhibited by standard fibers (see Chapter 12).

2.8.2 Photonic Bandgap Fiber

Figure 2.33 shows a two-dimensional cross-sectional end view of the structure of a photonic bandgap (PBG) fiber. In contrast to an index-guiding PCF, here the fiber has a hollow core that is surrounded by a cladding region which contains air holes running along the length of the fiber. Again the holes in the cladding region have a diameter d and a pitch Λ.

The functional principle of a photonic bandgap fiber is analogous to the role of a periodic crystalline lattice in a semiconductor, which blocks electrons from occupying a bandgap region. In a PBG fiber the hollow core acts as a defect in the photonic bandgap structure, which creates a region in which the light can propagate.

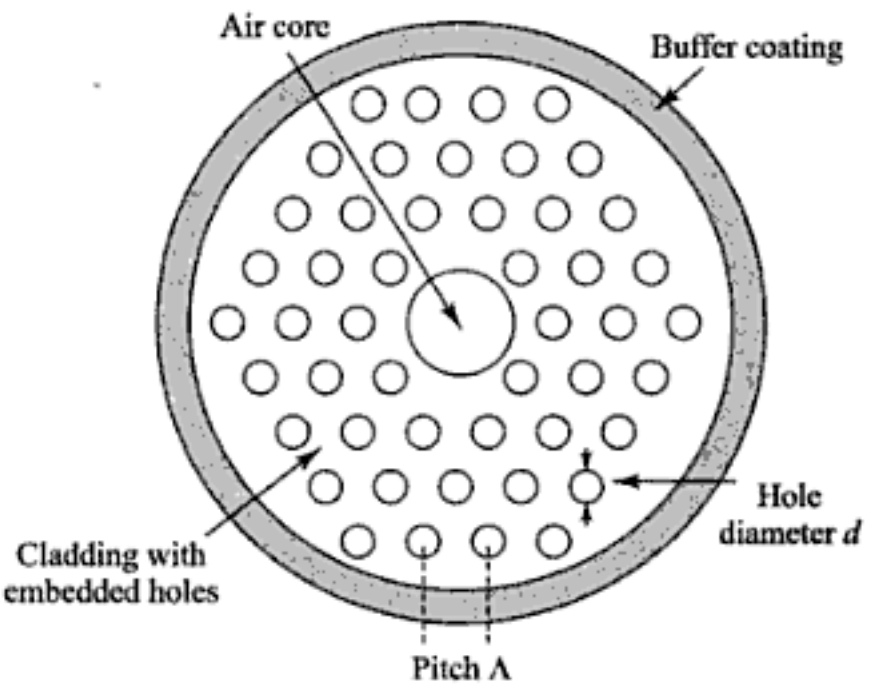

Fig. 2.33 *Cross-sectional end view of the structure of a photonic bandgap fiber*

2.9 Fiber Fabrication

Two basic techniques[55–58] are used in the fabrication of all-glass optical waveguides. These are the vapor-phase oxidation process and the direct-melt methods. The direct-melt method follows traditional glass-making procedures in that optical fibers are made directly from the molten state of purified components of silicate glasses. In the vapor-phase oxidation process, highly pure vapors of metal halides (e.g., $SiCl_4$ and $GeCl_4$) react with oxygen to form a white powder of SiO_2 particles. The particles are then collected on the surface of a bulk glass by one of four different commonly used processes and are sintered (transformed to a homogeneous glass mass by heating without melting) by one of a variety of techniques to form a clear glass rod or tube (depending on the process). This rod or tube is called a *perform*. It is typically around 10–25 mm in diameter and 60–120 cm long. Fibers are made from the preform[57–59] by using the equipment shown in Fig. 2.34. The perform is precision-fed into a circular heater called the *drawing furnace*. Here the preform end is softened to the point where it can be drawn into a very thin filament, which becomes the optical fiber. The turning speed of the takeup drum at the bottom of the draw tower determines how fast the fiber is drawn. This, in turn, will determine the thickness of the fiber, so that a precise rotation rate must be maintained. An optical fiber thickness monitor is used in a feedback loop for this speed regulation. To protect the bare glass fiber from external contaminants, such as dust and water vapor, an elastic coating is applied to the fiber immediately after it is drawn.

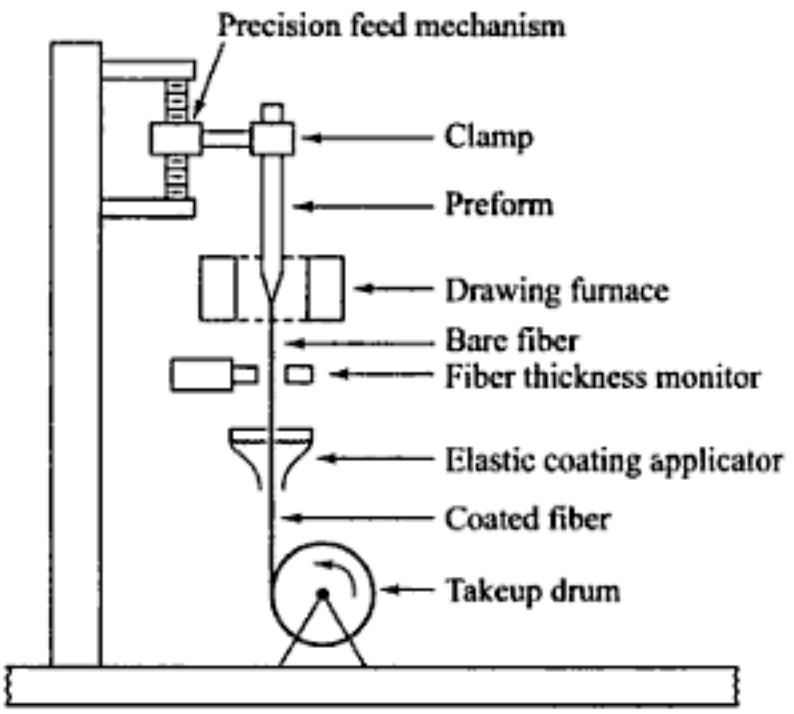

Fig. 2.34 *Schematic of a fiber-drawing apparatus*

2.9.1 Outside Vapor-Phase Oxidation

The first fiber to have a loss of less than 20 dB/km was made at the Corning Glass Works[60–62] by the *outside vapor-phase oxidation* (OVPO) process. This method is illustrated in Fig. 2.35. First, a layer of SiO_2 particles called a *soot* is deposited from a burner onto a rotating graphite or ceramic mandrel. The glass soot adheres to this bait rod and, layer by layer, a cylindrical, porous glass preform is built up. By properly controlling the constituents of the metal halide vapor stream during the deposition process, the glass compositions and dimensions desired for the core and cladding can be incorporated into the preform. Either step- or graded-index preforms can thus be made.

When the deposition process is completed, the mandrel is removed and the porous tube is then vitrified in a dry atmosphere at a high temperature (above 1400°) to a clear glass preform. This clear perform is subsequently mounted in a fiber-drawing tower and made into a fiber, as shown in Fig. 2.34. The central hole in the tube perform collapses during this drawing process.

2.9.2 Vapor-Phase Axial Deposition

The OVPO process described in Sec. 2.9.1 is a lateral deposition method. Another OVPO-type process is the *vapor-phase axial deposition* (VAD) method,[63, 64] illustrated in Fig. 2.36. In this method, the SiO_2 particles are formed in the same way as described in the OVPO process. As these particles emerge from the torches, they are deposited onto the end surface of a silica glass rod which acts as a seed. A porous preform is grown in the axial direction by moving the rod upward. The rod is also continuously rotated to maintain cylindrical symmetry of the particle deposition. As the porous preform moves upward, it is transformed into a solid, transparent rod preform by zone melting (heating in a narrow localized zone) with the carbon ring heater shown in Fig. 2.36. The resultant preform can then be drawn into a fiber by heating it in another furnace, as shown in Fig. 2.34.

Both step- and graded-index fibers in either muitimode or single-mode varieties can be made by the VAD method. The advantages of the VAD method are (1) the preform has no central hole as occurs with

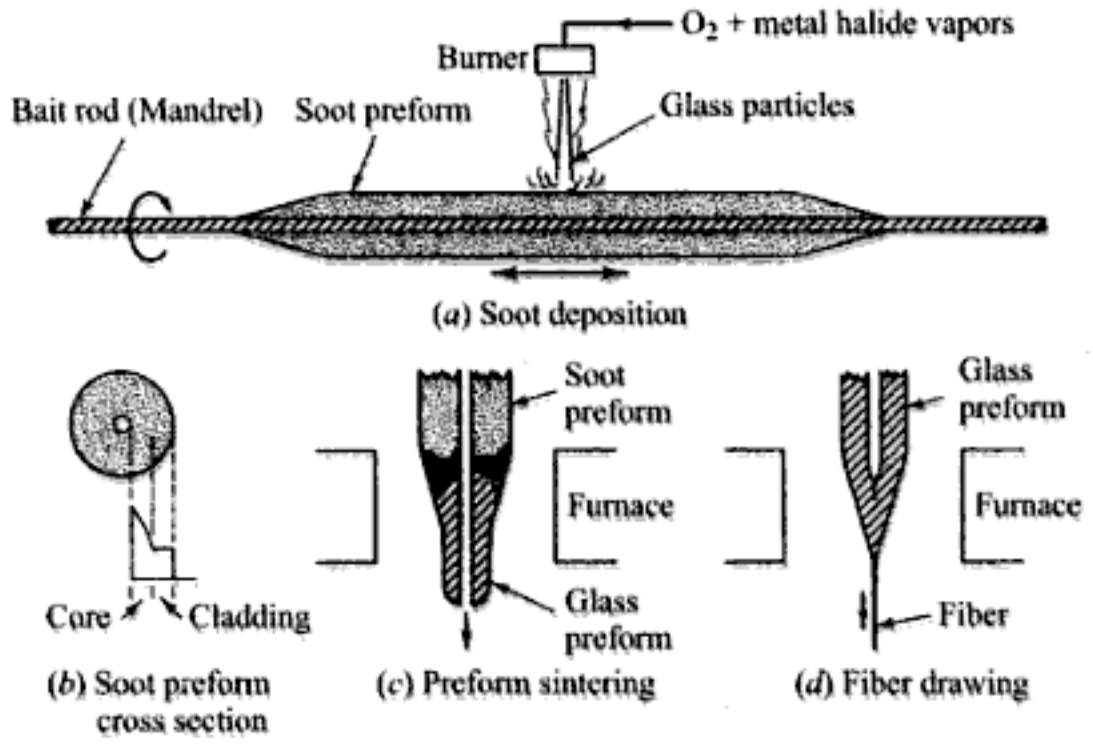

Fig. 2.35 *Basic steps in preparing a preform by the OVPO process. (a) Bait rod rotates and moves back and forth under the burner to produce a uniform deposition of glass soot particles along the rod; (b) Profiles can be step or graded index; (c) Following deposition, the soot preform is sintered into a clear glass preform; (d) fiber is drawn from the glass preform. (Reproduced with permission from Schultz.[55])*

the OVPO process, (2) the preform can be fabricated in continuous lengths which can affect process costs and product yields and (3) the fact that the deposition chamber and the zone-melting ring heater are tightly connected to each other in the same enclosure allows the achievement of a clean environment.

2.9.3 Modified Chemical Vapor Deposition

The *modified chemical vapor deposition* (MCVD) process shown in Fig. 2.37 was pioneered at Bell Laboratories,[43, 65–67] and widely adopted elsewhere to produce very low-loss graded-index fibers. The glass vapor particles, arising from the reaction of the constituent metal halide gases and oxygen, flow through the inside of a revolving silica tube. As the SiO_2 particles are deposited, they are sintered to a clear glass layer by an oxyhydrogen torch which travels back and forth along the tube. When the desired thickness of glass has been deposited, the vapor flow is shut off and the tube is heated strongly to cause it to collapse into a solid rod preform. The fiber that is subsequently drawn from this preform rod will have a core that consists of the vapor-deposited material and a cladding that consists of the original silica tube.

2.9.4 Plasma-Activated Chemical Vapor Deposition

Scientists at Philips Research invented the *plasma-activated chemical vapor deposition* (PCVD) process.[68–70] As shown in Fig. 2.38, the PCVD method is similar to the MCVD process in that deposition occurs within a silica tube. However, a nonisothermal microwave plasma operating at low pressure initiates the chemical reaction. With the silica tube held at temperatures in the range of 1000–1200°C to reduce mechanical stresses in the growing glass films, a moving microwave resonator operating at 2.45

GHz generates a plasma inside the tube to activate the chemical reaction. This process deposits clear glass material directly on the tube wall; there is no soot formation. Thus, no sintering is required. When one has deposited the desired glass thickness, the tube is collapsed into a preform just as in the MCVD case.

2.9.5 Photonic Crystal Fiber Fabrication

The fabrication of a photonic crystal fiber also is based on first creating a preform[71–74]. The perform is made by means of an array of hollow capillary silica tubes. To make a preform for an index-guiding fiber, the capillary tubes first are bundled in an array around a solid silica rod. For a photonic bandgap fiber, the hollow core is established by leaving an empty space at the center of the array. Following the array stacking processes, these configurations are fused together to create a preform and then made into a fiber using a conventional optical fiber drawing tower.

In the drawing process, the holes keep their original arrangement. This allows the creation of any type of array pattern (for example, close-packed arrays, a single circle surrounding a large solid core, or a star-shaped hollow core) and hole shape (for example, circular, hexagonal, or oval openings) in the final fiber.

In addition to using silica, polymer and soft glass materials, such as PMMA and SF6 or SF57 Schott (lead silicate) glass, also have been used to make photonic crystal fibersr[53,71–76]. For these fiber types the preform is made by an extrusion process. In an example extrusion process a glass

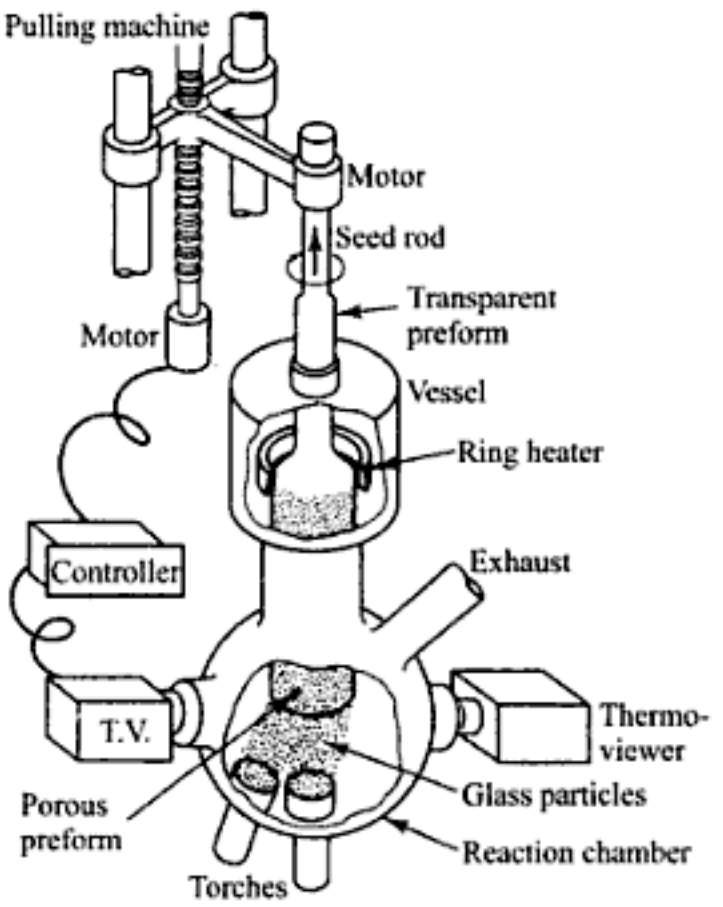

Fig. 2.36 *Apparatus for the VAD (vapor phase axial deposition) process. (Reproduced with permission from Izawa and Inagaki,[63] © 1980, IEEE)*

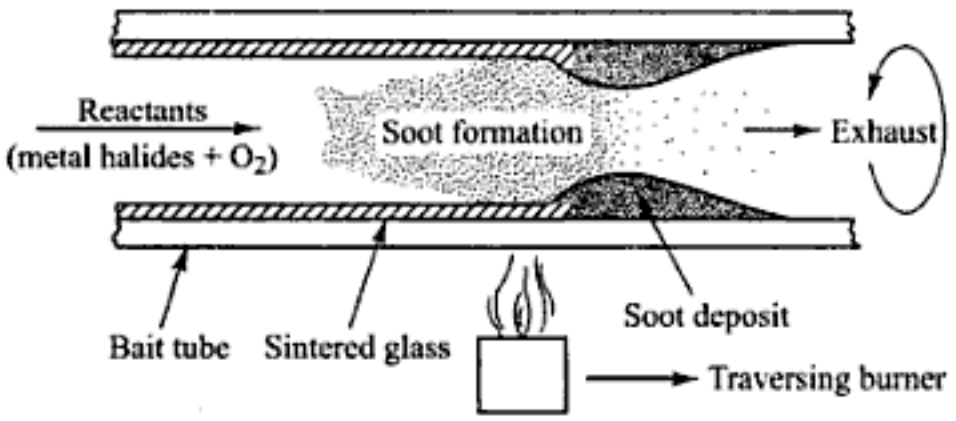

Fig. 2.37 *Schematic of MCVD (modified chemical vapor deposition) process. (Reproduced with permission from Schultz[55])*

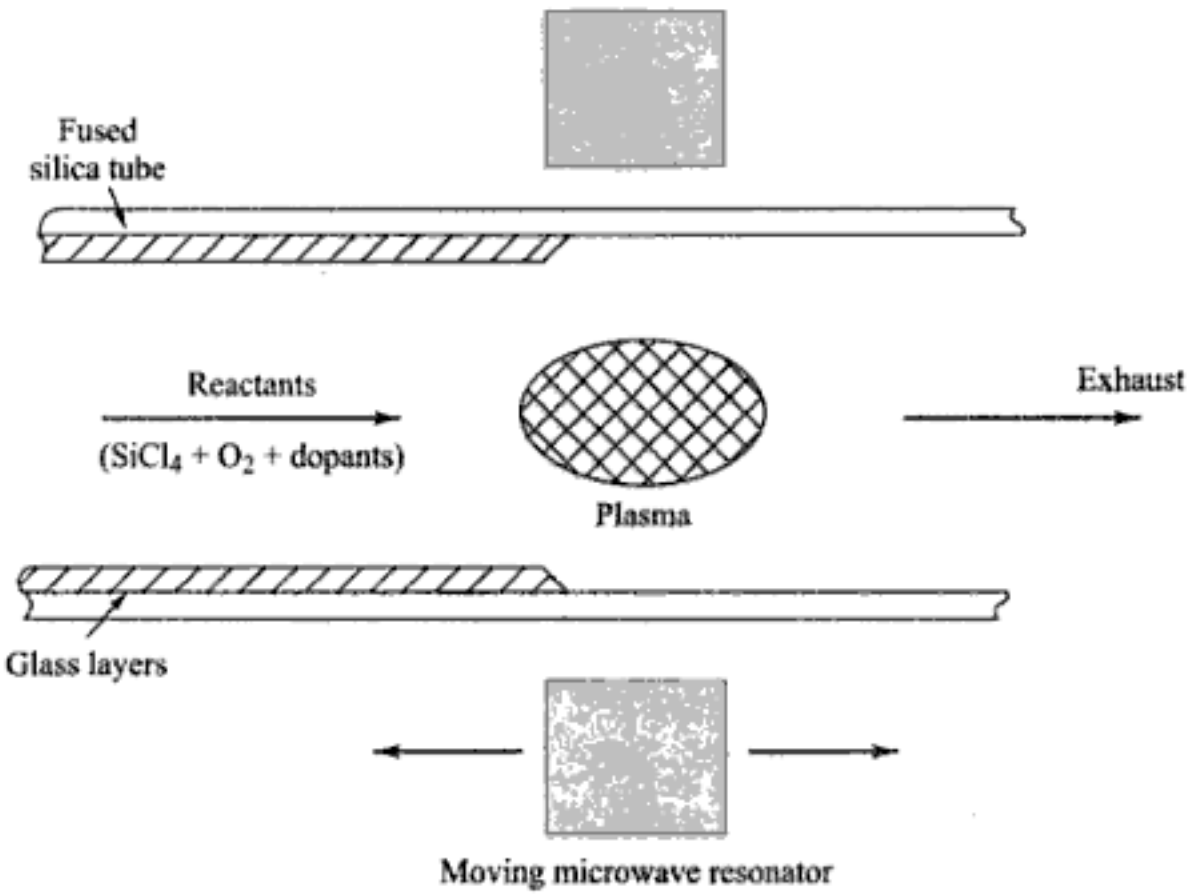

Fig. 2.38 *Schematic of PCVD (plasma-activated chemical vapor deposition) process*

disk is heated until it is soft and then is pressed through a die. The structure of the die determines the configuration of the fiber cross section. The extrusion time typically is around two hours. After the preform is fabricated, fibers are made using standard optical fiber drawing equipment.

2.10 Mechanical Properties of Fibers

In addition to the transmission properties of optical waveguides, their mechanical characteristics play a very important role when fibers are used as the transmission medium in optical communication systems[77–80]. Fibers must be able to withstand the stresses and strains that occur during the cabling process and the loads induced during the installation and service of the cable. During cable manufacture and installation, the loads applied to the fiber can be either impulsive or gradually varying. Once the cable is in place, the service loads are usually slowly varying loads, which can arise from temperature variations or a general settling of the cable following installation.

Strength and *static fatigue* are the two basic mechanical characteristics of glass optical fibers. Since the sight and sound of shattering glass are quite familiar, one intuitively suspects that glass is not a very strong material. However, the longitudinal breaking stress of pristine glass fibers is comparable to that of metal wires. The cohesive bond strength of the constituent atoms of a glass fiber governs its theoretical intrinsic strength. Maximum tensile strengths of 14 GPa (2×10^6 lb/in.^{2}) have been observed in short-gauge-length glass fibers. This is close to the 20-GPa tensile strength of steel wire. The difference between glass and metal is that, under an applied stress, glass will extend elastically up to its breaking strength, whereas metals can be stretched plastically well beyond their true elastic range. Copper wires,

for example, can be elongated plastically by more than 20 percent before they fracture. For glass fibers, elongations of only about 1 percent are possible before fracture occurs.

In practice, the existence of stress concentrations at surface flaws or microcracks limits the median strength of long glass fibers to the 700-to-3500-MPa ($1–5 \times 10^5$ lb/in.^{2}) range. The fracture strength of a given length of glass fiber is determined by the size and geometry of the severest flaw (the one that produces the largest stress concentration) in the fiber. A hypothetical, physical flaw model is shown in Fig. 2.39. This elliptically shaped crack is generally referred to as a *Griffith microcrack*[81]. It has a width w, a depth χ, and a tip radius ρ. The strength of the crack for silica fibers follows the relation

$$K = Y \chi^{1/2} \sigma \tag{2.82}$$

where the stress intensity factor K is given in terms of the stress σ in megapascals applied to the fiber, the crack depth χ in millimeters, and a dimensionless constant Y that depends on flaw geometry. For surface flaws, which are the most critical in glass fibers, $Y = \sqrt{\pi}$. From this equation the maximum crack size allowable for a given applied stress level can be calculated. The maximum values of K depend upon the glass composition but tend to be in the range 0.6–0.9 MN/m$^{3/2}$.

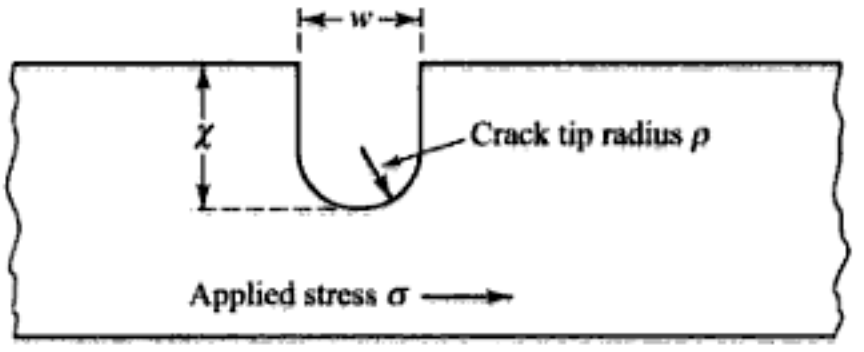

Fig. 2.39 *A hypothetical model of a microcrack in an optical fiber*

Since an optical fiber generally contains many flaws that have a random distribution of size, the fracture strength of a fiber must be viewed statistically. If $F(\sigma, L)$ is defined as the cumulative probability that a fiber of length L will fail below a stress level σ, then, under the assumption that the flaws are independent and randomly distributed in the fiber and that the fracture will occur at the most severe flaw, we have

$$F(\sigma, L) = 1 - e^{-LN(\sigma)} \tag{2.83}$$

where $N(\sigma)$ is the cumulative number of flaws per unit length with a strength less than σ. A widely used form for $N(\sigma)$ is the empirical expression

$$N(\sigma) = \frac{1}{L_0}\left(\frac{\sigma}{\sigma_0}\right)^m \tag{2.84}$$

where m, σ_0, and L_0 are constants related to the initial inert strength distribution. This leads to the so-called *Weibull expression*[82]

$$F(\sigma, L) = 1 - \exp\left[-\left(\frac{\sigma}{\sigma_0}\right)^m \frac{L}{L_0}\right] \tag{2.85}$$

A plot of the Weibull expression is shown in Fig. 2.40 for measurements formed on long-fiber samples[78, 83]. These data points were obtained by testing to destruction a large number of fiber samples. The fact that a single curve can be drawn through the data indicates that the failures arise from a single type of flaw. By careful environmental control of the fiber-drawing furnace, lengths of silica fiber greater than 50 km with a single failure distribution can be fabricated.

In contrast to strength, which relates to instantaneous failure under an applied load, *static fatigue* relates to the slow growth of pre-existing flaws in the glass fiber under humid conditions and tensile stress[78]. This gradual flaw growth causes the fiber to fail at a lower stress level than that which could be reached under a strength test. A flaw such as the one shown in Fig. 2.39 propagates through the fiber because of chemical erosion of the fiber material at the flaw tip. The primary cause of this erosion is the presence of water in the environment, which reduces the strength of the SiO_2 bonds in the glass. The speed of the growth reaction is increased when the fiber is put under stress. Certain fiber materials are more resistant to static fatigue than others, with fused silica being the most resistant of the glasses in water. In general, coatings that are applied to the fiber immediately during the manufacturing process afford a good degree of protection against environmental corrosion[84].

Another important factor to consider is *dynamic fatigue*. When an optical cable is being installed in a duct, it experiences repeated stress owing to surging effects. The surging is caused by varying degrees of friction between the optical cable and the duct or guiding tool in a manhole on a curved route. Varying stresses also arise in aerial cables that are set into transverse vibration by the wind. Theoretical and experimental investigations[85, 86] have shown that the time to failure under these conditions is related

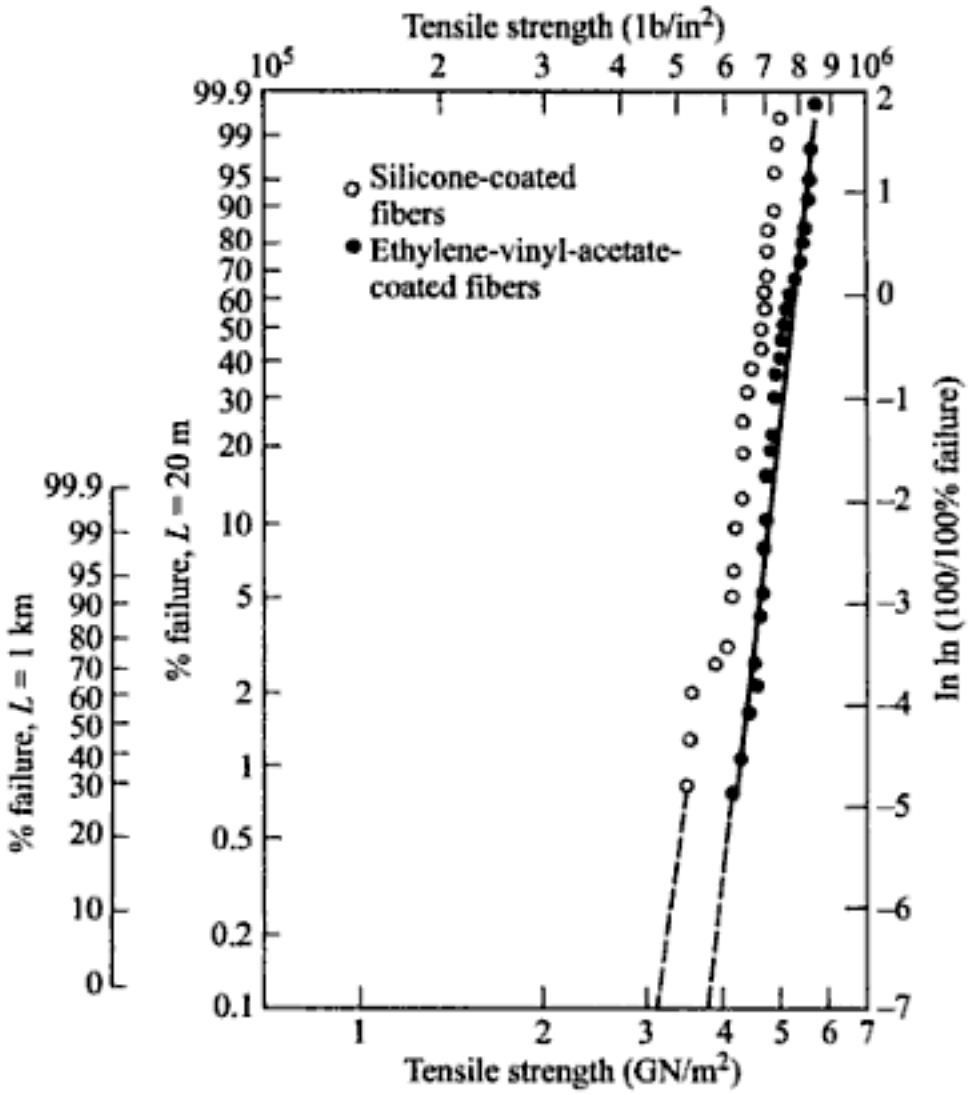

Fig. 2.40 *A Weibull type plot showing the cumulative probability that fibers of 20-m and 1-km lengths will fracture at the indicated applied stress. (Reproduced with permission from Miller, Hart, Vroom, and Bowden.[83])*

to the maximum allowable stress by the same lifetime parameters that are found from the cases of static stress and stress that increases at a constant rate.

A high assurance of fiber reliability can be provided by proof testing.[33, 87, 88] In this method, an optical fiber is subjected to a tensile load greater than that expected at any time during the cable manufacturing, installation, and service. Any fibers which do not pass the proof test are rejected. Empirical studies of slow crack growth show that the growth rate $d\chi/dt$ is approximately proportional to a power of the stress intensity factor; that is,

$$\frac{d\chi}{dt} = AK^b \tag{2.86}$$

Here, A and b are material constants and the stress intensity factor is given by Eq. (2.82). For most glasses, b ranges between 15 and 50.

If a proof test stress σ_p is applied for a time t_p, then from Eq. (2.86) we have

$$B\left(\sigma_i^{b-2} - \sigma_p^{b-2}\right) = \sigma_p^b t_p \tag{2.87}$$

where σ_i is the initial inert strength and

$$B = \frac{2}{b-2}\left(\frac{K}{Y}\right)^{2-b} \frac{1}{AY^b} \tag{2.88}$$

When this fiber is subjected to a static stress σ_s after proof testing, the time to failure t_s is found from Eq. (2.86) to be

$$B\left(\sigma_p^{b-2} - \sigma_s^{b-2}\right) = \sigma_s^b t_s \tag{2.89}$$

Combining Eqs (2.87) and (2.89) yields

$$B\left(\sigma_i^{b-2} - \sigma_s^{b-2}\right) = \sigma_p^b t_p + \sigma_s^b t_s \tag{2.90}$$

To find the failure probability F_s of a fiber after a time t_s after proof testing, we first define $N(t, \sigma)$ to be the number of flaws per unit length which will fail in a time t under an applied stress σ. Assuming thai $N(\sigma_i) \gg N(\sigma_s)$, then

$$N(t_s, \sigma_s) = N(\sigma_i) \tag{2.91}$$

Solving Eq. (2.90) for σ_i and substituting into Eq. (2.84), we have, from Eq. (2.91),

$$N(t_s, \sigma_s) = \frac{1}{L_0}\left\{\frac{\left[\left(\sigma_p^b t_p + \sigma_s^b t_s\right)/B + \sigma_s^{b-2}\right]^{1/(b-2)}}{\sigma_0}\right\}^m \tag{2.92}$$

The failure number $N(t_p, \sigma_p)$ per unit length during proof testing is found from Eq. (2-92) by setting $\sigma_s = \sigma_p$ and letting $t_s = 0$, so that

$$N(t_p, \sigma_p) = \frac{1}{L_0}\left[\frac{\left(\sigma_p^b t_p/B + \sigma_p^{b-2}\right)^{1/(b-2)}}{\sigma_0}\right]^m \tag{2.93}$$

Letting $N(t_s, \sigma_s) = N_s$, the failure probability F_s for a fiber after it has been proof tested is given by

$$F_s = 1 - e^{-L(N_s - N_p)} \tag{2.94}$$

Substituting Eqs (2.92) and (2.93) into Eq. (2.94), we have

$$F_s = 1 - \exp\left(-N_p L\left\{\left[\left(1 + \frac{\sigma_s^b t_s}{\sigma_p^b t_p}\right)\frac{1}{1+C}\right]^{m/(b-2)} - 1\right\}\right) \tag{2.95}$$

where $C = B/\sigma_p^2 t_p$, and where we have ignored the term

$$\left(\frac{\sigma_s}{\sigma_p}\right)^b \frac{B}{\sigma_s^2 t_p} \ll 1 \tag{2.96}$$

This holds because typical values of the parameters in this term are $\sigma_s/\sigma_p = 0.3 - 0.4$, $t_p = 10\,s$, $b > 15$, $\sigma_p = 350\ \text{MN/m}^2$, and $B = 0.05 - 0.5\ (\text{MN/m}^2)^2\text{s}$.

The expression for F_s given by Eq. (2.95) is valid only when the proof stress is unloaded immediately, which is not the case in actual proof testing of optical fibers. When the proof stress is released within a finite duration, the C value should be rewritten as

$$C \cong \gamma \frac{B}{\sigma_p^2 t_p} \tag{2.97}$$

where γ is a coefficient of slow-crack-growth effect arising during the unloading period.

2.11 Fiber Optic Cables

In any practical application of optical waveguide technology, the fibers need to be incorporated in some type of cable structure[89–95]. The cable structure will vary greatly, depending on whether the cable is to be pulled into underground or intrabuilding ducts, buried directly in the ground, installed on outdoor poles, or submerged under water. Different cable designs are required for each type of application, but certain fundamental cable design principles will apply in every case. The objectives of cable manufacturers have been that the optical fiber cables should be installable with the same equipment, installation techniques, and precautions as those used for conventional wire cables. This requires special cable designs because of the mechanical properties of glass fibers.

2.11.1 Cable Structures

One important mechanical property is the maximum allowable axial load on the cable, since this factor determines the length of cable that can be reliably installed. In copper cables the wires themselves are generally the principal load-bearing members of the cable, and elongations of more than 20 percent are possible without fracture. On the other hand, extremely strong optical fibers tend to break at 4-percent elongation, whereas typical good-quality fibers exhibit long-length breaking elongations of about 0.5–1.0 percent. Since static fatigue occurs very quickly at stress levels above 40 percent of the permissible

elongation and very slowly below 20 percent, fiber elongations during cable manufacture and installation should be limited to 0.1 – 0.2 percent.

Steel wire has been used extensively for reinforcing electric cables and also can be used as a *strength member* for optical fiber cables. For some applications it is desirable to have a completely nonmetallic construction, either to avoid the effects of electromagnetic induction or to reduce cable weight. In such cases, plastic strength members and high-tensile-strength synthetic yarns are used. A popular yarn is Kevlar®, which is a soft but tough yellow synthetic nylon material belonging to a generic yarn family known as *aramids*. Good fabrication practices will isolate the fibers from other cable components, keep them close to the neutral axis of the cable and allow the fibers to move freely when the cable is flexed or stretched.

The generic cable configuration shown in Fig. 2.41 illustrates some common materials that are used in the optical fiber cabling process. Individual fibers or modules of bundled fiber groupings and optional copper wires for powering in-line equipment are wound loosely around the central buffered strength member. A cable wrapping tape and other strength members such as Kevlar then encapsulate and bind these fiber groupings together. Surrounding all these components is a tough polymer *jacket* that provides crush resistance and handles any tensile stresses applied to the cable so that the fibers inside are not damaged. The jacket also protects the fibers inside against abrasion, moisture, oil, solvents, and other contaminants. The jacket type largely defines the application characteristics, for example, heavy-duty outside-plant cables for direct-burial and aerial applications have much thicker and tougher jackets than light-duty indoor cables.

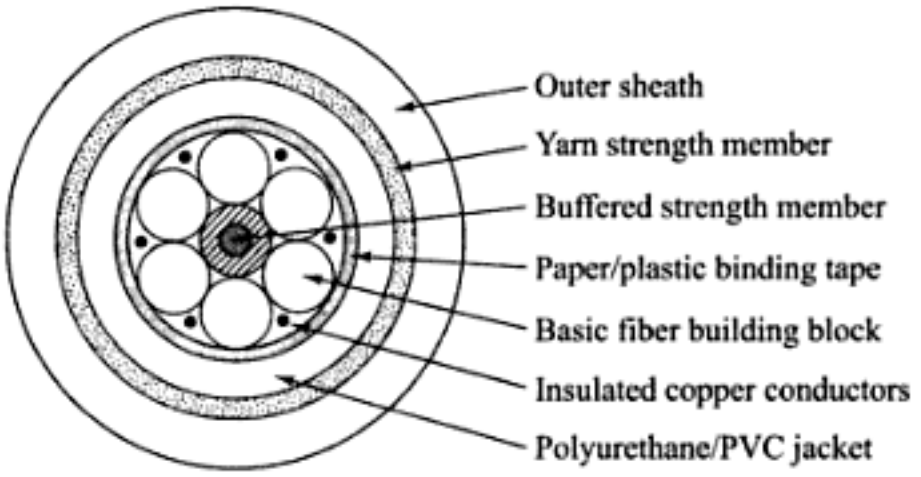

Fig. 2.41 *A typical six-fiber cable created by stranding six basic fiber-building blocks around a central strength member*

The two basic fiber optic cable structures are the *tight-buffered fiber cable* design and the *loose-tube cable* configuration. Cables with tight-buffered fibers nominally are used indoors whereas the loose-tube structure is intended for long-haul outdoor applications. A *ribbon cable* is an extension of the tight-buffered cable. In all cases the fibers themselves consist of the normally manufactured glass core and cladding which is surrounded by a protective 250-μm diameter coating.

As shown in Fig. 2.42, in the *tight-buffered* design each fiber is individually encapsulated within its own 900-μm diameter plastic buffer structure, hence the designation *tight-buffered design*. The 900-μm buffer is nearly four times the diameter and five times the thickness of the 250-μm protective coating material. This construction feature contributes to the excellent moisture and temperature performance of tight-buffered cables and also permits their direct termination with connectors. In a single-fiber module, a layer of amarid strength material surrounds the 900-μm fiber structure. This configuration then is encapsulated within a PVC outer jacket.

In the *loose-tube* cable configuration one or more standard-coated fibers are enclosed in a thermoplastic tube that has an inner diameter which is much larger than the fiber diameter as shown in Fig. 2.43. The fibers in the tube are slightly longer than the cable itself. The purpose of this construction is to isolate

the fiber from any stretching of the surrounding cable structure caused by factors such as temperature changes, wind forces, or ice loading. The tube is filled with either a *gel* or a dry *water-blocking material* that act as buffers, enable the fibers to move freely within the tube, and prevent moisture from entering the tube.

To facilitate the field operation of splicing cables that contain a large number of fibers, cable designers devised the fiber-ribbon structure. As shown in Fig. 2.44, the *ribbon cable* is an arrangement of fibers that are aligned precisely next to each other and then are encapsulated in a plastic buffer or jacket to form a long continuous ribbon. The number of fibers in a ribbon typically ranges from four to twelve. These ribbons can be stacked on top of each other to form a densely packed arrangement of many fibers (e.g., 144 fibers) within a cable structure.

There are many different ways in which to arrange fibers inside a cable. The particular arrangement of fibers and the cable design itself need to take into account issues such as the physical environment, the services that the optical link will provide, and any anticipated maintenance and repair that may be needed.

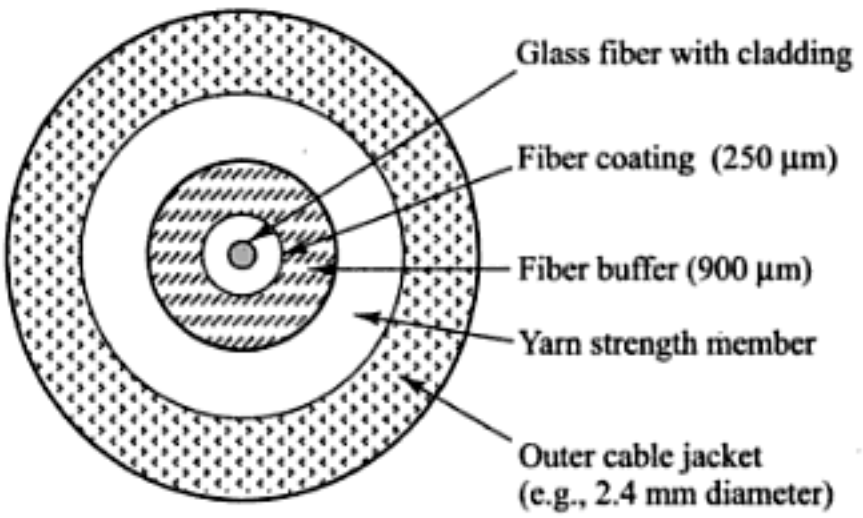

Fig. 2.42 *Construction of a simplex tight-buffered fiber cable module*

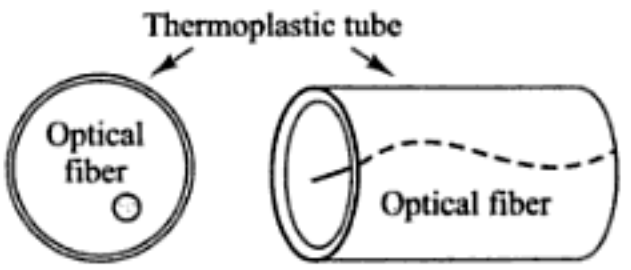

Fig. 2.43 *Concept of a loose-tube cable configuration*

2.11.2 Indoor Cable Designs

Indoor cables can be used for interconnecting instruments, for distributing signals among office users, for connections to printers or servers, and for short patch cords in telecommunication equipment racks. The three main types are described here.

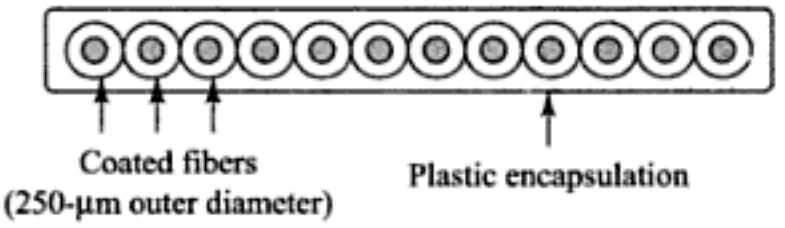

Fig. 2.44 *Example of a twelve-fiber ribbon cable module*

Interconnect cable serves light-duty low-fiber count indoor applications such as fiber-to-the-desk links, patch cords, and point-to-point runs in conduits and trays. The cable is flexible, compact, and lightweight with a tight-buffered construction. A popular indoor cable type is the *duplex cable,* which consists of two fibers that are encapsulated in an outer PVC jacket. Fiber optic *patch cords,* also known as *jumper cables,* are short lengths (usually less than 2 m) of simplex or duplex cable with connectors on both ends. They are used to connect lightwave test equipment to a fiber patch panel or to interconnect optical transmission modules within an equipment rack.

Breakout or ***fanout*** cable consists of up to 12 tight-buffered fibers stranded around a central strength member. Such cables serve low- to medium-fiber-count applications where it is necessary to protect individual jacketed fibers. The breakout cable allows easy installation of connectors on individual fibers in the cable. With such a cable configuration, routing the individually terminated fibers to separate pieces of equipment can be achieved easily.

Distribution cable consists of individual or small groupings of tight-buffered fibers stranded around a central strength member. This cable serves a wide range of network applications for sending data, voice, and video signals. Distribution cables are designed for use in intra-building cable trays, conduits, and loose placement in dropped-ceiling structures. A main feature is that they enable groupings of fibers within the cable to be branched (distributed) to various locations.

2.11.3 Outdoor Cables

Outdoor cable installations include aerial, duct, direct-burial, and underwater applications. Invariably these cables consist of a loose-tube structure. Many different designs and sizes of outdoor cables are available depending on the physical environment in which the cable will be used and the particular application.

Aerial cable is intended for mounting outside between buildings or on poles or towers. The two popular designs are the self-supporting and the facility-supporting cable structures. The *self-supporting cable* contains an internal strength member that permits the cable to be strung between poles without using any additional support mechanisms for the cable. For the *facility-supporting cable* first a separate wire or strength member is strung between the poles and then the cable is lashed or clipped to this member.

Armored cable for direct-burial or underground-duct applications has one or more layers of steel-wire or steel-sheath protective armoring below a layer of polyethylene jacketing as shown in Fig. 2.45. This not only provides additional strength to the cable but also protects it from gnawing animals such as squirrels or burrowing rodents, which often cause damage to underground cables. For example, in the

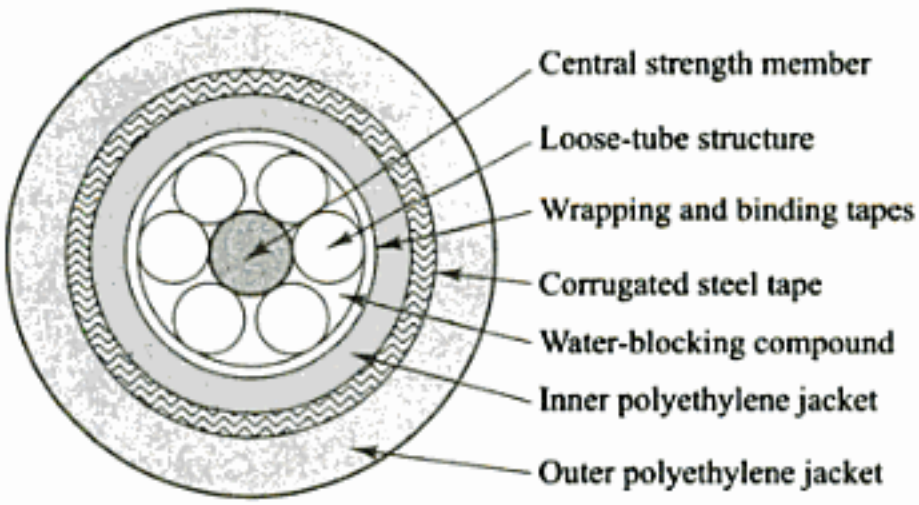

Fig. 2.45 *Example configuration of an armored outdoor fiber optic cable*

United States the plains pocket gopher *(Geomys busarius)* can destroy unprotected cable that is buried less than 2 m (6 ft) deep. Other cable components include a central strength member, wrapping and binding tapes, and water-blocking materials.

Underwater cable, also known as *submarine cable*, is used in rivers, lakes, and ocean environments. Since such cables normally are exposed to high water pressures, they have much more stringent requirements than underground cables. For example, as shown in Fig. 2.46 cables that can be used in rivers and lakes have various water-blocking layers, one or more protective inner polyethylene sheaths, and a heavy outer armor jacket. Cables that run under the ocean have further layers of armoring and contain copper wires to provide electrical power for submersed optical amplifiers or regenerators.

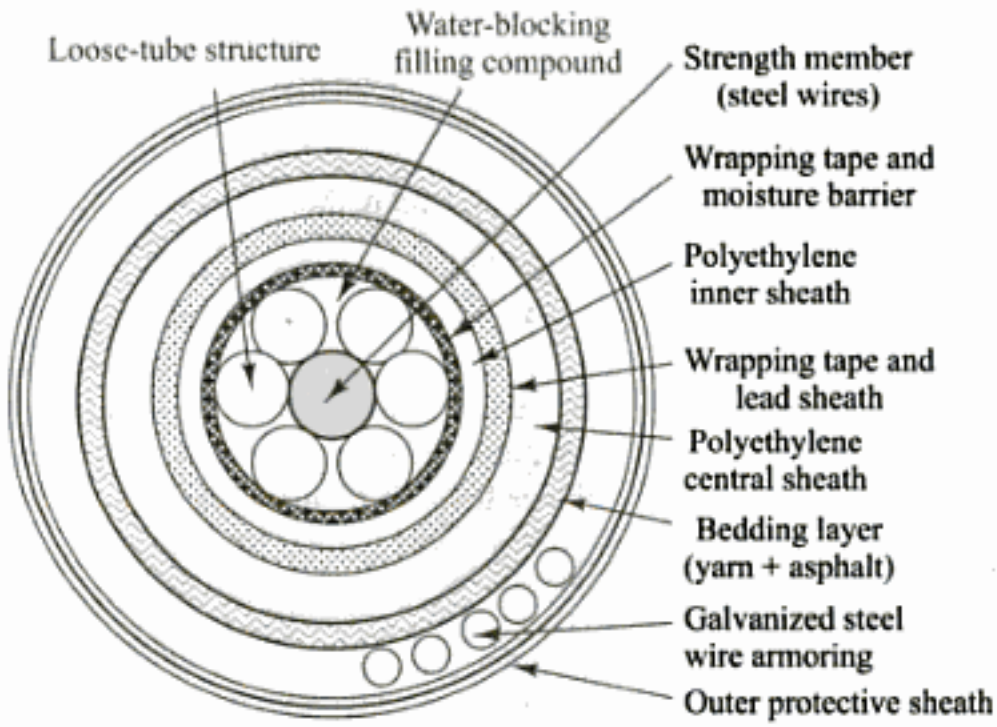

Fig. 2.46 *Example configuration of an underwater fiber optic cable*

2.11.4 Installation Methods

Workers can install optical fiber cables by plowing them directly into the ground, laying them in an outside trench, pulling or blowing them through ducts (both indoor and outdoor) or other spaces, suspending them on poles, or placing them underwater. Although each method has its own special handing procedures, they all need to adhere to a common set of precautions. These include avoiding sharp bends of the cable, minimizing stresses on the installed cable, periodically allowing extra cable slack along the cable route for unexpected repairs, and avoiding excessive pulling forces on the cable.

The ITU-T has published a number of L-series recommendations for the construction, installation, and protection of fiber optic cables in the outside plant.

Table 2.5 lists some of these recommendations and states their application.

Table 2.3 *Some ITU-T recommendations for optical fiber cable installations*

Recommendation Name	*Description*
L.35, *Installation of optical fiber cables in the access network*, Oct. 1998.	Gives guidance for installing optical cables in ducts, on poles, and through direct burial.
L.38, *Use of trenchless techniques for the construction of underground infrastructures for telecommunication cable installation*, Sept. 1999.	Describes underground drilling techniques for installing telecommunication cables without the need for disruptive excavation or plowing.
L.39, *Investigation of the soil before using trenchless techniques*, May 2000.	Describes soil-investigation techniques for obtaining information about the position of buried objects and the nature of the ground.
L.42, *Mini-trench installation techniques*, March 2003.	Describes a technique for putting duct-based underground optical cables in small trenches. This allows quicker installations, lower cost, and limited surface disruption.
L.43, *Micro-trench installation techniques*, March 2003.	Describes installing underground cables at a shallow depth in small grooves.
L.57, *Air-assisted installation of optical fiber cables*, May 2003.	Describes air-assisted methods for installation of optical fiber cables in ducts.

PROBLEMS

2.1 Consider an electric field represented by the expression

$$\mathbf{E} = \left[100e^{j30^\circ}\mathbf{e}_x + 20e^{-j50^\circ}\mathbf{e}_y + 40e^{j210^\circ}e_z\right]e^{j\omega t}$$

Express this as a measurable electric field as described by Eq. (2.2) at a frequency of 100 MHz.

2.2 A wave is specified by $y = 8\cos 2\pi(2t - 0.8z)$, where y is expressed in micrometers and the propagation constant is given in μm^{-1}. Find (*a*) the amplitude, (*b*) the wavelength, (*c*) the angular frequency, and (*d*) the displacement at time $t = 0$ and $z = 4$ μm.

2.3 Consider two plane waves X_1 and X_2 traveling in the same direction. If they have the same frequency ω but different amplitudes a_i and phases δ_i, then we can represent them by

$$X_1 = a_1\cos(\omega t - \delta_1)$$
$$X_1 = a_2\cos(\omega t - \delta_2)$$

According to the principle of superposition, the resultant wave X is simply the sum of X_1 and X_2. Show that X can be written in the form

$$X = A\cos(\omega t - \phi)$$

where

$$A^2 = a_1^2 + a_2^2 + 2a_1a_2\cos(\delta_1 - \delta_2)$$

and

$$\tan\phi = \frac{a_1\sin\delta_1 + a_2\sin\delta_2}{a_1\cos\delta_1 + a_2\cos\delta_2}$$

2.4 Elliptically polarized light can be represented by the two orthogonal waves given in Eqs (2.2) and (2.3). Show that elimination of the $(\omega t - kz)$ dependence between them yields

$$\left(\frac{E_x}{E_{0x}}\right)^2 + \left(\frac{E_y}{E_{0y}}\right)^2 - 2\frac{E_x}{E_{0x}}\frac{E_y}{E_{0y}}\cos\delta = \sin^2\delta$$

which is the equation of an ellipse making an angle α with the x axis, where α is given by Eq. (2.8).

2.5 Let $E_{0x} = E_{0y} = 1$ in Eq. (2.7). Using a computer or a graphical calculator, write a program to plot this equation for values of $\delta = (n\pi)/8$, where $n = 0, 1, 2, \ldots 16$. What does this show about the state of polarization as the angle δ changes?

2.6 Show that any linearly polarized wave may be considered as the superposition of left and right circularly polarized waves which are in phase and have equal amplitudes and frequencies.

2.7 Light traveling in air strikes a glass plate at an angle $\theta_i = 33°$, where θ_i is measured between the incoming ray and the glass surface. Upon striking the glass, part of the beam is reflected and part is refracted. If the refracted and reflected beams make an angle of 90° with each other, what is the refractive index of the glass? What is the critical angle for this glass?

2.8 A point source of light is 12 cm below the surface of a large body of water ($n = 1.33$ for water). What is the radius of the largest circle on the water surface through which the light can emerge?

2.9 A 45°–45°–90° prism is immersed in alcohol ($n = 1.45$). What is the minimum refractive index the prism must have if a ray incident normally on one of the short faces is to be totally reflected at the long face of the prism?

2.10 Show that the critical angle at an interface between doped silica with $n_1 = 1.460$ and pure silica with $n_2 = 1.450$ is 83.3°.

2.11 The reflection coefficient R_p for parallel polarized light is given by

$$R_p = \frac{n_1 \cos\varphi_2 - n_2 \cos\varphi_1}{n_1 \cos\varphi_2 + n_2 \cos\varphi_1}$$

Show that the condition $R_p = 0$ for the Brewster angle occurs when $\tan\varphi_1 = n_2/n_1$.

2.12 Calculate the numerical aperture of a step-index fiber having $n_1 = 1.48$ and $n_2 = 1.46$. What is the maximum entrance angle $\theta_{0,\max}$ for this fiber if the outer medium is air with $n = 1.00$?

2.13 Consider a dielectric slab having a thickness $d = 10$ mm and index of refraction $n_1 = 1.50$. Let the medium above and below the slab be air, in which $n_2 = 1$. Let the wavelength be $\lambda = 10$ mm (equal to the thickness of the waveguide).

(*a*) What is the critical angle for the slab waveguide?

(*b*) Solve Eq. (2.26*b*) graphically to show that there are three angles of incidence which satisfy this equation.

(*c*) What happens to the number of angles as the wavelength is decreased?

2.14 Derive the approximation of the right-hand side of Eq. (2.23) for $\Delta \ll 1$. What is the difference in the approximate and exact expressions for the value of NA if $n_1 = 1.49$ and $n_2 = 1.48$?

2.15 Using the expressions in Eqs (2.33) and (2.34) derived from Maxwell's curl equations, derive the radial and transverse electric and magnetic field components given in Eqs (2.35*a*) to (2.35*d*). Show that these expressions lead to Eqs (2.36) and (2.37).

2.16 Show that for $\nu = 0$, Eq. (2.55*b*) corresponds to TE_{0m} modes ($E_z = 0$) and that Eq. (2.56*b*) corresponds to TM_{0m} modes ($H_z = 0$).

2.17 Verify that $k_1^2 \approx k_2^2 \approx \beta^2$ when $\Delta \ll 1$, where k_1 and k_2 are the core and cladding propagation constants, respectively, as defined in Eq. (2.46).

2.18 A step-index multimode fiber with a numerical aperture of 0.20 supports approximately 1000 modes at an 850-nm wavelength.

(*a*) What is the diameter of its core?

(*b*) How many modes does the fiber support at 1320 nm?

(c) How any modes does the fiber support at 1550 nm?

2.19 (*a*) Determine the normalized frequency at 820 nm for a step-index fiber having a 25-μm core radius, $n_1 = 1.48$, and $n_2 = 1.46$.

(*b*) How many modes propagate in this fiber at 820 nm?

(*c*) How many modes propagate in this fiber at 1320 nm?

(*d*) How many modes propagate in this fiber at 1550 nm?

(*e*) What percent of the optical power flows in the cladding in each case?

2.20 Consider a fiber with a 25-μm core radius, a core index $n_1 = 1.48$, and $\Delta = 0.01$.

(*a*) If $\lambda = 1320$ nm, what is the value of V and how many modes propagate in the fiber?

(*b*) What percent of the optical power flows in the cladding?

(*c*) If the core–cladding difference is reduced to $\Delta = 0.003$, how many modes does the fiber support and what fraction of the optical power flows in the cladding?

2.21 Find the core radius necessary for single-mode operation at 1320 nm of a step-index fiber with $n_1 = 1.480$ and $n_2 = 1.478$. What are the numerical aperture and maximum acceptance angle of this fiber?

2.22 A manufacturer wishes to make a silica-core, step-index fiber with $V = 75$ and a numerical aperture NA = 0.30 to be used at 820 nm. If $n_1 = 1.458$, what should the core size and cladding index be?

2.23 Draw a design curve of the fractional refractive-index difference Δ versus the core radius a for a silica-core ($n_1 = 1.458$), single-mode fiber to operate at 1300 nm. Suppose the fiber we select from this curve has a 5-μm core radius. Is this fiber still single-mode at 820 nm? Which modes exist in the fiber at 820 nm?

2.24 Using the following approximation for W_0 given by Marcuse[96].

$W_0 = a(0.65 + 1.619V^{-3/2} + 2.879\ V^{-6})$

evaluate and plot $E(r)/E_0$ with r ranging from 0 to 3 for values of $V = 1.0, 1.4, 1.8, 2.2, 2.6,$ and 3.0. Here a is the fiber radius.

2.25 Commonly available single-mode fibers have beat lengths in the range 10 cm $< L_p <$ 2 m. What range of birefringent refractive-index differences does this correspond to for $\lambda =$ 1300 nm?

2.26 Plot the refractive-index profiles from n_1 to n_2 as a function of radial distance $r \leq a$ for graded-index fibers that have α values of 1, 2, 4, 8, and ∞ (step index). Assume the fibers have a 25-μm core radius, $n_1 = 1.48$, and $\Delta = 0.01$.

2.27 Calculate the number of modes at 820 nm and 1.3 μm in a graded-index fiber having a parabolic-index profile ($\alpha = 2$), a 25-μm core radius, $n_1 = 1.48$, and $n_2 = 1.46$. How does this compare to a step-index fiber?

2.28 Calculate the numerical apertures of (*a*) a plastic step-index fiber having a core refractive index of $n_1 = 1.60$ and a cladding index of $n_2 = 1.49$, (*b*) a step-index fiber having a silica core ($n_1 = 1.458$) and a silicone resin cladding ($n_2 = 1.405$).

2.29 When a preform is drawn into a fiber, the principle of conservation of mass must be satisfied under steady-state drawing conditions. Show that for a solid rod preform this is represented by the expression

$$s = S\left(\frac{D}{d}\right)^2$$

where D and d are the preform and fiber diameters, and S and s are the preform feed and fiber-draw speeds, respectively. A typical drawing speed is 1.2 m/s for a 125-μm outer-diameter fiber. What is the preform feed rate in cm/min for a 9-mm-diameter preform?

2.30 A silica tube with inside and outside radii of 3 and 4 mm, respectively, is to have a certain thickness of glass deposited on the inner surface. What should the thickness of this glass deposition be if a fiber having a core diameter of 50 μm and an outer cladding diameter of 125 μm is to be drawn from this perform using the MCVD fabrication process.

2.31 (*a*) The density of fused silica is 2.6 g/cm^3. How many grams are needed for a 1-km-long 50-μm-diameter fiber core?

(*b*) If the core material is to be deposited inside of a glass tube at a 0.5-g/min deposition rate, how long does it take to make the preform for this fiber?

2.32 During fabrication of optical fibers, dust particles incorporated into the fiber surface are prime examples of surface flaws that can lead to reduced fiber strength. What size dust particles are tolerable if a glass fiber having a 20-N/mm$^{3/2}$ stress intensity factor is to withstand a 700-MN/m^2 stress?

2.33 Static fatigue in a glass fiber refers to the condition where a fiber is stressed to a level σ_a, which is much less than the fracture stress associated with the weakest flaw. Initially, the fiber will not fail but, with time, cracks in the fiber will grow as a result of chemical erosion at the crack tip. One model for the growth rate of a crack of depth χ assumes a relation of the form given in Eq. (2.86).

(*a*) Using this equation, show that the time required for a crack of initial depth χ_i to grow to its failure size χ_f is given by

$$t = \frac{2}{(b-2)A(Y\sigma)^b}\left[\chi_i^{(2-b)/2} - \chi_f^{(2-b)/2}\right]$$

(*b*) For long, static fatigue times (on the order of 20 years), $K_i^{2-b} \ll K_f^{2-b}$ for large values of b. Show that under this condition the failure time is

$$t = \frac{2K_i^{2-b}}{(b-2)A\sigma^2 Y^2}$$

REFERENCES

1. See any general physics book or introductory optics book; for example:
   (*a*) D. Halliday, R. Resnick, and J. Walker, *Fundamentals of Physics*, Wiley, Hoboken, NJ, 7th ed., 2004.
   (*b*) E. Hecht, *Optics*, Addison-Wesley, Boston, 4th ed., 2002.
   (*c*) F. A. Jenkins and H. E. White, *Fundamentals of Optics*, McGraw-Hill, Burr Ridge, IL, 4th ed., 2001.
2. See any introductory electromagnetics book; for example:
   (*a*) W. H. Hayt, Jr. and J. A. Buck, *Engineering Electromagnetics*, McGraw-Hill, Burr Ridge, IL, 4th ed., 2006.
   (*b*) F. T. Ulaby, *Fundamentals of Applied Electromagnetics*, Prentice Hall, Upper Saddle River, NJ, 5th ed., 2007.
   (*c*) J. Franklin, *Classical Electromagnetism*, Prentice Hall, Upper Saddle River, NJ, 2005.
3. E. A. J. Marcatili, "Objectives of early fibers: Evolution of fiber types," in S. E. Miller and A. G. Chynoweth, eds., *Optical Fiber Telecommunications*, Academic, New York, 1979.
4. L. B. Felsen, "Rays and modes in optical fibers," *Electron. Lett.*, vol. 10, pp. 95–96, Apr. 1974.
5. A. W. Snyder and D. J. Mitchell, "Leaky rays on circular optical fibers," *J. Opt. Soc. Amer.*, vol. 64, pp. 599–607, May 1974.
6. A. W. Snyder and J. D. Love, *Optical Waveguide Theory*, Chapman & Hall, New York, 1983.
7. D. Marcuse, *Theory of Dielectric Optical Waveguides*, Academic, New York, 2nd ed., 1991.
8. H. G. Unger, *Planar Optical Waveguides and Fibers*, Clarendon, Oxford, 1977.
9. R. Syms and J. Cozens, *Optical Guided Waves and Devices*, McGraw-Hill, New York, 1992.
10. K. Kawano and T. Kitoh, *Introduction to Optical Waveguide Analysis: Solving Maxwell's Equation and the Schrödinger Equation*, Wiley, Hoboken, NJ, 2002.
11. J. A. Buck, *Fundamentals of Optical Fibers*, Wiley, Hoboken, NJ, 2nd ed., 2004.
12. R. Olshansky, "Leaky modes in graded index optical fibers," *Appl. Opt.*, vol. 15, pp. 2773–2777, Nov. 1976.
13. A. Tomita and L. G. Cohen, "Leaky-mode loss of the second propagation mode in single-mode fibers with index well profiles," *Appl. Opt.*, vol. 24, pp. 1704–1707, 1985.
14. E. Snitzer, "Cylindrical dielectric waveguide modes," *J. Opt. Soc. Amer.*, vol. 51, pp. 491–498, May 1961.
15. M. Koshiba, *Optical Waveguide Analysis*, McGraw-Hill, New York, 1992.
16. D. Marcuse, *Light Transmission Optics*, Van Nostrand-Reinhold, New York, 2nd ed., 1982.
17. R. Olshansky, "Propagation in glass optical waveguides," *Rev. Mod. Phys.*, vol. 51, pp. 341–367, Apr. 1979.
18. D. Gloge, "The optical fiber as a transmission medium," *Rep. Progr. Phys.*, vol. 42, pp. 1777–1824, Nov. 1979.
19. A. W. Snyder, "Asymptotic expressions for eigenfunctions and eigenvalues of a dielectric or optical waveguide," *IEEE Trans. Microwave Theory Tech.*, vol. MTT-17, pp. 1130–1138, Dec. 1969.
20. D. Gloge, "Weakly guiding fibers," *Appl. Opt.*, vol. 10, pp. 2252–2258, Oct. 1971.
21. D. Marcuse, "Gaussian approximation of the fundamental modes of graded index fibers," *J. Opt. Soc. Amer*, vol. 68, pp. 103–109, Jan. 1978.

22. H. M. DeRuiter, "Integral equation approach to the computation of modes in an optical waveguide," *J. Opt. Soc. Amer*, vol. 70, pp. 1519–1524, Dec. 1980.
23. A. W. Snyder, "Understanding monomode optical fibers," *Proc. IEEE*, vol. 69, pp. 6–13, Jan. 1981.
24. A. Jeffery, *Handbook of Mathematical Formulas and Integrals*, Academic, Third Edition, 2004.
25. M. Kurtz, *Handbook of Applied Mathematics for Engineers and Scientists*, McGraw-Hill, New York, 1991.
26. D. Zwillinger, ed., *Standard Mathematical Tables and Formulae*, CRC Press, Boca Raton, FL, 31th ed., 2003.
27. D. Marcuse, D. Gloge, and E. A. J. Marcatili, "Guiding properties of fibers," in S. E. Miller and A. G. Chynoweth, eds., *Optical Fiber Telecommunications*, Academic, New York, 1979.
28. R. M. Gagliardi and S. Karp, *Optical Communications*, Wiley, New York, 2nd ed., 1995.
29. D. Gloge, "Propagation effects in optical fibers," *IEEE Trans. Microwave Theory Tech.*, vol. MTT-23, pp. 106–120, Jan. 1975.
30. M. Artiglia, G. Coppa, P. DiVita, M. Potenza, and A. Sharma, "Mode field diameter measurements in single-mode optical fibers," *J. Lightwave Tech.*, vol. 7, pp. 1139–1152, Aug. 1989.
31. T. J. Drapela, D. L. Franzen, A. H. Cherin, and R. J. Smith, "A comparison of far-field methods for determining mode field diameter of single-mode fibers using both gaussian and Petermann definitions," *J. Lightwave Tech.*, vol. 7, pp. 1153–1157, Aug. 1989.
32. K. Petermann, "Constraints for fundamental mode spot size for broadband dispersion-compensated single-mode fibers," *Electron. Lett.*, vol. 19, pp. 712–714, Sept. 1983.
33. ITU-T Recommendation G.650, *Definition and Test Methods for the Relevant Parameters of Single-Mode Fibers*, Apr. 1997.
34. TIA/EIA FOTP-191, *Measurement of Mode Field Diameter of Single-Mode Fiber*, Sept. 1998.
35. F. Kapron, "Fiber-optic test methods," in F. Allard, ed., *Fiber Optics Handbook for Engineers and Scientists*, McGraw-Hill, New York, 1990.
36. D. K. Mynbaev and L. L. Scheiner, *Fiber-Optic Communications Technology*, Prentice Hall, Upper Saddle River, NJ, 2001.
37. I. P. Kaminow, "Polarization in optical fibers," *IEEE J. Quantum Electron.*, vol. QE-17, pp. 15–22, Jan. 1981.
38. S. C. Rashleigh, "Origins and control of polarization effects in single-mode fibers," *J. Lightwave Tech.*, vol. LT-1, pp. 312–331, June 1983.
39. X.-H. Zheng, W. M. Henry, and A. W. Snyder, "Polarization characteristics in the fundamental mode of optical fibers," *J. Lightwave Tech.*, vol. LT-6, pp. 1300–1305, Aug. 1988.
40. D. Gloge and E. Marcatili, "Multimode theory of graded core fibers," *Bell Sys. Tech. J.*, vol. 52, pp. 1563–1578, Nov. 1973.
41. B. E. A. Saleh and M. Teich, *Fundamentals of Photonics*, Chap. 8, Wiley, Hoboken, NJ, 2nd ed., 2007.
42. R. H. Doremus, *Glass Science*, Wiley, Hoboken, NJ, 2nd ed., 1994.
43. S. R. Nagel, "Fiber materials and fabrication methods," in S. E. Miller and I. P. Kaminow, eds., *Optical Fiber Telecommunications-II*, Academic, New York, 1988.
44. B. Mysen and P. Richet, *Silicate Glasses and Melts*, Elsevier, 2005.
45. B. J. Ainslie, "A review of the fabrication and properties of erbium-doped fibers for optical amplifiers," *J. Lightwave Tech.*, vol. 9, pp. 220–227, Feb. 1991.
46. W. Miniscalco, "Erbium-doped glasses for fiber amplifiers at 1500 nm," *J. Lightwave Tech.*, vol. 9, pp. 234–250, Feb. 1991.
47. E. Desurvire, *Erbium-Doped Fiber Amplifiers*, Wiley, Hoboken, NJ, 2002.
48. J. Zubia and J. Arrue, "Plastic optical fibers: An introduction to their technological processes and applications," *Opt. Fiber Technol.*, vol. 7, no. 2, pp. 101–140, Apr. 2001.
49. I. T. Monroy, H. P. A. vd Boom, A. M. J. Koonen, G. D. Khoe, Y. Watanabe, Y. Koike, and T. Ishigure, "Data transmission over polymer optical fibers," *Optical Fiber Tech.*, vol. 9, no. 3, pp. 159–171, July 2003.

50. T. A. Birks, J. C. Knight, and P. St. J. Russell, "Endlessly single-mode photonic crystal fiber," *Opt. Lett.*, vol. 22, pp. 961–963, July 1997.
51. J. C. Knight, J. Broeng, T. A. Birks, and P. St. J.Russell, "Photonic band gap guidance in optical fibers," *Science*, vol. 282, pp. 1476–1478, 20 Nov. 1998.
52. J. Broeng, D. Mogilevstev, S. E. Barkou, and A. Bjarklev, "Photonic Crystal Fibers: A New Class of Optical Waveguides," *Opt. Fiber Technol.*, vol. 5, pp. 305–330, July 1999.
53. P. St. J. Russell, "Photonic crystal fibers," *Science*, vol. 299, pp. 358–362, 17 Jan. 2003.
54. K. Saitoh and M. Koshiba, "Numerical modeling of photonic crystal fibers," *J. Lightwave Technology*, vol. 23, pp. 3580–3596, Nov. 2005.
55. P. C. Schultz, "Progress in optical waveguide processes and materials," *Appl. Opt.*, vol. 18, pp. 3684–3693, Nov. 1979.
56. W. G. French, R. E. Jaeger, J. B. MacChesney, S. R. Nagel, K. Nassau, and A. D. Pearson, "Fiber perform preparation," in S. E. Miller and A. G. Chynoweth, eds., *Optical Fiber Telecommunications*, Academic, New York, 1979.
57. R. E. Jaeger, A. D. Pearson, J. C. Williams, and H. M. Presby, "Fiber drawing and control," in S. E. Miller and A. G. Chynoweth, eds., *Optical Fiber Telecommunications*, Academic, New York, 1979.
58. D. J. DiGiovanni, D. P. Jablonowski, and M. F. Yan, "Advances in fiber design and processing," in I. P. Kaminow and T. L. Koch, eds., *Optical Fiber Telecommunications-IIIA*, Academic, New York, 1997.
59. Q. Jiang, F. Yang, and R. Pitchumani, "Analysis of coating thickness variation during optical fiber processing," *J. Lightwave Technology*, vol. 23, pp. 1261–1272, Mar. 2005.
60. F. P. Kapron, D. B. Keck, and R. D. Maurer, "Radiation losses in glass optical waveguides," *Appl. Phys. Lett.*, vol. 17, pp. 423–425, Nov. 1970.
61. P. C. Schultz, "Fabrication of optical waveguides by the outside vapor deposition process," *Proc. IEEE*, vol. 68, pp. 1187–1190, Oct. 1980.
62. R. V. VanDewoestine and A. J. Morrow, "Developments in optical waveguide fabrication by the outside vapor deposition process," *J. Lightwave Tech.*, vol. LT-4, pp. 1020–1025, Aug. 1986.
63. T. Izawa and N. Inagaki, "Materials and processes for fiber perform fabrication: Vapor-phase axial deposition," *Proc. IEEE*, vol. 68, pp. 1184–1187, Oct. 1980.
64. H. Murata, "Recent developments in vapor-phase axial deposition," *J. Lightwave Tech.*, vol. LT-4, pp. 1026–1033, Aug. 1986.
65. S. R. Nagel, J. B. MacChesney, and K. L. Walker, "Modified chemical vapor deposition," in T. Li, ed., in *Optical Fiber Communications, Vol. 1, Fiber Fabrication*, Academic, New York, 1985.
66. E. M. Dianov and V. M. Mashinsky, "Germania-based core optical fibers," *J. Lightwave Technology*, vol. 23, pp. 3500–3508, Nov. 2005.
67. Y. Chigusa, Y. Yamamoto, T. Yokokawa, T. Sasaki, T. Taru, M. Hirano, M. Kakui, M. Onishi, and E. Sasaoka, "Low-loss pure-silica-core fibers and their possible impact on transmission systems," *J. Lightwave Technology*, vol. 23, pp. 3541–3550, Nov. 2005.
68. P. Geittner and H. Lydtin, "Manufacturing optical fibers by the PCVD process, *Philips Tech. Rev. (Netherlands)*, vol. 44, pp. 241–249, May 1989.
69. T. Hünlich, H. Bauch, R. T. Kersten, V. Paquet, and G. F. Weidmann, "Fiber perform fabrication using plasma technology: A review," *J. Opt. Commun.*, vol. 8, pp. 122–129, Dec. 1987.
70. H. Lydtin, "PCVD: A technique suitable for large-scale fabrication of optical fibers," *J. Lightwave Tech.*, vol. LT-4, pp. 1034–1038, Aug. 1986.
71. S. C. Xue, M. C. J. Large, G. W. Barton, R. I. Tanner, L. Poladian, and R. Lwin, "Role of material properties and drawing conditions in the fabrication of microstructured optical fibers," *J. Lightwave Technology*, vol. 24, pp. 853–860, Feb. 2006.
72. V. V. Ravi Kumar, A. George, W. Reeves, J. Knight, P. Russell, F. Omenetto, and A. Taylor, "Extruded soft glass photonic crystal fiber for ultrabroad supercontinuum generation," *Optics Express*, vol. 10, pp. 1520–1525, Dec. 2002.
73. J. Y. Y. Leong, P. Petropoulos, J. H. V. Price, H. Ebendorff-Heidepriem, S. Asimakis,

R. Moore, K. Frampton, V. Finazzi, X. Feng, T. M. Monro, D. J. Richardson, "High nonlinearity dispersion-shifted lead-silicate holey fibers for efficient 1-μm pumped supercontinuum generation," *J. Lightwave Tech.*, vol. 24, pp. 183–190, Jan. 2006.

74. H. Ebendorff-Heidepriem, P. Petropoulos, R. Moore, K. Frampton, D.J. Richardson, and T. M. Monro, "Fabrication and optical properties of lead silicate glass holey fibers," *J. Non-Crystalline Solids*, vol. 345&346, pp. 293–296, Aug. 2004.
75. G. Barton, M. A. van Eijkelenborg, G. Henry, M. C. J. Large, and J. Zagari, "Fabrication of microstructured polymer optical fibers," *Opt. Fiber Technol.*, vol. 10, pp. 325–335, Oct. 2004.
76. X. Feng, A. K. Mairaj, D. W. Hewak, and T. M. Monro, "Nonsilica glasses for holey fibers," *J. Lightwave Tech.*, vol. 23, pp. 2046–2054, June 2005.
77. D. Kalish, D. L. Key, C. R. Kurkjian, B. K. Turiyal, and T. T. Wang, "Fiber characterization – Mechanical," in S. E. Miller and A. G. Chynoweth, eds., *Optical Fiber Telecommunications*, Academic, New York, 1979.
78. C. R. Kurjian J. T. Krause, and M. J. Matthewson, "Strength and fatigue of silica optical fibers," *J. Lightwave Technology*, vol. 7, pp. 1360–1370, Sept. 1989.
79. G. S. Glaesemann and D. J. Walter, "Methods for obtaining long-length strength distributions for reliability prediction," *Optical Engineering*, vol. 30, pp. 746–748, June 1991.
80. K. Yoshida, T. Satoh, N. Enomoto, T. Yagi, H. Hihara, and M. Oku, "Studies on the strength of optical fiber fabricated by a hybridized process," *J. Lightwave Technology*, vol. 14, pp. 2513–2518, Nov. 1996.
81. K. B. Broberg, *Cracks and Fracture*, Academic, New York, 1999.
82. P. D. T. O'Conner, *Practical Reliability Engineering*, Wiley, Hoboken, NJ, 4th ed., 2002.
83. T. J. Miller, A. C. Hart, W. I. Vroom, and M. J. Bowden, "Silicone and ethylene-vinyl-acetate-coated laser-drawn silica fibers with tensile strengths > 3.5 GN/m^2 (500 kpsi) in > 3 km lengths," *Electron. Lett.*, vol. 14, pp. 603–605, Aug. 1978.
84. K. E. Lu, G. S. Glaesemann, R. V. Van Dewoestine, and G. Kar, "Recent developments in hermetically coated optical fiber," *J. Lightwave Tech.*, vol. 6, pp. 240–244, Feb. 1988.
85. Y. Katsuyama, Y. Mitsunaga, H. Kobayashi, and Y. Ishida, "Dynamic fatigue of optical fiber under repeated stress," *J. Appl. Phys.*, vol. 53, pp. 318–321, Jan. 1982.
86. V. Annovazzi-Lodi, S. Donati, S. Merlo, and G. Zapelloni, "Statistical analysis of fiber failures under bending-stress fatigue," *J. Lightwave Tech.*, vol. 15, pp. 288–293, Feb. 1997.
87. TIA/EIA FOTP-31C, *Proof Testing Optical Fibers by Tension*, Feb. 1999.
88. TIA/EIA FOTP-28, *Method for Measuring Dynamic Tensile Strength and Fatigue of Optical Fibers by Tension*, Apr. 1999.
89. B. Wiltshire and M. H. Reeve, "A review of the environmental factors affecting optical cable design," *J. Lightwave Tech.*, vol. 6, pp. 179–185, Feb. 1988.
90. C. H. Gartside, III, P. D. Patel, and M. R. Santana, "Optical fiber cables," in S. E. Miller and I. P Kaminow, eds., *Optical Fiber Telecommunications-II*, Academic, New York, 1988.
91. K. Hogari, S. Furukawa, Y. Nakatsuji, S. Koshio, and K. Nishizawa, "Optical fiber cables for residential and business premises," *J. Lightwave Tech.*, vol. 16, pp. 207–213, Feb. 1998.
92. A. L. Crandall, C. R. Herron, R. B. Washburn, "Controlling axial load forces on optical fiber cables during installation," Paper NWC3, *OFC/NFOEC 2005 Conf. Program*, Anaheim, CA, March 6–11, 2005.
93. G. Mahlke and P. Gössing, *Fiber Optic Cables: Fundamentals, Cable Design, System Planning*, Wiley, Hoboken, NJ, 4th ed., 2001.
94. O. L. Storaasli, "Compatibility of fiber optic microduct cables with various blowing installation equipment," Paper NWC2, *OFC/NFOEC 2005 Conf. Program*, Anaheim, CA, March 6–11, 2005.
95. TIA/EIA-590-A, *Standard for Physical Location and Protection of Below-Ground Fiber Optic Cable Plant*, July 2001.
96. D. Marcuse, "Loss analysis of single-mode fiber splices," *Bell Sys. Tech. J.*, vol. 56, pp. 703–718, May–June 1977.

CHAPTER 3

Signal Degradation in Optical Fibers

In Chapter 2 we showed the structure of optical fibers and examined the concepts of how light propagates along a cylindrical dielectric optical waveguide. Here, we shall continue the discussion of optical fibers by answering two very important questions:

1. What are the loss or signal attenuation mechanisms in a fiber?
2. Why and to what degree do optical signals get distorted as they propagate along a fiber?

Signal attenuation (also known *as fiber loss* or *signal loss)* is one of the most important properties of an optical fiber, because it largely determines the maximum unamplified or repeaterless separation between a transmitter and a receiver. Since amplifiers and repeaters are expensive to fabricate, install, and maintain, the degree of attenuation in a fiber has large influence on system cost. Of equal importance is signal distortion. The distortion mechanisms in a fiber cause optical signal pulses to broaden as they travel along a fiber. If these pulses travel sufficiently far, they will eventually overlap with neighboring pulses, thereby creating errors in the receiver output. The signal distortion mechanisms thus limit the information-carrying capacity of a fiber.

3.1 Attenuation

Attenuation of a light signal as it propagates along a fiber is an important consideration in the design of an optical communication system, since it plays a major role in determining the maximum transmission distance between a transmitter and a receiver or an in-line amplifier. The basic attenuation mechanisms in a fiber are absorption, scattering, and radiative losses of the optical energy.[1–5] Absorption is related to the fiber material, whereas scattering is associated both with the fiber material and with structural imperfections in the optical waveguide. Attenuation owing to radiative effects originates from perturbations (both microscopic and macroscopic) of the fiber geometry.

This section first discusses the units in which fiber losses are measured and then presents the physical phenomena giving rise to attenuation.

3.1.1 Attenuation Units

As light travels along a fiber, its power decreases exponentially with distance. If $P(0)$ is the optical power in a fiber at the origin (at $z = 0$), then the power $P(z)$ at a distance z further down the fiber is

$$P(z) = P(0)e^{-\alpha_p z} \tag{3.1a}$$

where

$$\alpha_p = \frac{1}{z}\ln\left[\frac{P(0)}{P(z)}\right] \tag{3.1b}$$

is the fiber *attenuation coefficient* given in units of, for example, km^{-1}. Note that the units for $2z\alpha_p$ can also be designated by *nepers* (see Appendix D).

For simplicity in calculating optical signal attenuation in a fiber, the common procedure is to express the attenuation coefficient in units of *decibels per kilometer,* denoted by dB/km. Designating this parameter by α, we have

$$\alpha(\text{dB/km}) = \frac{10}{z}\log\left[\frac{P(0)}{P(z)}\right] = 4.343\ \alpha_p\ (\text{km}^{-1}) \tag{3.1c}$$

This parameter is generally referred to as the *fiber loss* or the *fiber attenuation.* It depends on several variables, as is shown in the following sections, and it is a function of the wavelength.

Example 3.1 An ideal fiber would have no loss so that $P_{out} = P_{in}$. This corresponds to a 0-dB/km attenuation, which, in practice, is impossible. An actual low-loss fiber may have a 3-dB/km average loss at 900 nm, for example. This means that the optical signal power would decrease by 50 percent over a 1-km length and would decrease by 75 percent (a 6-dB loss) over a 2-km length, since loss contributions expressed in decibels are additive.

Example 3.2 As sec. 1.3 describes optical powers are commonly expressed in units of *dBm,* which is the decibel power level referred to 1 mW. Consider a 30-km long optical fiber that has an attenuation of 0.4 dB/km at 1310 nm. Suppose we want to find the optical output power P_{out} if 200 μW of optical power is launched into the fiber. We first express the input power in dBm units:

$$P_{in}\,(\text{dBm}) = 10\log\left[\frac{P_{in}(\text{W})}{1\,\text{mW}}\right]$$

$$= 10\log\left[\frac{200\times10^{-6}\,\text{W}}{1\times10^{-3}\,\text{W}}\right] = -7.0\ \text{dBm}$$

From Eq. (3.1*c*) we then have that the output power level (in dBm) at $z = 30$ km is

$$P_{out}\,(\text{dBm}) = 10\log\left[\frac{P_{out}(\text{W})}{1\,\text{mW}}\right]$$

$$= 10\log\left[\frac{P_{in}(\text{W})}{1\,\text{mW}}\right] - \alpha z$$

$$= -7.0\ \text{dBm} - (0.4\ \text{dB/km})\ (30\ \text{km})$$

$$= -19.0\ \text{dBm}$$

In unit of watts, the output power is

$$P(30\ \text{km}) = 10^{-19.0/10}\ (1\ \text{mW}) = 12.6.\times10^{-3}\ \text{mW}$$

$$= 12.6\ \mu\text{W}$$

3.1.2 Absorption

Absorption is caused by three different mechanisms:

1. Absorption by atomic defects in the glass composition.
2. Extrinsic absorption by impurity atoms in the glass material.
3. Intrinsic absorption by the basic constituent atoms of the fiber material.

Atomic defects are imperfections in the atomic structure of the fiber material. Examples are missing molecules, high-density clusters of atom groups, or oxygen defects in the glass structure. Usually, absorption losses arising from these defects are negligible compared with intrinsic and impurity absorption effects. However, they can be significant if the fiber is exposed to ionizing radiation, as might occur in a nuclear reactor environment, in medical radiation therapies, in space missions that pass through the earth's Van Allen belts, or in accelerator instrumentation.[6–9] In such applications, high radiation doses may be accumulated over several years.

Radiation damages a material by changing its internal structure. The damage effects depend on the energy of the ionizing particles or rays (e.g., electrons, neutrons, or gamma rays), the radiation flux (dose rate), and the fluence (particles per square centimeter). The total dose a material receives is expressed in units of rad(Si), which is a measure of radiation absorbed in bulk silicon. This unit is defined as

$$1 \text{ rad(Si)} = 100 \text{ erg/g} = 0.01 \text{ J/kg}$$

The basic response of a fiber to ionizing radiation is an increase in attenuation owing to the creation of atomic defects, or attenuation centers, that absorb optical energy. The higher the radiation level, the larger the attenuation, as Fig. 3.1*a* illustrates. However, the attenuation centers will relax or anneal out with time, as shown in Fig. 3.1*b*.

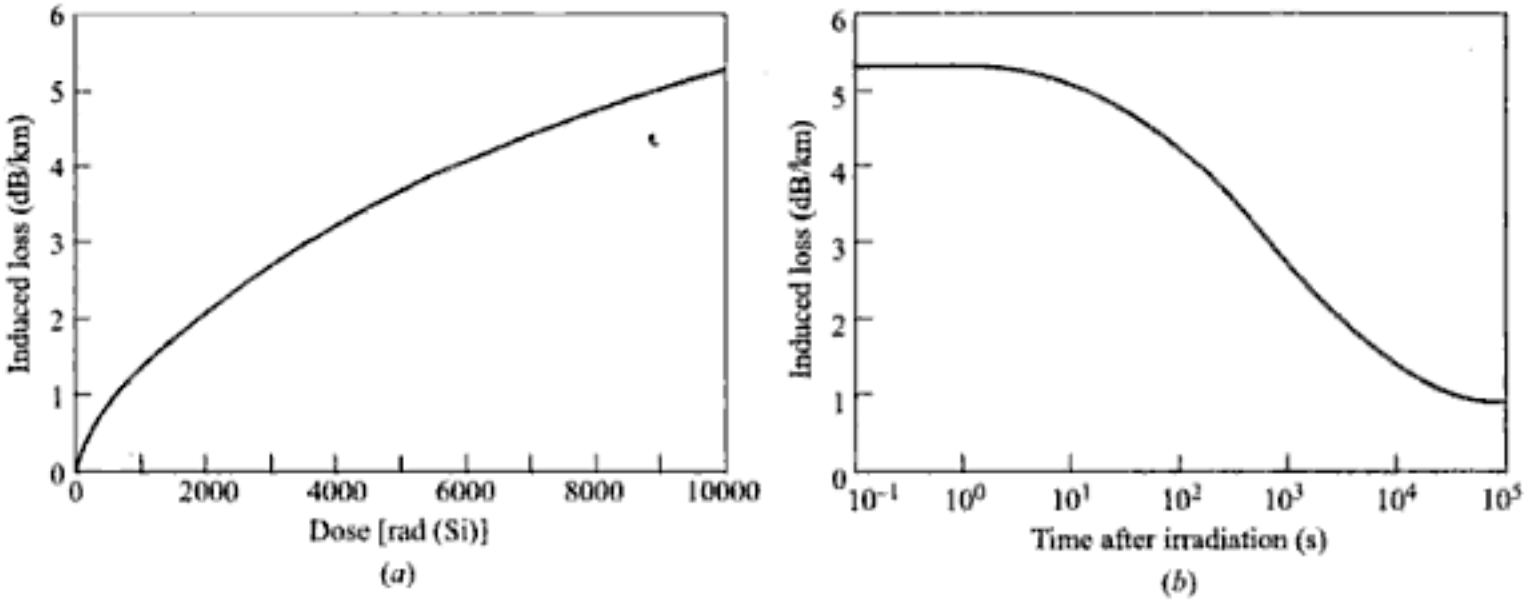

Fig. 3.1 *Effects of ionizing radiation on optical fiber attenuation. (a) Loss increase during steady irradiation to a total dose of 10^4 rad (SiO_2). (b) Subsequent recovery as a function of time after radiation has stopped. (Modified with permission from West et al.,[7] © 1994, IEEE.)*

The dominant absorption factor in silica fibers is the presence of minute quantities of impurities in the fiber material. These impurities include OH^- (water) ions that are dissolved in the glass and transition metal ions such as iron, copper, chromium, and vanadium. Transition metal impurity levels were around 1 part per million (ppm) in glass fibers made in the 1970s, which resulted in losses ranging from 1 to 4 dB/km, as Table 3.1 shows. Impurity absorption losses occur either because of electron transitions between the energy levels within these ions or because of charge transitions between ions. The absorption peaks of the various transition metal impurities tend to be broad, and several peaks may overlap, which

further broadens the absorption in a specific region. Modern vapor-phase fiber techniques for producing a fiber preform (see Sec. 2.9) have reduced the transition-metal impurity levels by several orders of magnitude. Such low impurity levels allow the fabrication of low-loss fibers.

The presence of OH ion impurities in a fiber preform results mainly from the oxyhydrogen flame used in the hydrolysis reaction of the $SiCl_4$, $GeCl_4$, and $POCl_3$ starting materials. Water impurity concentrations of less than a few parts per billion (ppb) are required if the attenuation is to be less than 20 dB/km. The high levels of OH ions in early fibers resulted in large absorption peaks at 725, 950, 1240, and 1380 nm. Regions of low attention lie between these absorption peaks.

The peaks and valleys in the attenuation curves resulted in the designation of the various *transmission windows* shown in Fig. 3.2. By reducing the residual OH content of fibers to below 1 ppb, standard commercially available single-mode fibers have nominal attenuations of 0.4 dB/km at 1310 nm (in the O-band) and less than 0.25 dB/km at 1550 nm (in the C-band). Further elimination of water ions diminishes the absorption peak around 1440 nm and thus opens up the E-band for data transmission, as indicated by the dashed line in Fig. 3.2. Optical fibers that can be used in the E-band are known by names such *low-water-peak* or *full-spectrum fibers*.

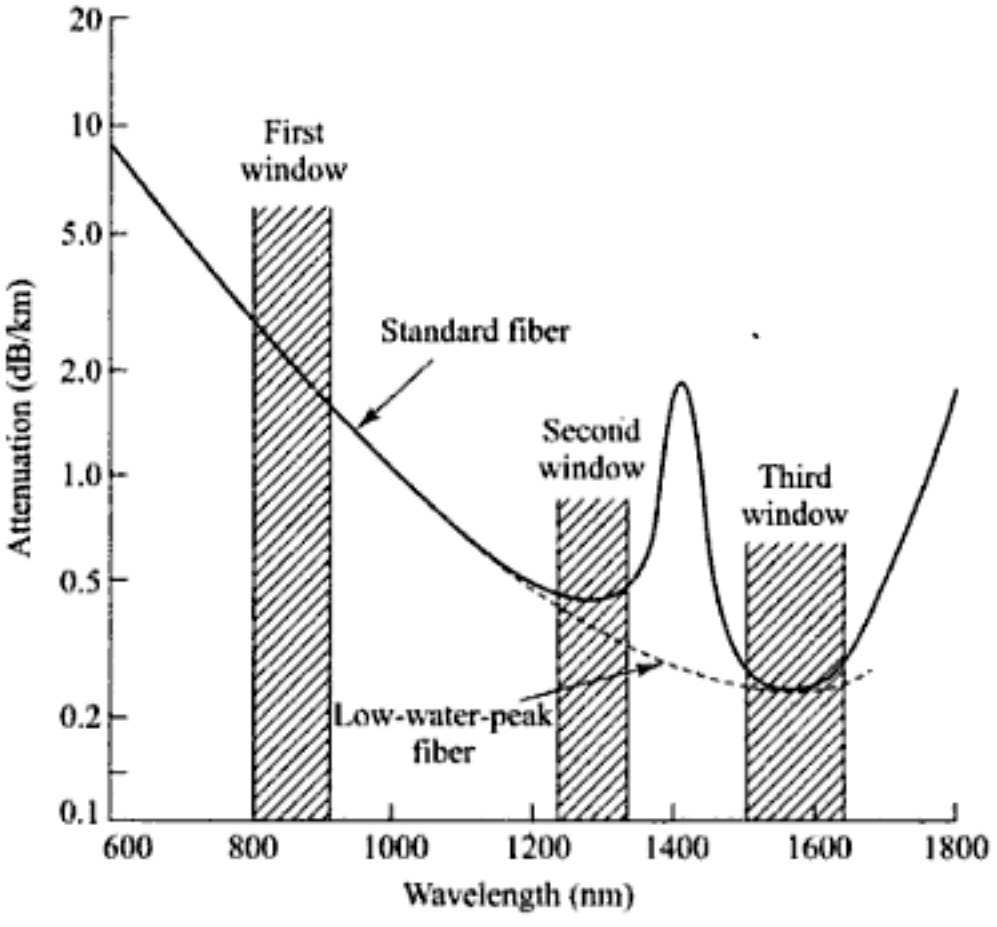

Fig. 3.2 *Optical fiber attenuation as a function of wavelength yields nominal values of 0.5 dB/km at 1310 nm and 0.3 dB/km at 1550 nm for standard single-mode fiber. Absorption by water molecules causes the attenuation peak around 1400 nm for standard fiber. The dashed curve is the attenuation for low-water-peak fiber*

Table 3.1 *Examples of absorption loss in silica glass at different wavelengths due to 1 ppm of water-ions and various transition-metal impurities*

Impurity	*Loss due to 1 ppm of Impurity (dB/km)*	*Absorption Peak (nm)*
Iron: Fe^{2+}	0.68	1100
Iron: Fe^{3+}	0.15	400
Copper: Cu^{2+}	1.1	850
Chromium: Cr^{2+}	1.6	625
Vanadium: V^{4+}	2.7	725
Water: OH^-	1.0	950
Water: OH^-	2.0	1240
Water: OH^-	4.0	1380

Intrinsic absorption is associated with the basic fiber material (e.g., pure SiO_2) and is the principal physical factor that defines the transparency window of a material over a specified spectral region. It occurs when the material is in a perfect state with no density variations, impurities, material inhomogeneities, and so on. Intrinsic absorption thus sets the fundamental lower limit on absorption for any particular material.

Intrinsic absorption results from electronic absorption bands in the ultraviolet region and from atomic vibration bands in the near-infrared region. The electronic absorption bands are associated with the band gaps of the amorphous glass materials. Absorption occurs when a photon interacts with an electron in the valence band and excites it to a higher energy level, as is described in Sec. 2.1. The ultraviolet edge of the electron absorption bands of both amorphous and crystalline materials follow the empirical relationship[1, 3]

$$\alpha_{uv} = Ce^{E/E_0} \tag{3.2a}$$

which is known as Urbach's rule. Here, C and E_0 are empirical constants and E is the photon energy. The magnitude and characteristic exponential decay of the ultraviolet absorption are shown in Fig. 3.3. Since E is inversely proportional to the wavelength λ, ultraviolet absorption decays exponentially with increasing wavelength. In particular, the ultraviolet loss contribution in dB/km at any wavelength can be expressed empirically as a function of the mole fraction x of GeO_2 as[10]

$$\alpha_{uv} = \frac{154.2x}{46.6x + 60} \times 10^{-2} \exp\left(\frac{4.63}{\lambda}\right) \tag{3.2b}$$

As shown in Fig. 3.3, the ultraviolet loss is small compared with scattering loss in the near-infrared region.

In the near-infrared region above 1.2 μm, the optical waveguide loss is predominantly determined by the presence of OH ions and the inherent infrared absorption of the constituent material. The inherent infrared absorption is associated with the characteristic vibration frequency of the particular chemical bond between the atoms of which the fiber is composed. An interaction between the vibrating bond and the electromagnetic field of the optical signal results in a transfer of energy from the field to the bond, thereby giving rise to absorption. This absorption is quite strong because of the many bonds present in the fiber. An empirical expression for the infrared absorption in dB/km for GeO_2-SiO_2 glass is[10]

$$\alpha_{IR} = 7.81 \times 10^{11} \times \exp\left(\frac{-48.48}{\lambda}\right) \tag{3.3}$$

These mechanisms result in a wedge-shaped spectral-loss characteristic. Within this wedge, losses as low as 0.148 dB/km at 1.57 μm in a single-mode fiber have been measured.[11, 12] A comparison[13] of the infrared absorption induced by various doping materials in low-water content fibers is shown in Fig. 3.4. This indicates that for operation at longer wavelengths GeO_2-doped fiber material is the most desirable. Note that the absorption curve shown in Fig. 3.3 is for a GeO_2 doped fiber.

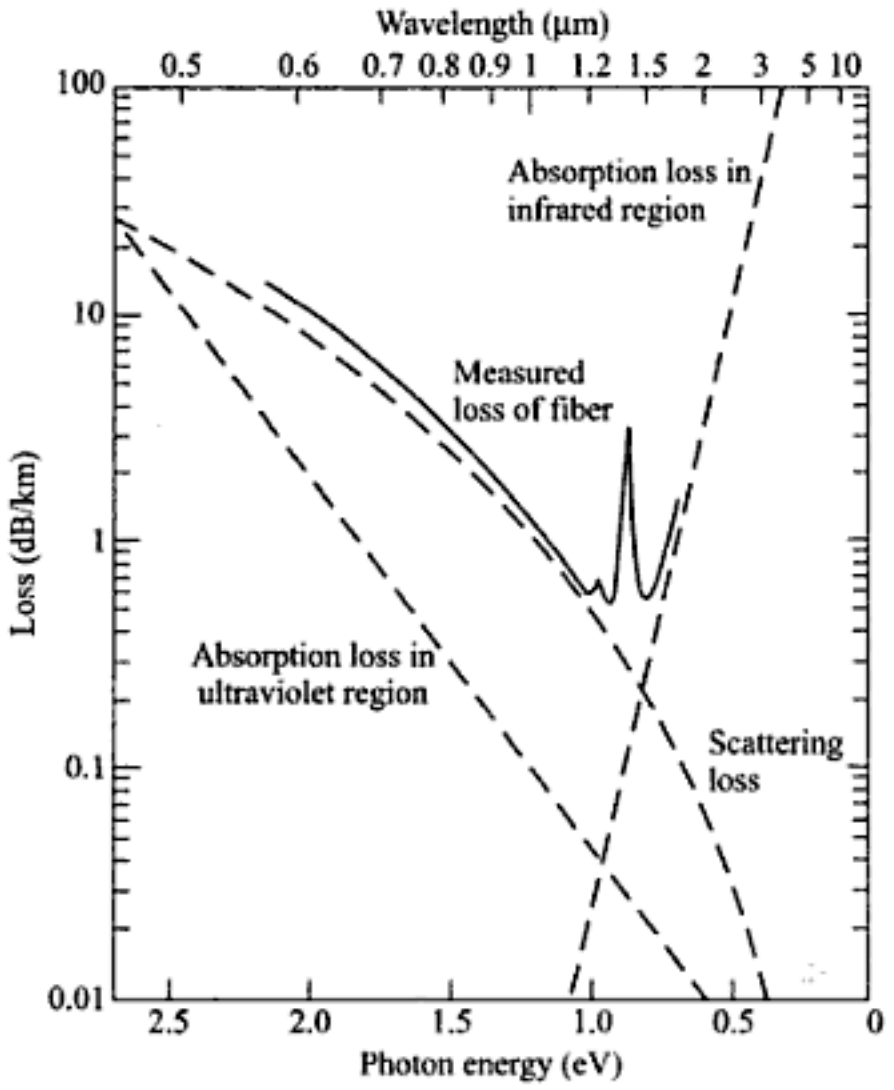

Fig. 3.3 *Optical fiber attenuation characteristics and their limiting mechanisms for a GeO_2–doped low-loss low-water-content silica fiber. (Reproduced with permission from Osanai et al.[13])*

3.1.3 Scattering Losses

Scattering losses in glass arise from microscopic variations in the material density, from compositional fluctuations, and from structural inhomogeneities or defects occurring during fiber manufacture. As Sec. 2.7 describes glass is composed of a randomly connected network of molecules. Such a structure naturally contains regions in which the molecular density is either higher or lower than the average density in the glass. In addition, since glass is made up of several oxides, such as SiO_2, GeO_2, and P_2O_5

compositional fluctuations can occur. These two effects give rise to refractive-index variations which occur within the glass over distances that are small compared with the wavelength. These index variations cause a Rayleigh-type scattering of the light. Rayleigh scattering in glass is the same phenomenon that scatters light from the sun in the atmosphere, thereby giving rise to a blue sky.

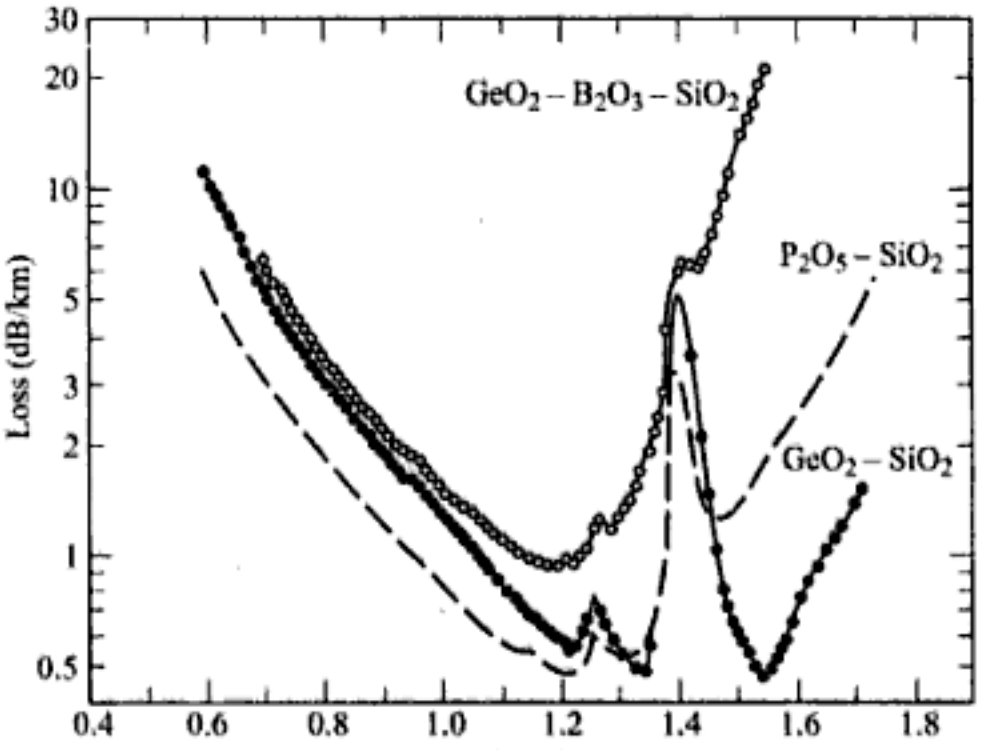

Fig. 3.4 *A comparison of the infrared absorption induced by various doping materials in low-loss silica fibers. (Reproduced with permission from Osanai et al.[13])*

The expressions for scattering-induced attenuation are fairly complex owing to the random molecular nature and the various oxide constituents of glass. For single-component glass the scattering loss at a wavelength λ resulting from density fluctuations can be approximated by[3, 14] (in base e units)

$$\alpha_{\text{scat}} = \frac{8\pi^3}{3\lambda^4} (n^2 - 1)^2 k_B T_f \beta_T \tag{3.4a}$$

Here, n is the refractive index, k_B is Boltzmann's constant, β_T is the isothermal compressibility of the material, and the fictive temperature T_f is the temperature at which the density fluctuations are frozen into the glass as it solidifies (after having been drawn into a fiber). Alternatively, the relation[3, 15] (in base e units)

$$\alpha_{\text{scat}} = \frac{8\pi^3}{3\lambda^4} n^8 p^2 k_B T_f \beta_T \tag{3.4b}$$

has been derived, where p is the photoelastic coefficient. A comparison of Eqs (3.4*a*) and (3.4*b*) is given in Prob. 3.6. Note that Eqs (3.4*a*) and (3.4*b*) are given in units of *nepers* (that is, base e units). As shown in Eq. (3.1), to change this to decibels for optical power attenuation calculations, multiply these equations by $10 \log e = 4.343$.

Example 3.3 For pure silica glass an approximate equation for the Rayleigh scattering loss is given by

$$\alpha(\lambda) \approx \alpha_0 \left(\frac{\lambda_0}{\lambda}\right)^4$$

where α_0 = 1.64 dB/km at λ_0 = 850 nm. This formula predicts scattering losses of 0.291 dB/km at 1310 nm and 0.148 dB/km at 1550 nm.

For multicomponent glasses the scattering is given by[3]

$$\alpha = \frac{8\pi^3}{3\lambda^4}(\delta n^2)^2\, \delta V \tag{3.5}$$

where the square of the mean-square refractive-index fluctuation $(\delta n^2)^2$ over a volume of δV is

$$(\delta n^2)^2 = \left(\frac{\partial n}{\partial \rho}\right)^2 (\delta\rho)^2 + \sum_{i=1}^{m}\left(\frac{\partial n^2}{\partial C_i}\right)(\delta C_i)^2 \tag{3.6}$$

Here, $\delta\rho$ is the density fluctuation and δC_i, is the concentration fluctuation of the ith glass component. The magnitudes of the composition and density fluctuations are generally not known and must be determined from experimental scattering data. Once they are known the scattering loss can be calculated.

Structural inhomogeneities and defects created during fiber fabrication can also cause scattering of light out of the fiber. These defects may be in the form of trapped gas bubbles, unreacted starting materials, and crystallized regions in the glass. In general, the preform manufacturing methods that have evolved have minimized these extrinsic effects to the point where scattering that results from them is negligible compared with the intrinsic Rayleigh scattering.

Since Rayleigh scattering follows a characteristic λ^{-4} dependence, it decreases dramatically with increasing wavelength, as is shown in Fig. 3.3. For wavelengths below about 1 μm it is the dominant loss mechanisms in a fiber and gives the attenuation-versus-wavelength plots their characteristic downward trend with increasing wavelength. At wavelengths longer than 1 μm, infrared absorption effects tend to dominate optical signal attenuation.

Combining the infrared, ultraviolet, and scattering losses, we get the results shown in Fig. 3.5 for multimode fibers and Fig. 3.6 for single-mode fibers.[16] Both of these figures are for typical commercial-grade silica fibers. The losses of multi-mode fibers are generally higher than those of single-mode fibers. This is a result of higher dopant concentrations and the accompanying larger scattering loss due to greater compositional fluctuation in multimode fibers. In addition, multimode fibers are subject to higher-order-mode losses owing to perturbations at the core–cladding interface.

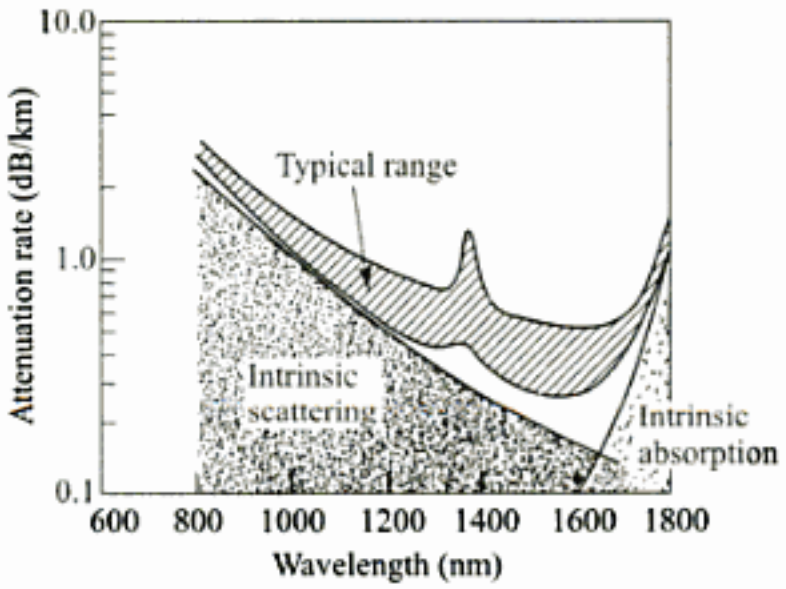

Fig. 3.5 *Typical spectral attenuation range for production-run graded-index multimode fibers. (Reproduced with permission from Keck,[16] © 1985, IEEE)*

The McGraw-Hill Companies

FOURTH EDITION

Optical Fiber Communications

This book on Optical Fiber Communication presents the fundamental principles for understanding and applying optical fiber technology to sophisticated modern telecommunication systems.

Salient features:

- Comprehensive treatment of optical-link constituents.
- Design principles of digital and analog optical fiber transmission links.
- Operating principles of WDM and its components are explained.
- Architecture and performance of Optical Networks explained in detail.

New to this edition:

- New chapter on Nonlinear Effects
- Revised chapter on Performance Measurements and Monitoring
- New sections on
  - Optical Spectral Band
  - Fiber Standards and the Selection of Fibers
  - Raman Fiber Amplifiers
  - Specialty Fibers and Photonic Crystal Fibers
  - Coherent Detection
  - Power Penalties and Error Control

Advance praise for the book:

"A classic book with comprehensive coverage touching every key topic in Optical Fiber Communications. Inculcates thorough understanding of the fundamental principles coupled with state-of-the-art and the emerging OFC technology"

http://www.mhhe.com/keiser/ofc4e for supplements

Visit us at www.tatamcgrawhill.com

ISBN-13: 978-0-07-064810-4
ISBN-10: 0-07-064810-7

9 780070 648104

acsmerizers.com

Tata McGraw-Hill